

# Towards clinical assessment of cerebral blood flow regulation using ultrasonography : model applicability in clinical studies

**Citation for published version (APA):**

Martens, E. G. H. J. (2012). *Towards clinical assessment of cerebral blood flow regulation using ultrasonography : model applicability in clinical studies*. [Phd Thesis 1 (Research TU/e / Graduation TU/e), Biomedical Engineering]. Technische Universiteit Eindhoven. <https://doi.org/10.6100/IR732194>

**DOI:**

[10.6100/IR732194](https://doi.org/10.6100/IR732194)

**Document status and date:**

Published: 01/01/2012

**Document Version:**

Publisher's PDF, also known as Version of Record (includes final page, issue and volume numbers)

**Please check the document version of this publication:**

- A submitted manuscript is the version of the article upon submission and before peer-review. There can be important differences between the submitted version and the official published version of record. People interested in the research are advised to contact the author for the final version of the publication, or visit the DOI to the publisher's website.
- The final author version and the galley proof are versions of the publication after peer review.
- The final published version features the final layout of the paper including the volume, issue and page numbers.

[Link to publication](#)

**General rights**

Copyright and moral rights for the publications made accessible in the public portal are retained by the authors and/or other copyright owners and it is a condition of accessing publications that users recognise and abide by the legal requirements associated with these rights.

- Users may download and print one copy of any publication from the public portal for the purpose of private study or research.
- You may not further distribute the material or use it for any profit-making activity or commercial gain
- You may freely distribute the URL identifying the publication in the public portal.

If the publication is distributed under the terms of Article 25fa of the Dutch Copyright Act, indicated by the "Taverne" license above, please follow below link for the End User Agreement:

[www.tue.nl/taverne](http://www.tue.nl/taverne)

**Take down policy**

If you believe that this document breaches copyright please contact us at:

[openaccess@tue.nl](mailto:openaccess@tue.nl)

providing details and we will investigate your claim.

# **Towards Clinical Assessment of Cerebral Blood Flow Regulation using Ultrasonography**

Model Applicability in Clinical Studies

A catalogue record is available from the Eindhoven University of Technology Library

ISBN: 978-90-386-3135-6

Copyright ©2012 by Esther Martens

All rights reserved. No part of this book may be reproduced, stored in a database or retrieval system, or published, in any form or in any way, electronically, mechanically, by print, photo print, microfilm or any other means without prior written permission of the author.

Cover design: Ana Soares and Esther Martens

Printed by the Universiteitsdrukkerij TU Eindhoven, Eindhoven, The Netherlands.

# **Towards Clinical Assessment of Cerebral Blood Flow Regulation using Ultrasonography**

Model applicability in clinical studies

## **PROEFSCHRIFT**

ter verkrijging van de graad van doctor aan de  
Technische Universiteit Eindhoven, op gezag van de  
Rector Magnificus, prof.dr.ir. C.J. van Duijn, voor een  
commissie aangewezen door het College voor  
Promoties in het openbaar te verdedigen  
op maandag 14 mei 2012 om 16.00 uur

door

**Esther Gerardina Hubertina Johanna Martens**

geboren te Sittard

Dit proefschrift is goedgekeurd door de promotoren:

Prof. dr. ir. F.N. van de Vosse

en

Prof. dr. W.H. Mess

Co-promotor:

Dr. ir. J.P.H. Reulen

# CONTENTS

Chapter 1	Introduction	7
Chapter 2	Extra- and intracranial blood flow velocities in Alzheimer's disease and mild cognitive impairment	19
Chapter 3	Dynamic cerebral autoregulation in subjects with Alzheimer's disease, mild cognitive impairment and controls: evidence for increased peripheral vascular resistance with possible predictive value.	39
Chapter 4	The visually-evoked cerebral blood flow response in women with a recent history of pre-eclampsia and/or eclampsia	57
Chapter 5	Parameter reliability and blood pressure dynamics in the assessment of neurovascular coupling of Alzheimer and cognitively impaired patients	71
Chapter 6	Application of a physiology-based model for visually-evoked blood flow response analysis	95
Chapter 7	General Discussion	119
	Summary	129
	Samenvatting	133
	Dankwoord	137
	Curriculum Vitae	141



# **CHAPTER 1**

## **Introduction in Cerebral Blood Flow and its Regulation**



## Introduction

### 1.1 History of brain function imaging

It is hard to imagine how current daily clinical practice would look like without functional imaging techniques such as (functional) magnetic resonance imaging (fMRI), positron emission tomography (PET) and functional transcranial Doppler ultrasonography (fTCD). The wide spread application of these techniques covers clinical utilities such as diagnosis of cancer or brain diseases and monitoring of stroke, but also research purposes such as investigation of functional connectivity i.e. correlation between functional responses of brain areas to a certain stimulus. If it had not been for some early pioneers who were intrigued by how the brain can perform its functions, how it responds to increased metabolic demands and if and how neuronal activity is coupled to vascular changes, brain function imaging might not have been so well-anchored in today's research and clinical practice.

The exploration of the functional organization of the brain has been ongoing already since the end of the 19<sup>th</sup> century [1, 2]. The first to describe cerebral blood flow changes during mental activity is generally regarded to be Mosso, who in the late 1800's monitored changes in brain volume or temperature induced by brain activity in patients with skull defects [2]. In the same period, Broca examined circulatory changes induced by temperature changes which were supposed to reflect mental activity [1]. In 1890, Roy and Sherrington confirmed the tight coupling between neuronal activity, metabolism and cerebral blood flow, known today as 'functional hyperaemia' [3, 4]. They proposed that diffusion of vascular mediators in response to increased neuronal activity led to the relaxation of vascular smooth muscle and accessory cerebral blood flow increase. However, interest in this research area almost vanished at the beginning of the 20<sup>th</sup> century due to lack of sophisticated tools and contradicting evidence suggesting no relation between brain activity and circulation [1, 5].

Apart from a remarkable clinical study reported by Fulton in 1928, showing that cortical blood flow changes are related to complexity of a visual stimulation task, it was not until the end of World War II that brain circulation and metabolism regained attention in new studies. Together with his colleagues, Kety was the first to develop quantitative methods for measuring brain blood flow and metabolism in humans using in-vivo tissue autoradiography [1]. Further maturation of this technique to a predecessor of the PET imaging technique led to the demonstration that blood flow changes regionally during changes in brain functional activity. Although its potential importance was recognized, the measurement technique was received with caution by then. Later with the development of x-ray computed tomography followed by further improvement to precursors of the current PET, human functional brain mapping research got a boost. Moreover, the parallel progression of cognitive neuroscience, being at a point where experimental designs perfectly matched with emerging functional brain imaging techniques, contributed substantially to the revival of brain function imaging [1]. With the development of

the first methods to detect regional changes in cerebral blood flow in the 1960s, the base for modern brain function imaging was established [2].

### 1.1 Cerebral blood flow and its regulation

For preservation of its vital functions, the brain is largely dependent of a sufficient delivery of oxygen and nutrients. These metabolic factors are transported to the different brain areas via the blood circulation. The cerebral vasculature is anatomically organized by a ring like structure with branches to anterior, medial and posterior located brain areas. This so-called circle of Willis protects the brain for hypo-perfusion by providing alternative pathways in case of vessel obstruction or occlusion. As shown in figure 1, blood flow to the anterior areas and the mid brain is provided by the carotid arteries in the neck. The common carotid artery bifurcates in the external carotid artery, which is responsible for the facial perfusion, and the internal carotid artery which is responsible for the blood supply to the circle of Willis. The internal carotid artery transits into the large middle cerebral artery (MCA), which supplies the largest brain area i.e. the medial temporal area. Blood flow to the posterior areas is provided by the basilar artery which arises from the vertebral arteries. The basilar artery enters the brain circulation splitting into the two posterior cerebral arteries (PCAs) of which the P1 segment is the part in the circle of Willis and the P2 segment its branch outside the circle.

Control of cerebral blood flow is crucial for proper brain function. Blood supply to the brain is essentially regulated by 2 control mechanisms, i.e. neurovascular coupling and cerebral autoregulation. Autoregulation ensures constant adequate blood supply through compensation for blood pressure variations by dilation or narrowing of the microvasculature. Neurovascular coupling adjusts blood supply to the local metabolic need by adaptation of microcirculatory resistance and volume.

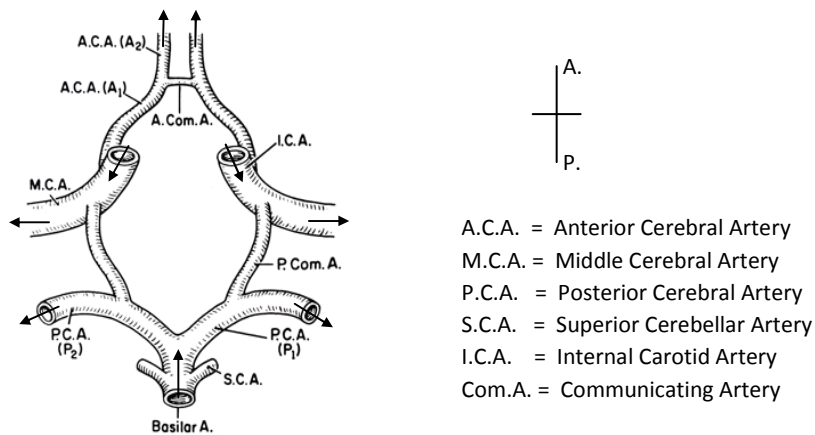


Figure 1.1 Anatomical representation of the circle of Willis, inferior view, adopted from Newell and Aaslid [15]. Notice the symmetry e.g. only the left middle cerebral artery is denoted with M.C.A., whereas right M.C.A. is not labeled.

### ***Cerebral autoregulation***

The brain is largely protected against ischemia and vascular damage by its control mechanisms. Cerebral autoregulation keeps the blood flow constant over a certain range of perfusion pressures (about 50-150 mmHg) by adapting microcirculatory diameters and hence, microcirculatory resistance and volume. At the lower limit of cerebral autoregulation, maximal vasodilation or vascular expansion is attained, which means that if the pressure drops further beyond the lower limit of approximately 50 mmHg, the cerebral blood flow will also start to decrease. In this case, the cerebral autoregulation mechanism is not able anymore to protect the brain against ischemia. At the upper limit of cerebral autoregulation, i.e. at a perfusion pressure of about 150 mmHg, the microvasculature has attained a state of maximal vasoconstriction or vascular contraction. Beyond this limit, the cerebral autoregulation mechanism loses its protective power, since further increase of the pressure will result in an increased flow which might harm the endothelial wall of the arteries.

### ***Neurovascular Coupling***

The neurovascular coupling mechanism also protects the brain against ischemia and vascular damage, but it acts locally and it becomes active under different circumstances compared to cerebral autoregulation. The input for the neurovascular coupling mechanism is not the pressure, but a local change in neuronal activity [2]. In case a brain area is more active it will consume more energy and its metabolic reserves will start to deplete. This leads to local vasodilation of the microcirculatory vessels which results in an increase in blood flow. This blood flow response is called the functional hyperaemic response: because of more brain activity i.e. more active functioning of a local brain area, the blood flow will increase to protect this brain area from ischemia.

### **1.3 Neurovascular biology**

The cellular basis underlying the aforementioned regulatory tools and hence, interpretation of acquired data, are still incompletely understood [8]. Since Willis found nerve fibres in cerebral vessels in the late 1600s, more neurobiological investigators started to describe the innervation of extra-cerebral vessels [9]. With emerging anatomical and functional studies in the last century, a more prominent role in the establishment of the vascular response was ascribed to astrocytes, but solid experimental evidence was absent until recently [7]. These special type of nerve cells are situated in a unique anatomical position, because of their close relationship with neurons as well as blood vessels [6, 7]. Together with glia and pericytes, they form a so-called functional neurovascular unit constituting a base for the establishment of the functional hyperaemic or neurovascular coupling response [2].

Functional hyperaemia is effectuated by adjustment of the cerebrovascular tone of the micro-vessels which changes cerebrovascular resistance. Most of the resistance, about 40-50% [2, 5], is determined by the pial arteries and intraparenchymal arterioles i.e. the arterioles that run along the surface of the brain. Their anatomical morphology and the structural changes they undergo when penetrating deeper into the brain are shown in figure 1.2a. The pial artery consists from inside to outside of an endothelial layer, a

smooth muscle cell layer and a leptomeningeal cell layer [2]. Larger arteries are separated from their surrounding by the Virchow-Robin space. However, as the pial artery penetrates deeper into the brain tissue, the Virchow-Robin space disappears, bringing the vascular membrane in direct contact with the end-feet of astrocytes [2, 9]. Capillaries consist of an endothelial cell layer surrounded by contractile cells, the pericytes [7].

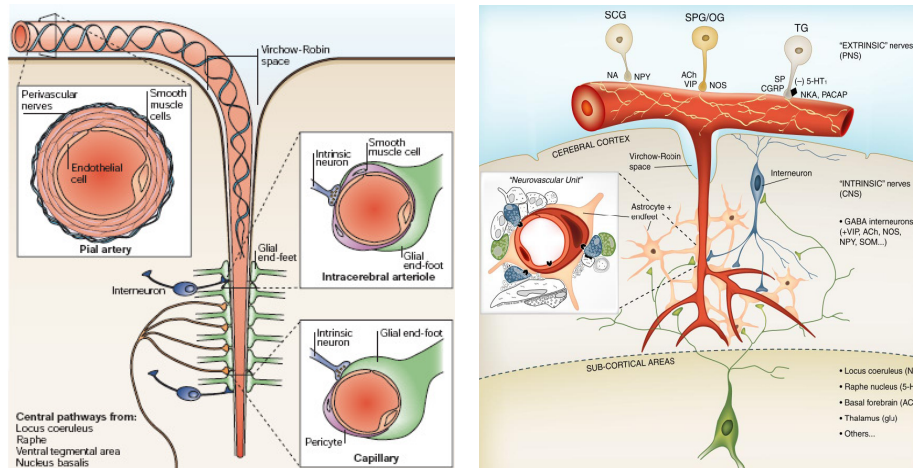


Figure 1.2 a. The neurovascular functional unit (left, from ref. [2])  
 b. Schematic representation of neurovascular unit in its environment (right, ref. [9])

### Neurovascular unit

Astrocytes constitute together with perivascular neurons, glia and the vascular smooth muscle and endothelial cells a neurovascular unit which main functions are to maintain local homeostasis and to protect the brain against ischemia or injury [2]. They seem to have a key role in coordinating the neurovascular coupling [11] for several reasons. First, they are thought to be able to sense activity, second, they may regulate the function of a million synapses in their domain and third astrocytic end feet surround the blood vessels. The arrangement of axonal varicosities adjacent to astrocytic end feet surrounding the blood vessel wall within the neurovascular unit, indicates that perivascularly released neurotransmitters or mediators can directly activate receptors on vascular and astroglial cells to alter microvascular tone [9]. In this way, cerebral blood flow changes can be actively controlled by smooth muscle tone changes resulting in dilation or constriction of pial arteries and intraparenchymal arterioles [11, 12].

### Neuronal innervation pathways

Different neuronal pathways can be distinguished for cerebrovascular innervation i.e. extrinsic and intrinsic innervation as shown in figure 1.2b. Extrinsic innervation of pial arteries originates from peripheral nerves of which signals are transmitted via specific

types of ganglia to extrinsic nerve endings on pial arteries. When the Virchow-Robin space disappears, arteries receive neural input only from neurons located in the brain itself, therefore called intrinsic innervation. Specifically in the cerebral cortex, intrinsic innervation may be induced by afferents from subcortical pathways or from local cortical interneurons [9]. Subcortical pathways originate from some nuclei (nucleus basalis, raphe nucleus, locus coeruleus), which send projection fibers to cortical microvessels and surrounding astrocytes to induce release of vasoactive mediators via receptors on astrocytes, endothelium or smooth muscle. Interneurons integrate incoming afferent signals which can alter the tone of neighbouring intraparenchymal micro-vessels and pial vessels precisely adapting perfusion to local changes in neuronal activity [9, 2].

#### ***Vasoactive agents***

Synaptical activity induces neuronal and astrocytic release of neurotransmitters, which are either vasoactive themselves or stimulate production of vasoactive agents. A variety of mediators has been proposed to play a dominant role in the functional hyperaemic response, but it is highly likely that multiple vasoactive agents concert to realize a flow response [2, 17]. Important roles in the astrocytic signaling pathway seem to be reserved for glutamate and  $\gamma$ -Aminobutyric acid (GABA) released from neurons which may induce  $\text{Ca}^{2+}$  waves in astrocytes. These in turn activate  $\text{K}^+$  channels and P2Y receptors on astrocytic end feet, which are involved in gliavascular signalling and brain water permeability regulation [1, 11]. Hypoxia, hypoglycemia and vasoagents which are not neurotransmitters such as  $\text{K}^+$ ,  $\text{H}^+$ ,  $\text{Ca}^{2+}$ , adenosine, prostaglandins have been investigated as possible trigger for or as mediator in functional hyperemia revealing that none of them can induce functional hyperemia on their own [2, 17].

#### ***Flow distribution in the vascular territory***

Smooth muscle cells and pericytes convert chemical signals originating from endothelial cells, neurons and astrocytes into changes in vascular diameter. The smooth muscle cells are triggered to constrict or relax by induced changes in  $\text{Ca}^{2+}$  concentration and alterations in phosphorylation of the myosine chain [2]. In addition, intravascular pressure changes the contraction state of smooth muscle cells, which counteract to prevent changes in flow rate. Smooth muscle cells are linked via gap junctions probably involved in intramural propagation of vascular signals [2].

When in a certain micro-environment vasodilatation occurs, intravascular pressure will become out of balance and shifts in blood volume need to restore balance [2]. Since capillary and venular volume increase lag behind arteriole volume increase, intraluminal distending pressure increase is thought to occur secondary to arteriolar dilatation, which increases capillary volume [11]. Pericytes are suggested to control vascular dimensions, flow in capillaries and to adjust distribution of red-blood-cell flux among capillaries [11].

Arteries upstream of the local vasodilatation site need to relax as well so that cerebral blood flow is increased effectively and stealing will be prevented i.e. cerebral perfusion pressure is maintained in the whole area supplied by the mother artery [2,11]. Local vasodilatation is proposed to be propagated upstream in a retrograde fashion [2]. Figure 1.3 shows retrograde communication between endothelial cells through gap junc-

tions between endothelial cells or smooth muscle cells. This is a mechanism proposed for conducting vasomotor responses of cerebral arterioles and capillaries to upstream arteries. Diameter changes in capillaries may be mediated by pericytes and the dilatory signal conducted along capillary endothelium to upstream arterioles where further dilations could occur.

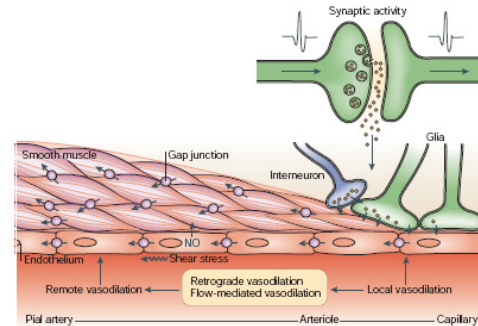


Figure 1.3 Local vasodilatation is propagated upstream in a retrograde fashion via intramural signalling, so that steal effects within the mother vessels' territory can be prevented (from ref [2]).

#### 1.4 Cerebrovascular alterations in Alzheimer's disease

Cerebral hypoperfusion and disturbed cerebral blood flow regulation are associated with several pathological conditions. Neurobiological studies suggest that cerebrovascular alterations are involved in hypertension, Alzheimer's disease and ischemic stroke [2, 10]. In Alzheimer's disease, cerebrovascular disturbances may become manifest already before the onset of clinical symptoms, which implies that they may be detectable in the prodromal phase.

##### **Alzheimer's disease**

Accumulation of amyloid  $\beta$  peptide ( $A\beta$ ) resulting in plaque deposition in the brain and blood vessels and alteration of neurofilaments to neurofibrillary tangles are the main features of Alzheimer's disease [2].  $A\beta$  plays a key role in the progression of the disease by promoting development of neuronal dysfunction and neurodegeneration. Oxidative stress, ion channel dysfunction, inflammation and apoptosis are mediators for the toxic effect of  $A\beta$  on brain cells. Emerging evidence suggests that vascular factors are involved in the pathogenesis of Alzheimer's disease, since it shares risk factors for vascular diseases [11]. Cerebral ischemic lesions have been shown to interact with Alzheimer pathology to enhance dementia. Also, in comparison to healthy aging controls Alzheimer patients have more severe atherosclerosis in the large vessels of the circle of Willis, which produces substantial vascular narrowing leading to hypoperfusion [2].

$A\beta$  deposition does not only affect neurons, but also has profound effects on blood vessels. Cerebrovascular effects of  $A\beta$  are dependent of reactive oxygen species (ROS) production and hence, on oxidative stress conditions [2, 10].  $A\beta$  induces NADPH oxi-

dase-dependent ROS production in microglia and astrocytes. Increased ROS production leads to impaired endothelium dependent relaxation because of reduced NO availability. Reduced vasodilatory capacity hampers functional hyperemic responsiveness. Furthermore, oxidative stress alters enzymes that are crucial to vascular function.

The progression of vascular dysregulation in Alzheimer's disease undergoes a few steps, starting with reduced flow because of neuronal death and synaptic loss [2]. Several studies provide evidence supporting that brain hypoperfusion pushes oxidative stress, cognitive decline and neurodegeneration e.g. regional microvessel degeneration is found to be independent of disease stage and abundant senile plaques are also observed in cognitively normal elderly after autopsy [13]. Progression of amyloid deposition in cerebral arterioles will impair smooth muscle cells capability to relax and prohibits vasodilation mechanically. Finally atherosclerosis in the vessels of the circle of Willis reduces global cerebral blood flow in this further impairing the ability of neural stimuli to increase cerebral blood flow. Assessment of cerebral blood flow regulation could therefore be essential for early diagnosis of Alzheimer's disease.

### 1.5 Ultrasound assessment of cerebral blood flow regulation

Cerebral blood flow and its regulation may be examined by a variety of techniques including Blood oxygen level dependent Magnetic Resonance Imaging (BOLD MRI), Positron Emission Tomography (PET), Single Photon Emission Computer Tomography (SPECT), Near Infrared Spectroscopy (NIRS) and duplex or Transcranial Doppler (TCD) ultrasonography. For the purpose of screening of subjects for a suspected pathology, ultrasonography is preferable over other techniques because of its advantages as non-invasiveness, flexibility in use, superior time resolution and cost-effectiveness.

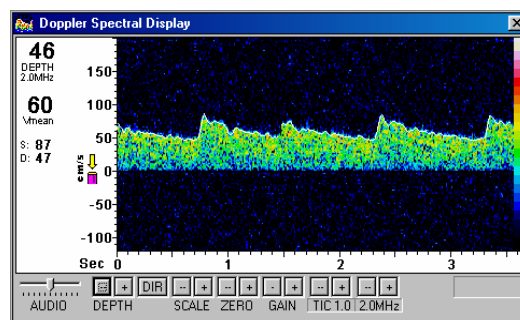


Figure 1.4 Doppler velocity spectrum measured in the Middle Cerebral Artery (MCA) during a few heart beats. Coloring reflects the amount of blood cells having the specified velocity. Usually the envelop corresponding to blood cells with maximum velocity are recorded and processed by beat-to-beat detection of peak-systolic, mean or end-diastolic values.

#### Measurement Principles

Ultrasonography can be performed using a Duplex scanner, which provides both the B-mode i.e. echo image and Doppler velocity spectrum, or using a 'blind' transcranial

Doppler device (B-TCD), which provides only the Doppler velocity spectrum without imaging information. For cerebral vessel imaging or blood flow velocity recording, ultrasound is usually insonated via the temporal window i.e. a thin spot in the bone near the ear. When the ultrasound signal encounters a transition between media (tissues) with different characteristic acoustic impedances, part of it will be reflected (echo) and the remaining part will travel further through the tissue. The acoustic impedance of a material depends on the speed of sound through a medium and its density. When ultrasound travels through tissue, it will become attenuated dependent of absorption within the tissue (energy to heat conversion). The time difference between the emitted ultrasound pulses and their echo's provides information about the distance of the transition to the transducer i.e. about depth. Echo's originating from deeper lying tissues will be weaker than those coming from superficial tissues. The amplitude of the echoes or intensities of the reflected ultrasound signals may be depicted as gray values. To generate a 2D image ultrasound pulses are subsequently sent from an array of piezo-electric elements in the transducer. The reflected echo amplitudes along the array of scan lines can be converted to gray values obtaining a 2D echo image or Brightness mode image [14].

Blood flow velocity recordings rely on the classical Doppler principle but differ in that the source (ultrasound transducer) is not moving with respect to the observer (red blood cell) i.e. the source is stationary whereas the observer has a velocity. The ultrasound transducer emits pulses to the red blood cells which reflect them by another frequency than the frequency of the emitted pulses. This results in a frequency shift between the emitted and reflected ultrasound signal from which the blood flow velocity can be determined according to [14]:

$$v = \frac{c \cdot (f_t - f_r)}{2 \cdot f_t \cdot \cos \theta} \quad (1)$$

With  $v$  representing the blood flow velocity,  $\theta$  the insonation angle,  $c$  the speed of sound in blood and  $f_t$  and  $f_r$  the frequencies of the emitted and reflected ultrasound pulses respectively.

Equation 1 shows that the measured blood flow velocity, i.e. the blood flow velocity component in the direction of the ultrasound beam, depends on the insonation angle between the emitted ultrasound beam and the movement direction of the red blood cells in the vessel. Since duplex allows simultaneous reproduction of the echo image and the Doppler signal, it is possible to visualize where the blood flows enabling localisation of the vessels. In this way, the blood flow axis and thus the insonation angle of the ultrasound beam can be determined and automatically corrected for [14].

#### ***Assessment of cerebral blood flow regulation***

The use of ultrasonography for investigation of cerebral blood flow and its regulation has evolved to an important diagnostic tool [15]. Transcranial Doppler ultrasonography (TCD) can be applied to study cerebral autoregulation and vasoreactivity to gain understanding of cerebral hemodynamic mechanisms. Regarding the study of stimulus-



evoked blood flow changes, Aaslid was first to demonstrate the use of TCD to measure visually-evoked blood flow responses [15, 16]. Nowadays, cerebral autoregulation and neurovascular coupling are often examined in clinical studies by use of transfer function analysis to evaluate the clinical value of ultrasonography for specific patient groups.

For the assessment of cerebral autoregulation function, the extent to which blood pressure fluctuations are transferred into the cerebral blood flow is examined. Generally, the transfer function or input-output relation between the simultaneously measured finger blood pressure and blood flow velocity in the middle cerebral artery is determined in the frequency domain [18]. The gain of this transfer function represents the amplification factor between the blood pressure fluctuations and the cerebral blood flow velocity fluctuations. The phase shift of the same transfer function denotes the lag between blood pressure and blood flow velocity fluctuations. Transfer function gain and phase are measures for cerebral autoregulation function.

To assess neurovascular coupling, the visually-evoked cerebral blood flow velocity response is measured in the P2 segment of the PCA using transcranial Doppler ultrasonography. A visual block stimulus consisting of repeated steps of, e.g., '40s stimulus on' - '20s stimulus off' is presented to the subject, while simultaneously the blood flow is measured. For the visual stimulus paradigm, amongst others a flash light, text reading, reversal checkerboard pattern or a cartoon may be used [19, 20]. A colored cartoon is most often used as visual stimulus paradigm since it evokes the largest response. The Visually-Evoked blood Flow Response (VEFR) can be obtained by averaging the individual (step) response cycles and expressing them relative to baseline, i.e. the mean cerebral blood flow velocity 10s before the stimulus is switched on. The VEFR can be fitted with the step response of a control system model, so that a patient-specific set of 5 model parameter values is obtained [19, 20]. Figure 1.5 shows a typical example of a VEFR and its model fit. In terms of the response, model parameter  $K$  specifies the mean % CBFV difference between the "stimulus-off" and "stimulus-on" periods, whereas  $\omega_n$  characterizes the oscillation of the system as if it were undamped. Parameter  $T_v$  modulates the initial flow response and  $\zeta$  describes the damping of the system. Finally,  $T_d$  is the time delay between stimulus onset and flow response start.

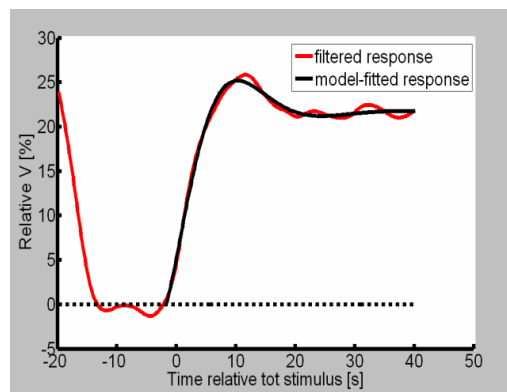


Figure 1.5 Example of a visually-evoked blood flow response and its model-fit.

## 1.6 Aim

Ultrasonographic assessment of cerebral blood flow regulation may have (great) potential for diagnostics, screening and therapeutic decisions in clinic. For instance, it may be a suitable tool for the early detection of Alzheimer's disease [21]. Also, it may be used as a screening tool for increased risk of stroke after the experience of preeclampsia, since experience of preeclampsia increases the chance to die from cerebral hemorrhage 5-fold [22]. In addition, ultrasonography is a non-invasive technique, which is flexible in use, cost-effective and has a high temporal resolution. However, currently the interpretation of outcomes for cerebral blood flow regulation assessment is difficult due to large spread and lack of success yet in differentiating between pathological and normal regulation. Therefore, it is important both to enable assessment of cerebrovascular control by reliable parameters and to determine its clinical value for pathological populations. The work in this thesis is aimed at putting a step forward towards development of reliable and clinically relevant parameters for cerebral blood flow regulation assessment using ultrasonography.

## 1.7 Outline of the Thesis

First, duplex ultrasonography will be applied to examine blood flow velocities (BFV) in intra- and extracranial vessels of patients with Alzheimer's disease (AD), mild cognitive impairment (MCI) and healthy controls (HC). This study, described in chapter 2, aims to reveal the potential of ultrasonography as a diagnostic tool for discrimination of AD, MCI and HC based on their BFV distributions throughout the extracranial supplying carotid vessels and intracranial circulation. Subsequently, in chapter 3, cerebral autoregulation characteristics will be investigated in the same study cohort of AD and MCI patients and HC by comparison of their pressure - flow velocity transfer functions. These enable also identification of parameters of a windkessel model providing patient-specific values for vascular properties such as resistance and compliance.

As a next step, the focus will shift to local blood flow regulation i.e. the neurovascular coupling mechanism. First, visually-evoked blood flow responses (VEFRs) are studied in a relative young study population of formerly (pre-)eclamptic patients and age-matched healthy controls in chapter 4. Several studies provide evidence for altered cerebral hemodynamics during (pre)eclampsia, but long-term effects are unknown. Then, the standard VEFR analysis procedure, applied in chapter 4, will be compared to a newly introduced VEFR analysis procedure including parameter reliability consideration and blood pressure dynamics, in chapter 5. Both procedures are applied to the study cohort of AD, MCI and HC and consequences for study outcomes will be discussed. To enable linkage of VEFR behavior to vascular properties, a physiological model of the visual cortex vasculature including different regulatory processes is introduced and tested in chapter 6. Possible pathological regulatory deficits for AD can be simulated to evaluate their effect on VEFR behavior.

## References

- [1] Raichle, M., *Behind the scenes of functional brain imaging: A historical and physiological perspective*. Proc. Natl. Acad. Sci. USA, 1998 95:p. 765-772.
- [2] Iadecola, C., *Neurovascular regulation in the normal brain and in Alzheimer's disease*. Nat Rev Neurosci, 2004. 5(5): p. 347-60.
- [3] Zonta, M., et al., *Neuron-to-astrocyte signaling is central to the dynamic control of brain microcirculation*. Nat Neurosci, 2003. 6(1): p. 43-50.
- [4] Paulson, O.B. and E.A. Newman, *Does the release of potassium from astrocyte endfeet regulate cerebral blood flow?* Science, 1987. 237(4817): p. 896-8.
- [5] Edvinsson L, Krause D. *Cerebral Blood Flow and Metabolism*. 2nd edition, Philadelphia: ©Lippincott Williams & Wilkins 2002.
- [6] Filosa, J.A. and V.M. Blanco, *Neurovascular coupling in the mammalian brain*. Exp Physiol, 2007. 92(4): p. 641-6.
- [7] Iadecola, C. and M. Nedergaard, *Glial regulation of the cerebral microvasculature*. Nat Neurosci, 2007. 10(11): p. 1369-76.
- [8] Paemeleire, K., *The cellular basis of neurovascular metabolic coupling*. Acta Neurol Belg, 2002. 102(4): p. 153-7.
- [9] Hamel, E., *Perivascular nerves and the regulation of cerebrovascular tone*. J Appl Physiol, 2006. 100(3): p. 1059-64.
- [10] Girourd H, Iadecola C. *Neurovascular coupling in the normal brain and in hypertension, stroke, and Alzheimer disease*. J Appl Physiology, 2006. 100: p 328-35.
- [11] Koehler R.C. et al., *Astrocytes and the regulation of cerebral blood flow*. Trends in Neurosciences 2008. 32(3): p.160-9.
- [12] Kuschinsky W. Chapter *Neuronal-vascular coupling, a unifying hypothesis*. Plenum Press, New York 1997.
- [13] de la Torre JC, *Vascular basis of Alzheimer's pathogenesis*. Ann N Y Acad Sci 2002;977:196-215.
- [14] Evans DH, McDicken WN. *Doppler Ultrasound; Physics, instrumentation and Signal Processing*. 2<sup>nd</sup> edition. Wiley, Chichester, 2000
- [15] Newell DW, Aaslid R. *Transcranial Doppler*. New York: ©Raven Press 1992.
- [16] Aaslid R. *Visually evoked dynamic blood flow response of the human circulation*. Stroke 1987; 18:771-775
- [17] Lok J, Gupta P, GUo S et al. *Cell-cell signaling in the neurovascular unit*. Neurochem Res 2007, 32:2032-45.
- [18] Tiecks FP, Lam AM, Aaslid R, Newell DW. *Comparison of static and dynamic cerebral autoregulation measurements*. Stroke 1995; 26(6): 1014-1019.
- [19] Rosengarten B, Huwendiek O, Kaps M. *Neurovascular coupling and cerebral autoregulation can be described in terms of a control system*. Ultrasound in medicine & biology 2001;27:189-93.
- [20] Rosengarten B, Huwendiek O, Kaps M, *Neurovascular coupling in terms of a control system: validation of a second-order linear system model*. Ultrasound in medicine & biology 2001;27:631-5.
- [21] de la Torre JC, *Vascular risk factor detection and control may prevent Alzheimer's disease*. Ageing Res Rev 2010;9:218-25.
- [22] Irgens HU, Reisaeter L, Irgens LM, Lie RT. *Long term mortality of mothers and fathers after preeclampsia: population based cohort study*. BMJ 2001; 323: 1213-1217

# **CHAPTER 2**

## **Extra- and Intracranial Blood Flow Velocities in Alzheimer's Disease and Mild Cognitive Impairment**

Based on:

Martens EGHJ, Shijaku E, Aalten P, Ramakers IHGB, Verhey FRJ, Mess WH, Reulen JPH.  
*Extra- and Intracranial Blood Flow Velocities in Alzheimer's Disease and Mild Cognitive Impairment*. Submitted (2012)

## Abstract

Structural and functional changes in cerebral vasculature are increasingly thought to play a prominent role in the progression to Alzheimer's disease. Of particular relevance for possible prevention and early detection of Alzheimer's disease, is the study of these changes in patients with an increased probability of developing into Alzheimer's disease i.e. patients classified as mild cognitive impairment. This study aims to compare blood flow velocities measured on multiple sites throughout the extra- and intracranial circulation between patients with Alzheimer's disease (AD), patients with mild cognitive impairment (MCI) and healthy controls (HC).

Extra- and intracranial arteries of 18 AD, 21 MCI and 20 HC matched on age and sex were examined using Duplex ultrasonography. Blood Flow Velocities (BFV) were measured on multiple sites in the carotid arteries and intracranial basal arteries.

Compared to HC and MCI, AD BFV were bilaterally significantly lowered at the proximal site of the internal carotid artery (ICA), but similar at mid and distal sites. No significant group differences were found at proximal, mid and distal sites of the common carotid arteries or in the external carotid arteries. Intracranially, the same pattern for AD vs. MCI and HC was observed in the middle (MCA) and posterior cerebral arteries (PCA) i.e. significantly lowered AD BFV in the proximal MCA and PCA P1-segment, but similar values remotely, i.e. in the distal MCA and P2-segment. MCI vs. HC differed significantly for systolic BFV in bilateral proximal MCAs.

Remarkably, AD is clearly distinguishable from MCI and HC based on BFV measured on proximal in contrast to distal sites of intra- and extracranial vessels. In view of reported vascular alterations in AD, this is likely to result from a diameter reduction at distal sites. MCI BFV measured in the intracranial anterior circulation are in general intermediate between AD and HC, whereas MCI BFV measured in the extracranial or intracranial posterior circulation are similar to HC. Our findings do not only suggest that cerebrohemodynamic alterations are detectable during AD progression, but also that extensive ultrasonographic screening of intra- and extracranial arteries is useful for monitoring BFV decline in the MCI stage. Future follow-up of MCI patients can reveal the predictive value of location-specific BFV for conversion to AD.

## 2.1 Introduction

Over the last decade research on Alzheimer's disease (AD) has increasingly focused on the role of cerebrovascular factors in the pathogenesis of AD [6, 10, 19]. Neurobiological studies show that the structure of cerebral vessels in AD can be profoundly altered: large cerebral vessels may have severe ather-osclerotic plaques [10], whereas in arterioles cerebral amyloid angiopathy is deposited [5]. Lesions may also be present in the capillaries giving rise to endothelium compression and thickened basement membrane. Furthermore, deposition of  $\beta$ -amyloid is suggested to impair the ability of arteriolar smooth muscle to relax, comprising vasodilatation [10]. These findings suggest that structural and functional changes in cerebral vasculature play a prominent role in the progression to AD.

Of particular relevance for possible prevention and early detection of AD is the study of cerebrovascular changes in patients with an increased probability of developing into AD, in particular patients classified as mild cognitive impairment (MCI). Patients with MCI do not meet the criteria for dementia, but do have cognitive impairments [15]. Iadecola hypothesized that cerebrovascular alterations are already evident before the onset of clinical symptoms, i.e. in the latent phase of AD. This implies that basic blood flow alterations may be detectable in the prodromal stage of AD.

Current studies are especially dedicated to the identification of clinical, neuroimaging and biological markers to distinguish AD and MCI disease stages [9, 24]. Regarding neuroimaging techniques, Positron Emission Tomography (PET) and Single Photon Emission Computer Tomography (SPECT) studies show quite promising results in diagnosis and detection of AD based on blood flow assessment [12]. However, considering radiation and costs, SPECT, PET and MRI are not the ideal screening tools for prediction or diagnosis of AD.

Ultrasonography is increasingly posed as a screening tool for AD, because of its non-invasiveness, low costs, easy applicability and low patient burden [6, 18]. In previous studies blood **volume flow (BVF)** of the cervical arteries were measured using duplex ultrasonography. BVF was reduced particularly in the internal carotid arteries (ICA) in AD compared to healthy controls (HC), which was mainly an effect of reduced velocity rather than diameter [14]. In a subsequent study, MCI BVF in the ICA was found to be intermediate between AD and HC [13]. Furthermore, 2 year follow-up in the same cohort revealed that, based on a cut-off baseline **BVF** value of 558 ml/min (median), AD conversion could be predicted with a specificity of 72% and sensitivity of 68%.

Also intracranial vessels of MCI patients have been examined using duplex ultrasound. Blood **Flow Velocity (BFV)** was significantly decreased bilaterally in the middle cerebral arteries (MCA, depth 50-55 mm) and anterior cerebral arteries (ACA, depth of 60-70 mm), but unaffected in the basilar arteries as compared to controls [25]. Doepp et al [7] investigated both extracranial carotid volume flows and intracranial MCA flow velocity in AD, vascular dementia (VD) and controls. They found volume flows and MCA flow velocities significantly reduced both in AD and vascular dementia (VD) as compared to HC.

Recently, a TCD study was reported in which BFV has been measured in multiple extra- and intracranial vascular segments of AD, HC and a small MCI group [18]. In addition to

significantly increased pulsatility index (PI) values, they found significantly lowered BFV in several extra- and intracranial vascular segments in AD. However, these findings were not consistent for all measurement locations and for left and right side, which may be due to lack of angle correction compromising reliability of TCD findings. Duplex ultrasonography may be more sensitive for detection of BFV and PI differences. Nonetheless, these findings indicate that specific sites in the extra- and intracranial circulation are affected in AD.

In this study, duplex ultrasonography has been applied to systematically evaluate BFVs at multiple bilateral sites in both extra- and intracranial arteries of not only AD patients and HC, but also patients at risk for AD i.e. MCI patients. Since duplex scanner availability in hospitals can be limited, it has been tested whether Duplex BFV findings were reproducible with TCD. The aim of our study is to compare BFV maps constructed of all measured intra- and extracranial BFV in different disease stages e.g. AD and MCI as compared to HC. Our major research hypothesis is that MCI BFV in extracranial carotid vessels and intracranial basal arteries and their branches are intermediate between those of AD and HC.

## 2.2 Methods

### *Study population*

The study population consists of 18 patients with possible/probable AD, 21 MCI patients and 20 HC. All participants gave informed consent according to the declaration of Helsinki. The study was approved by the local ethics committee.

Patients are selected from the Maastricht Memory Clinic, a university affiliated outpatient clinic for subjects with cognitive impairment [26]. All patients were subjected to a standardized assessment at baseline which included a detailed history provided by the patient and a psychiatric, neurological, and physical examination, appropriate laboratory tests, a neuropsychological assessment, and neuroimaging (CT or MRI) [26].

AD patients were diagnosed according to the DSM-IV criteria for dementia [1] and NINCDS-ADRDA criteria [15]. MCI was defined as having subjective and objective cognitive impairment, no significant impairments in daily living and no dementia. Patients living in a nursing home at the start of the study or without a reliable informant were excluded from the study. Also patients with a possible diagnosis of vascular dementia, according to NINDS/AIREN criteria [19] were excluded. Final exclusion criteria were use of psychopharmacological medication, abuse of alcohol and/or drugs, diabetes and heart disease.

Participants with a possible stenosis (> 50%) of extra- and/or intracranial vessels as assessed by extra and transcranial non-invasive colour duplex investigation were excluded. Also participants without a temporal "bone" window were excluded.

Healthy subjects were recruited via a pre-existing bank of volunteer subjects of the Maastricht Aging Study (MAAS) [11] and were randomly matched for age, sex and educational level. When entering the study, these subjects were subjected to a neuropsychological assessment, comparable to the AD and MCI patients.

Table 1. Demographic data of the study participants

Characteristics	AD [N=18]	MCI [N=21]	HC [N=20]	P-val	Post hoc
	Mean ± SD	Mean ± SD	Mean ± SD		
Age (Years)	72 ± 7	70 ± 7	70 ± 6	F	0,667
MMSE	19.7 ± 5.4	27.7 ± 1.4	29.0 ± 1.2	F	0,000 A,B **
Height (cm)	166 ± 8	167 ± 8	168 ± 7	H	0,566
Weight (kg)	73 ± 7	74 ± 12	72 ± 12	H	0,888
MBP (mmHg)	105 ± 9	101 ± 9	103 ± 12	H	0,412
Education (%)					
high   med   low	17   28   56	43   14   43	20   35   45	$\chi^2$	0,270
Sex (♂ - ♀)	10 - 8	11 - 10	9 - 11	$\chi^2$	0,797

F: Anova |  $\chi^2$ : Pearson Chi Square | H: Kruskal-Wallis | A: AD≠MCI | B: AD≠HC

\*\* : ANOVA with Sidak correction,  $p < 0.001$

Demographics of the study population are shown in table 1. Except for MMSE, no demographic parameter differed between groups. Relevant neuroimaging data (CT or MRI) for the diagnosis of AD or MCI, gathered in the aforementioned regular patient care, were also analyzed. Table 2 shows the MRI characteristics for AD and MCI, i.e. white matter hyperintensity score (Fazekas WMH) and atrophy measures, i.e. atrophy-related white matter changes (ARWMC total), global cortical atrophy (GCA) [8] and medial-temporal atrophy (MTA) [22].

Table 2. MRI characteristics i.e. white matter and atrophy measures for AD and MCI

MRI characteristics	AD [N=18]	MCI [N=17]	P-val
	Mean ± SD	Mean ± SD	
Fazekas WMH (0-3)	1,1 ± 0,8	0,9 ± 0,5	M 0,463
ARWMC total (0-30)	4,9 ± 4,2	4,0 ± 2,9	M 0,757
GCA (0-3)	1,7 ± 1,0*	0,8 ± 0,7	M 0,014
MTA (0-4)	3,1 ± 1,2*	2,1 ± 1,4	M 0,032

\*  $p < 0.05$

#### Color Duplex Ultrasound Examination

Extracranial systolic and diastolic BFV were measured bilaterally in the common (CCA: proximal, middle and distal), external (ECA) and internal carotid artery (ICA: proximal, middle and distal). Measurement locations were chosen equally distant over the trajectory that could be visualized in B-mode resulting in inter-location distances of approximately 2 cm for the CCA and 1.5 cm for the ICA. Intracranial systolic, mean and diastolic BFV were determined bilaterally in the anterior (ACA), middle (MCA) and posterior cerebral arteries (PCA, P1 and P2 segment). The MCA was measured at two insonation depths with means of 56 mm (D1) and 46 mm (D2).

Extracranial vessels were also qualitatively screened for the presence of plaques and degree of possible stenosis and the CCA also for vessel wall thickening. Intra- and ex-



tracranial duplex investigations were carried out with a HP Sonos 5500 device using a Philips S4 i.e. 2-4 MHz sector array probe and Philips 11-3L i.e. 3-11MHz linear array probe, respectively. The experienced ultrasound examiner was blinded to diagnosis. All participants were insonated under standard resting conditions (supine position in a partly darkened room). Angle-corrected BFV were measured with the sample volume expanded over the entire vessel diameter. In several subjects BFV were only measurable in part of the vessels or vessel segments or only for left or right side.

#### ***Transcranial Doppler ultrasonography without B-mode ('Blind' TCD)***

Since our duplex examinations were part of a larger study protocol in which dynamic cerebral autoregulation was tested as well, also MCA BFV measured with a 2 MHz pulsed wave TCD system (Multidop X4, DWL, Sipplingen) were available for our study cohort. These recordings were averaged over a 10-minute-interval as representatives for 'blind' MCA BFV (B-MCA BFV). The MCA was insonated at a mean depth of 48.6 mm (std 3 mm, range 44-57mm, N=53)

#### ***Statistical Methods***

Data were statistically analyzed using the Statistical Package for Social Sciences (SPSS) version 17.0. Statistical relevant group differences were investigated by independent Student t-test and Chi-square analysis. Analysis of Covariance (ANCOVA) with Sidak correction was performed to account for possible confounders. Mann-Whitney-U- tests were applied in case parameters were not normally distributed. A p-value < 0.05 was regarded as significant.

## **2.3 Results**

#### **Extracranial BFV (CCA, ECA and ICA)**

Since age was a significant confounder for right systolic and diastolic BFV in the proximal ICA, all extracranial BFV were corrected for age in statistical analyses. Systolic and diastolic BFV at the **proximal** site of the ICA were significantly lowered bilaterally in AD as compared to HC and MCI (see figure 1). AD and MCI BFV differences remained significant when GCA, MTA or ARWMC total were included as confounders. No significant differences were found between MCI and HC.

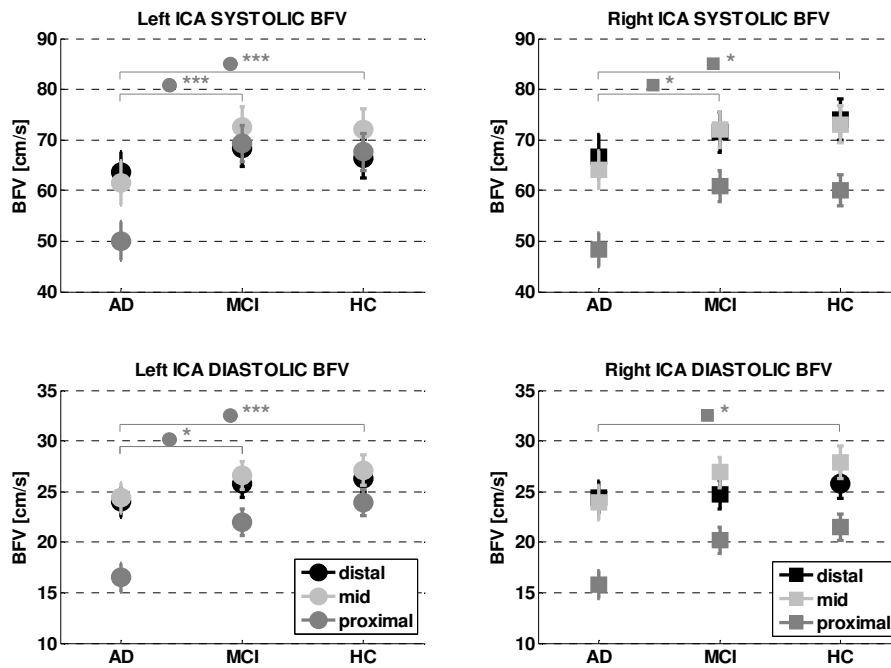


Figure 1. Age-corrected left and right side systolic and diastolic ICA BF Velocities (group mean and standard error of the mean) as measured on three sites (distal, mid and proximal) in AD, MCI and HC. Significance levels according to ANCOVA with Sidak correction: \*  $p < 0.05$ , \*\*  $p < 0.01$ , \*\*\*  $p < 0.005$

Discriminant analysis showed that based on left ICA proximal diastolic BFV an **82 %** correct classification of AD vs. HC was obtained (sensitivity 89%, specificity 75%), whereas this was 68% based on right. Similarly, based on left ICA proximal systolic BFV **82 %** was correctly classified as AD vs. MCI (sensitivity 83%, specificity 81%) whereas this was 74% for right.

#### Intracranial BFV (ACA, MCA and PCA)

##### **Anterior Cerebral Artery (ACA) BFV**

Right and left ACA BFVs were measured at a mean insonation depth of 70 mm (right  $N=44$ , range 60-86 mm, left  $N=42$ , range 58-79 mm). A significantly lowered systolic, mean and diastolic BFV was found for AD vs. HC only in the **right** ACA (figure 2). For MCI, only a trend was observed towards lower right mean and bilateral diastolic BFV compared to HC. Except for left diastolic BFV, mean MCI BFVs were intermediate between corresponding AD and HC values.

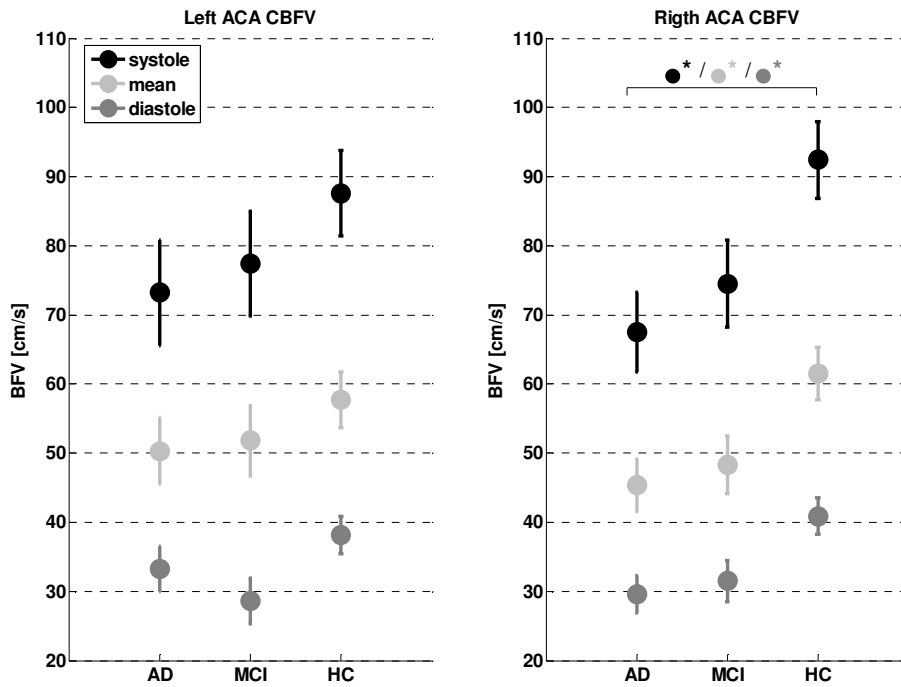


Figure 2. Right and left side ACA systolic, mean and diastolic CBFV group means and standard errors. Significant differences are found for the right side values between AD and HC ( \*  $p < 0.05$ ).

### Posterior Cerebral Artery (PCA) BFV

#### Insonation depth P1 (PCA-P1)

Right and left side PCA-P1 BFVs were measured at a mean depth of 67 mm (N=52, range 50-80 mm). Bilateral **systolic** PCA-P1 BFV were significantly lowered in AD vs. HC (figure 3a). In addition, left **mean** PCA-P1 BFV were significantly lowered for AD vs. HC and AD vs. MCI.

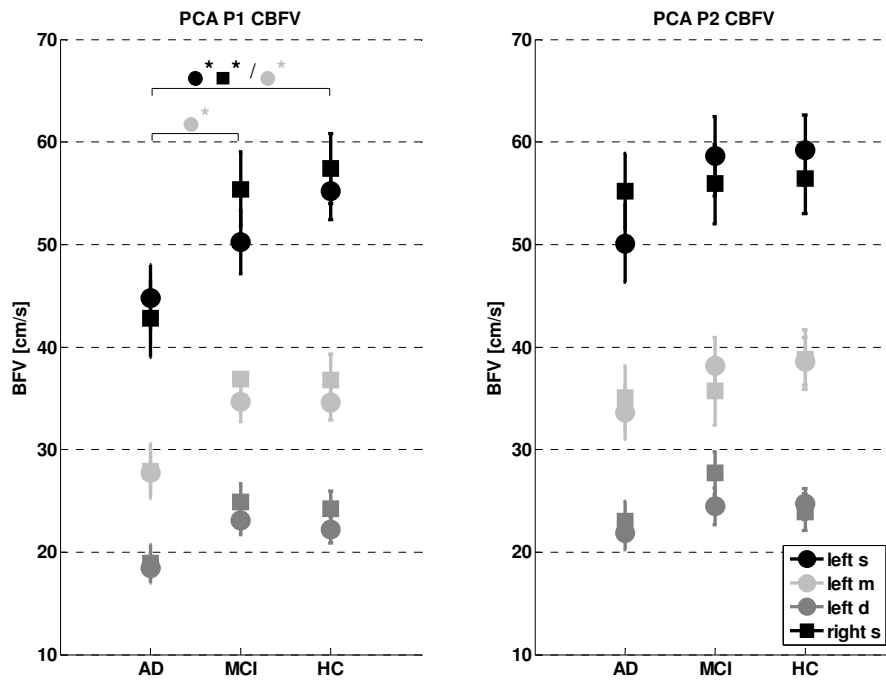


Figure 3. Right and left side group-averaged PCA-P1 (a) and PCA-P2 (b) systolic, mean and diastolic BFV for AD, MCI and HC (raw values, \* $p < 0.05$ )

#### Insonation depth P2 (PCA-P2)

PCA-P2 BFVs were not significantly different between the three groups (see figure 3b). Systolic, mean and diastolic PCA-P2 BFVs were also not significantly different from their corresponding PCA-P1 values for AD, MCI and HC.

#### **Middle Cerebral Artery (MCA) BFV**

Right and left side MCA BFVs were measured at insonation depths D1 and D2 with for all subjects  $D1 > D2$ . At the left side  $D2 - D1$  difference was  $-12 \pm 5$  mm (range: -34 to -4 mm) and the right side  $-11.3 \pm 5$  mm (range -22 to -2 mm).

#### Insonation depth D1(MCA-D1)

Since insonation depth was a significant confounder for right systolic, mean and diastolic MCA BFV, all MCA BFV (D1 and D2) values are corrected for insonation depth. Systolic, mean and diastolic MCA-D1 BFV were significantly lowered in AD vs. HC bilaterally for depth D1 (mean = 56 mm, std = 4 mm, range 45-65 mm). Also, a bilateral significantly lowered systolic MCA-D1 BFV was found for MCI vs. HC, whereas a trend was found for mean and diastolic values.

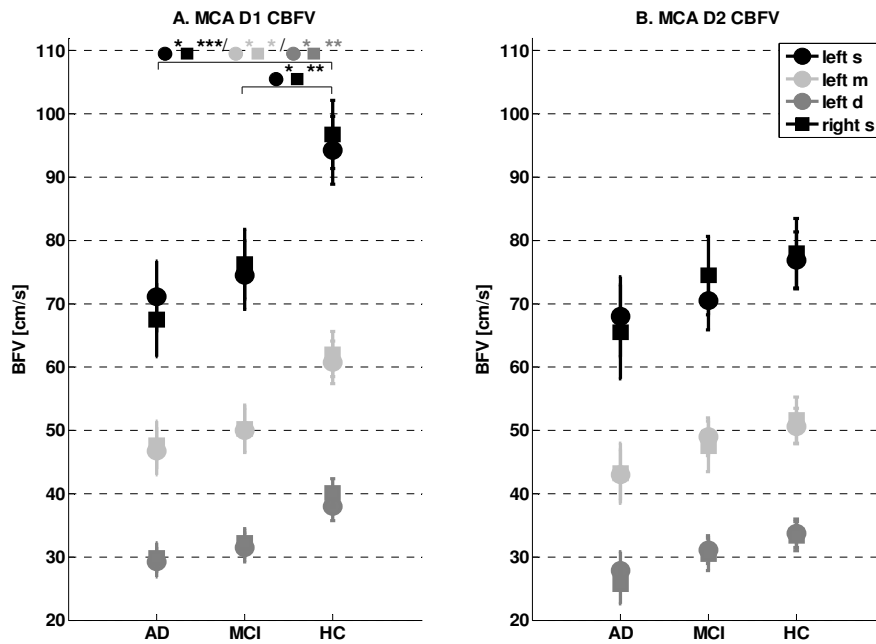


Figure 4. Right and left side group-averaged MCA-D1 (A) and MCA-D2 (B) systolic, mean and diastolic BFV (values corrected for confounder insonation depth, \*\*\* $p < 0.005$ , \*\* $p < 0.01$ , \* $p < 0.05$ )

#### Insonation depth 2 (MCA-D2)

After correction for the D2 (mean= 45 mm, std=6 mm, range 34-60 mm), no significant differences in MCA-D2 BFV were found between groups (figure.4b).

#### TCD "blind" MCA BFV (B-MCA)

Right and left side B-MCA BFVs were measured at an insonation depth of  $48 \pm 2.8$  mm (range 44-57 mm). Significantly lowered left side systolic, mean and diastolic B-MCA BFV were found for AD vs. HC (figure 5a), whereas for the right side a significantly lowered mean B-MCA BFV and trends for lower systolic and diastolic BFV were observed (figure 5b). Compared to MCI, AD BFV showed a trend for lowered left mean and diastolic values, whereas HC BFVs were similar.

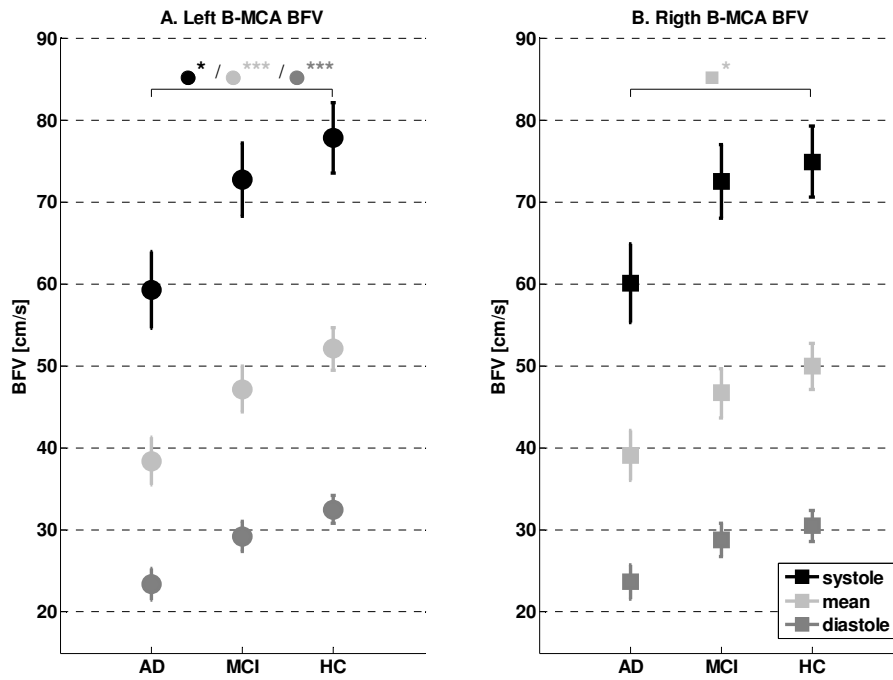


Fig.5. Right and left side group-averaged B-MCA systolic, mean and diastolic BFV for AD, MCI and HC

**Overview: BFV map**

Figure 6 gives an overview of the measurements locations (circles) throughout the extra- and intracranial circulation. Sites where significant group differences were found are indicated by the large black-filled circles. Group-averaged BFV values are shown in table 3 with systolic BFV values presented for the extracranial arteries and mean BFV values for the intracranial circulation. Notably, significant differences are bilaterally found at the proximal measurement site of the ICA, P1 segment of the PCA and depth D1 of the MCA (location denoted as M1). In addition, right ACA BFV (location denoted as A1) were significantly different between AD and HC, but not for AD vs. MCI. MCI and HC were differentiable on bilateral systolic BFV at the proximal MCA (denoted by additional encircling).

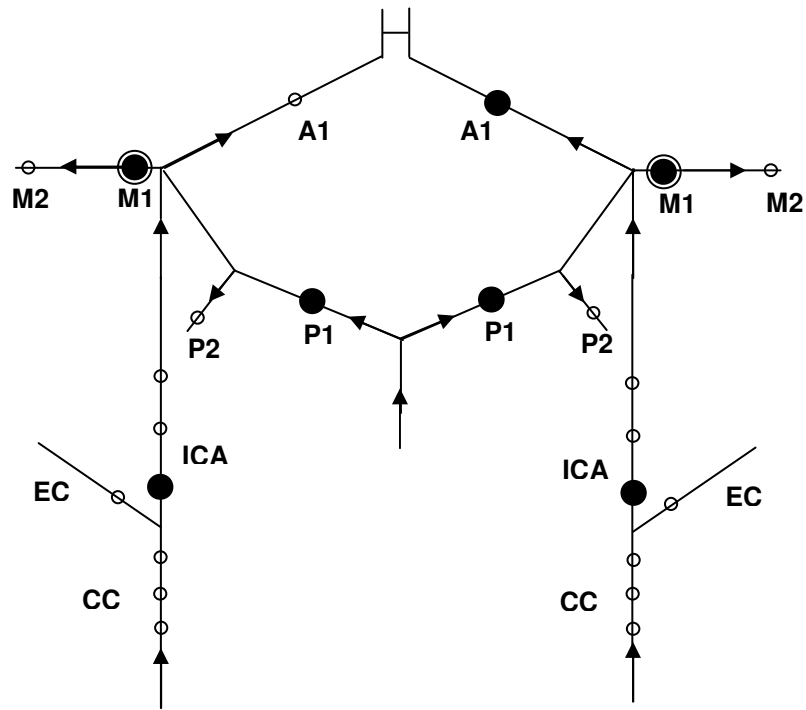


Figure 6. Overview of extra- and intracranial measurement sites. Sites where significantly different BFV values between AD vs. MCI and/or HC were found are indicated by the enlarged black filled circles. Encircling of M1 indicates that here also a significant BFV difference between MCI and HC is found.

Table 3. Overview of **extracranial systolic BFV** and **intracranial mean raw BFV** values and p-values.

<b>Location</b>	<b>AD</b>	<b>MCI</b>	<b>HC</b>	<b>p-value</b>
L CCA, prox	77	85	85	<0.394
R CCA, prox	70	76	68	<0.419
L CCA, mid	80	91	91	<0.135
R CCA, mid	76	84	90	<0.085
L CCA, dist	72	77	76	<0.408
R CCA, dist	66	76	75	<0.167
L ECA	71	82	79	<0.228
R ECA	70	90	84	<0.064
<b>L ICA, prox</b>	<b>49</b>	<b>70</b>	<b>68</b>	<b>AD-HC, AD-MCI &lt;0.005</b>
<b>R ICA, prox</b>	<b>48</b>	<b>61</b>	<b>60</b>	<b>AD-HC, AD-MCI &lt;0.05</b>
L ICA, mid	61	73	72	<0.109
R ICA, mid	66	72	74	<0.291
L ICA, dist	63	69	67	<0.629
R ICA, dist	66	69	66	<0.783
L ACA	50	52	58	<0.452
<b>R ACA</b>	<b>45</b>	<b>48</b>	<b>62</b>	<b>AD-HC &lt;0.05, AD-MCI&lt;0.07</b>
<b>L MCA, prox</b>	<b>47</b>	<b>49</b>	<b>62</b>	<b>AD-HC &lt;0.01, MCI-HC&lt;0.05</b>
<b>R MCA, prox</b>	<b>47</b>	<b>51</b>	<b>61</b>	<b>AD-HC &lt;0.05</b>
L MCA, dist	43	49	50	<0.372
R MCA, dist	43	48	52	<0.351
<b>L PCA P1</b>	<b>28</b>	<b>35</b>	<b>35</b>	<b>AD-HC, AD-MCI &lt;0.05</b>
<b>R PCA P1</b>	<b>28</b>	<b>37</b>	<b>37</b>	<b>AD-HC, AD-MCI &lt;0.06</b>
L PCA P2	34	38	37	<0.329
R PCA P2	35	36	39	<0.635



## 2.4 Discussion

### Extracranial Vessels

Significant age-corrected extracranial BFV differences were found between AD vs. HC or MCI bilaterally in the proximal ICA (except for right diastole). No significant differences were found between MCI and HC for proximal ICA or between groups for CCA, ECA and mid and distal ICA. Proximal ICA BF **velocity** of AD is a factor 0.75 of MCI or HC (left: 0.7/right: 0.8), which is similar but slightly higher than the factor 0.6 reported for **volume** flow [14]. This difference may be due to the slightly higher MMSE in our AD group (20 vs.18) or to the contribution of both velocity and diameter to volume flow. Our findings are consistent with those of Roher et al. [18], who also found significantly decreased ICA BFVs in AD vs. HC using TCD. Furthermore, sensitivity (83 vs. 82%) and specificity (81 vs. 93%) for AD vs. HC classification based on our proximal ICA BFV are close to reported values for MRI brain atrophy measures e.g. cortical thickness [3].

In contrast to proximal findings, mid and distal ICA BFV are similar for all groups. Assuming no bifurcations along the trajectory between the proximal to distal ICA measurement sites, the ICA diameter in AD may either be dilated at the proximal site or be narrowed at the mid and distal site. A pathology involving an enlarged vessel diameter is dolichoectasia [21]. Dolichoectasia is a dilatative arteriopathy consisting of an enlarged diameter combined with an increased arterial length causing ischemic stroke. However, this pathology is often seen in vertebrobasilar arteries and less frequently in the (internal) carotid arteries [21, 2]. A reduced distal vessel diameter, on the other hand, could be speculated to result from local vessel wall thickening. As a consequence of cerebral amyloid deposition, the cardiovascular system faces increased cerebrovascular resistance possibly leading to cardiovascular compensatory actions to accomplish a sufficient blood supply to the brain at the expense of locally increased pressure. Exposure to increased pressure may have evoked a long term adaptive response by thickening of the vessel wall. Another possibility we can not exclude is that geometric and tapering differences may be responsible for our findings. These speculations show that it is highly recommendable to measure ICA vessel diameters to provide conclusive evidence on this topic.

### Intracranial Vessels

#### **Right ACA**

Right ACA BFV were significantly decreased in AD compared to HC. Contrary to another study investigating ACA BFV [25], we found no significant difference between MCI and HC for left ACA and only a trend for right ACA BFV. This may be ascribed to differences between Sun and our study regarding the more precise ultrasound modality applied in our study (TCD vs. Duplex), insonation depth (60-70 vs. 58-86 mm) or to stricter inclusion criteria for vascular risk factors in our study. Right ACA BFV correlate significantly with outcomes of several neuropsychological tests, but this will be discussed in detail in another publication.

#### **PCA P1 and P2**

PCA P1 BFV are bilaterally significantly lowered in AD compared to MCI and HC, whereas PCA P2 BFV in AD are similar to MCI or HC. This finding could be interpreted as a reduced P1 flow in AD which recovers to 'normal' values in P2. However, this is

unlikely, since P1 and P2 flow should be approximately equal assuming insignificant flow to the posterior communicating artery. Therefore, two hypotheses may explain our P1 and P2 BFV findings in AD as compared to MCI or HC: either the diameter of the P1-segment must be enlarged or the diameter of the P2-segment reduced compared to the normal condition. An enlarged P1 diameter could also be speculated to result from intracranial dilatative arteriopathy (dolichoectasia) [17] just as we suggested to explain our ICA findings. Dolichoectasia pathophysiology is unknown, but debated to be either a cause or a consequence of atherosclerosis. However, described consequences of AD pathology for large intracranial arteries are structural alterations such as increased atherosclerotic plaques [5]. Plaque deposition resulting from Alzheimer disease is associated with reduced vessel diameters and increased vessel stiffness. A reduction of P2 diameter seems therefore the more obvious explanation for our findings. Still, knowledge of diameter values in AD is required to support either one of the hypotheses.

#### ***MCA D1 and D2***

Our mean BFV on MCA D1 (~56mm) are quite consistent with reported BFV for 20 AD (47 vs. 43 cm/s) and 12 HC (59 vs. 61cm/s) measured on a depth of 50-60mm using duplex ultrasonography [7]. Regarding MCI vs. HC, we found bilateral systolic BFV to differ significantly on D1. These findings are less pronounced than those of Sun et al. [25], who also found mean and diastolic TCD BFV to differ significantly between MCI and HC. As discussed for ACA, this may be due to MMSE, duplex vs. TCD use, insonation depth or inclusion criteria.

Similar to PCA findings, MCA D1 BFV is significantly decreased, whereas MCA D2 BFV seems preserved in AD. This pattern is also observed for MCI vs. HC for systolic values. Postulated BFV hypotheses for P1 vs. P2 may also be applicable to explain MCA D1 vs. D2 findings for the different groups. Thus, for the MCA the same theory may apply, i.e. distal vessel stiffness is increased in AD and to a lesser extent in MCI, possibly accompanied by a diameter reduction.

Our duplex findings are only partly consistent with TCD findings of Roher et al. [18]. They report a significantly lowered right proximal MCA BFV for AD vs. HC and only a trend for left side measurements, but they find pronounced BFV differences bilateral at the distal MCA site. Although this may be ascribed to the inferior accuracy of TCD in comparison to duplex, we can not exclude the possibility that distal BFV are reduced since in our findings we also observe a decreasing pattern in the order HC-MCI-AD although differences are not significant.

#### ***Duplex vs. TCD***

Also TCD BFV differed significantly between AD and HC for bilateral mean and left systolic and diastolic values. However, TCD BFV has been measured at an (group-averaged) insonation depth (48 mm), which lies intermediate between the depths adjusted to acquire proximal (56mm) and distal (45 mm) MCA BFV by duplex ultrasonography. Considering lowered proximal and similar distal duplex BFV in AD as compared to HC, the less pronounced group difference in TCD BFV can be speculated either to arise from earlier addressed site-specificity of AD pathology or from its methodological inferiority compared to duplex. Still, distal duplex BFV may be overestimated in AD due to increased vascular tortuosity which results in excessive angle correction. This suggests that TCD findings may reflect rather a pathological than a methodological effect. On the

other hand, default receiver gate times and burst lengths of TCD and Duplex systems are in the order of 5-7.5  $\mu$ s, which correspond to quite large sample volumes of  $\sim$ 0.75-1.2 cm. This implies that the TCD sample volume may have had overlap with distal as well as proximal duplex sample volumes, which compromises comparison of TCD vs. duplex BFV. Therefore, it is recommended for future studies to measure BFV at exactly the same insonation depth with TCD and duplex ultrasonography to evaluate TCD sensitivity.

#### **Recommendations for future research**

A major disadvantage of ultrasonography is that velocities rather than volume flows can be measured in the upper part of the internal carotid artery and the intracranial vessels. A possible approach to also assess intracranial volume flows could be started by adding volume flow measurement in the cervical arteries to our measurement protocol. However, to enable volume flow distribution assessment at remote bifurcations (i.e. ratio's for branches, i.e. ICA flow to MCA/ACA flows) diameter values should be available. Generic values for cerebral vessel diameters are available for the healthy population, but they already vary considerably. Therefore, assessment of generic diameter for the basal intracranial vessels by for example applying MR angiography in a large population of Alzheimer patients does not seem an option. An optimal approach for patient-specific volume flow assessment would be to combine ultrasonography for BFV measurement with MR angiography for diameter measurement. In most clinics, MR images are routinely made for all patients with memory complaints to check for hippocampus atrophy. Additional MR angiography is feasible although contrast-enhancement, i.e. a bolus injection, is required. The currently optimal accuracy depends on field of view (FOV) and coil. A FOV of 0.35 x 0.35 x 0.6 mm has been reported [4], implying that detection of flow differences of minimally  $\sim$ 3 ml/min are possible assuming a BFV of 50 cm/s and detectable diameter change of 0.35mm. In other words, the MCA diameter being about 3.1 mm needs to change for example by  $\sim$ 11% to become detectable. Since MR coil development evolves rapidly, resolution will improve fast. It is conceivable that acquisition of blood volume flow maps based on combined ultrasonographic BFV measurement and MR angiographic diameter detection will be sufficiently sensitive to differentiate MCI from AD and HC.

A follow-up study in our MCI group and monitoring of newly admitted patients with memory complaints may reveal whether location-specific BFV decline can predict conversion to AD. In addition, we strongly recommend prospective studies applying our measurement protocol in all MCI patients. An optimal setting would be to extensively examine all patients who present themselves at the memory clinic with memory complaints by use of duplex ultrasonography, TCD for comparison and MR angiography. Follow-up will reveal which MCI patients have converted to AD and which MCI patients are stable. Comparison of baseline BFV between converters and stable MCI patients can identify which BFV measurement sites may be predictive for AD development.

## **2.5 Conclusion**

This study provides evidence that BFV differences between AD, MCI and HC measured with duplex ultrasonography are location-specific even within a single vessel. AD BFV are mainly decreased at proximal sites, but preserved at distal sites. This is highly likely to result from AD pathology manifesting by diameter reductions at distal locations. MCI BFV measured in the intracranial anterior circulation are in general intermediate between AD and HC, whereas MCI BFV measured in the extracranial or intracranial posterior circulation are similar to HC. The considerable advantages of ultrasonography for clinical practice and the detectable location-specific BFV decline in AD and MCI make it worthwhile to implement it as a standard screening tool for MCI patients. Following all future MCI patients entering the memory clinic enables comparison of cerebral hemodynamics of MCI converters vs. non-converters.

## References

- [1] Association AP ed. (1994) Diagnostic and Statistical Manual of Mental Disorders, American Psychiatric Association, Washington, DC.
- [2] Caplan LR. Dilatative arteriopathy (dolichoectasia): what is known and not known. *Annals of Neurology* 2005; 57(4):469-71.
- [3] Cho Y, Seong JK, Jeong Y, Shin SY. Individual subject classification for Alzheimer's disease based on incremental learning using a spatial frequency representation of cortical thickness data. *Neuroimage* 2011, doi:10.1016/j.neuroimage.2011.09.085.
- [4] Choi JW, Roh HG, Moon WJ, Chun YI, Kang CH. Optimization of MR parameters of 3D TOF MRA for various intracranial stents at 3.0T MRI. *Neurointervention* 2011; 6:71-77.
- [5] de la Torre JC, Vascular basis of Alzheimer's pathogenesis. *Ann N Y Acad Sci* 200; 977:196-215.
- [6] de la Torre JD, Vascular risk factor detection and control may prevent Alzheimer's disease. *Ageing Res Rev* 2010; 218-25.
- [7] Doepp F, Valdeuza JM, Schreiber SJ. Transcranial and extracranial ultrasound assessment of cerebral hemodynamics in vascular and Alzheimer's disease. *Neurol Res* 2006; 8:645-649.
- [8] Fazekas F, Chawluk JB, Alavi A, Hurtig HI, Zimmerman RA. MR signal abnormalities at 1.5T in Alzheimer's dementia and normal aging. *AJR Am J Röntgenol* 1987; 149: 351-356
- [9] Heister D, Brewer JB, Magda S, Blennow K, McEvoy LK. Predicting MCI outcome with clinically available MRI and CSF biomarkers. *Neurology* 2011; 77: 1619-28.
- [10] Iadecola C. Neurovascular regulation in the normal brain and in Alzheimer's disease. *Nat Rev Neurosci* 2004; 5:347-60.
- [11] Jolles J, Houx PJ, Boxtel van MPJ, Ponds RWHM. The Maastricht Aging Study: determinants of cognitive aging. *Neuropsych Publishers*. Maastricht 1995.
- [12] Maalikjy Akkawi N, Agosti C, Anzola GP, Borroni B, Magoni M, Pezzini A, Rozzini L, Vignolo LA, Padovani A. Transient global amnesia: a clinical and sonographic study. *Euro Neurol* 2003; 49:67-71.
- [13] Maalikjy Akkawi N, Borroni B, Agosti C, Magoni M, Broli M, Pezzini A, Padvani A. Volume cerebral blood flow reduction in pre-clinical stage of Alzheimer's disease: evidence from an ultrasonographic study. *J Neurol* 2005; 252: 559-63.
- [14] Maalikjy Akkawi N, Borroni B, Agosti C, Pezzini A, Magoni M, Rozzini L, Promettie P, Romanelli G, Vignolo LA, Padovani A. Volume reduction in cerebral blood flow in patients with Alzheimer's disease: a sonographic study. *Dement Geriatr Cogn Disord* 2003; 16: 163-9.
- [15] McKhann G, Drachman D, Folstein M, Katzman R, Price D, Stadlan EM. Clinical diagnosis of Alzheimer's disease: report of the NINCDS-ARDRA Work Group under the auspices of Department of Health and Human Services Task Force on Alzheimer's Disease. *Neurology* 1984; 34: 939-44.
- [16] Petersen RC, Smith GE, Waring SC, Ivnik FJ, Tangalos EG, Kokmen E. Mild cognitive impairment: clinical characterization and outcome. *Arch Neurol* 1999; 56:303-8.
- [17] Pico F, Labreuche J, Seilhean D, Duyckaerts C, Hauw J, Amarenco P. Association of small vessel disease with dilatative arteriopathy of the brain. *Stroke* 2007; 38: 1197-1202.
- [18] Roher AE, Garami Z, Tyas SL, Maarouf CL, Kokjohn TA, Belohlavek M, Vedders LJ, Conner D, Sabbagh NM, Beach TG, Emmerling MR. Transcranial Doppler ultrasound blood flow velocity and pulsatility index as systemic indicators for Alzheimer's disease. *Alzheimer's Disease & Dementia* 2011; 7:445-55.
- [19] Roman GC, Tatemichi TK, Erkinjuntti T, Cummings JL, Masdeu JC, Garcia JH, Amaducci L, Orgogozo JM, Brun A, Hofman A et al. Vascular dementia: diagnostic criteria for re-

- search studies. Report of the NINDS-AIREN International Workshop. *Neurology* 1993; 43: 250-60.
- [20] Roman GC. Alzheimer's disease research: have we forgotten the cerebrovascular circulation? *Alzheimer disease and associated disorders* 2008; 22:1-3.
- [21] Sadahiro H, Ishihara H, Goto H, Oka H, Shirao S, Yoneda H, Suzuki M. Repeated cerebral ischemia caused by extracranial carotid artery dolichoectasia. *J Neuroimaging* 2011; XX:1-5.
- [22] Scheltens P, Leys D, Barkhof F, Huglo D, Weinstein HC, Vermersch P, Kuiper M, Steinling M, Wolters EC, Valk J. Atrophy of medial temporal lobes on MRI in 'probable' Alzheimer's disease and normal ageing: diagnostic value and neuropsychological correlates. *J Neurol Neurosurg Psychiatry* 199; 55:967-72.
- [23] Sitzer M, Puac D, Buehler A, Steckel DA, Von Kegler S, Markus HS, Steinmetz H. Internal carotid artery angle of origin: a novel risk factor for early carotid atherosclerosis. *Stroke* 2003; 34: 950-55.
- [24] Stefani A, Sancesario G, Pierantozzi M, Leone G, Galati S, Hainsworth AH, Diomedei M. CSF biomarkers, impairment of cerebral hemodynamics and degree of cognitive decline in Alzheimer's and mixed dementia. *J Neurol sci* 2009; 83:109-15.
- [25] Sun ZW, Zhu YX, Liu HY, Liu J, Zhu XQ, Zhou JN, Liu RY. Decreased cerebral blood flow velocity in apolipoprotein E epsilon4 allele carriers with mild cognitive impairment. *Eur J Neurol* 007; 14:150-55.
- [26] Verhey F, Jolles J, Ponds R et al (1993). Diagnosing dementia: a comparison between a monodisciplinary and multidisciplinary approach. *J Neuropsychiatry Clin Neuroscience*, 5, 78-85.



# CHAPTER 3

## Dynamic Cerebral Autoregulation in patients with Alzheimer's disease and Mild cognitive impairment

Based on:

Gommer ED, Martens EGHJ, Aalten P, Shijaku E, Verhey F, Mess WH, Ramakers IHGB, Reulen JPH. *Dynamic cerebral autoregulation in subjects with Alzheimer's disease, mild cognitive impairment and controls: evidence for increased peripheral vascular resistance*. *Journal of Alzheimer's Disease* (2012) Vol 30 (4), in press



## Abstract

Cerebrovascular dysfunction plays a role not only in vascular causes of cognitive impairment but also in Alzheimer's disease (AD). We hypothesized that cerebral autoregulation is impaired in patients with AD compared to patients with mild cognitive impairment (MCI) and control subjects. Dynamic cerebral autoregulation (dCA) was investigated in 17 AD patients, in 19 patients MCI subjects and in 20 controls (C). The 3 groups were matched for age, sex and level of education.

The electrocardiogram and non-invasive finger arterial blood pressure were measured and transcranial doppler ultrasonography was used to measure cerebral blood flow velocity in right and left middle cerebral artery (MCA). Also cerebrovascular resistance index CVRi was computed. dCA in supine position was quantified based on spontaneous blood pressure variations by computation of the linear transfer function between arterial blood pressure as input and MCA cerebral blood flow velocity as output resulting in transfer function gain and phase. dCA gain and phase were evaluated for different frequency bands of autoregulation. Results were also evaluated using a 3-parameter windkessel model (WKM).

CVRi was significantly higher in AD ( $2.9 \pm 0.2$ ) compared to both MCI ( $2.3 \pm 0.1$ ,  $p=0.02$ ) and C ( $2.1 \pm 0.1$  mmHg/cm,  $p=0.002$ ). Five MCI patients who converted to AD during the course of the study also had higher CVRi compared to non-converters ( $2.8 \pm 0.6$  vs. mean  $2.1 \pm 0.5$  mmHg/cm,  $p<0.05$ ). For all groups no significant differences in dCA gain and phase were found. In terms of the WKM approach, in the order C→MCI→AD groups showed about equal arterial resistance and peripheral compliance, but increased peripheral vasculature resistance ( $26 \pm 2$  vs.  $36 \pm 3$  mmHg/ml in C resp. AD,  $p=0.004$ ).

In conclusion, AD patients compared to MCI patients and controls have increased CVRi, whereas dCA parameters do not seem to differentiate AD patients. For MCI patients CVRi might have predictive value in developing AD.

### 3.1 Introduction

Dementia is one of the principal neurological disorders in elderly. Recent studies [1-3] have indicated that vascular risk factors are involved in the pathogenesis of cognitive disorders and dementia. For adequate function, the brain is critically dependent on continuous blood supply. Therefore, the cerebral vasculature is endowed with neurovascular control mechanisms that assure that the blood supply of the brain is commensurate to the energy needs of its cellular constituents. The regulation of cerebral blood flow (CBF) during brain activity involves the coordinated interaction of neurons, glia, and vascular cells. Alterations of the vascular regulatory mechanisms may lead to brain dysfunction and disease. A more and more emerging view is that cerebrovascular dysregulation is a feature not only of cerebrovascular pathologies, such as stroke, but also of neurodegenerative conditions, such as Alzheimer's disease (AD) [1]. First epidemiological studies have shown that risk factors for vascular diseases are important risk factors for AD [4]. Small ischemic lesions substantially aggravate the dementia [5]. Interaction of cerebral ischemia with AD pathology enhances the clinical manifestations of the disease. Moreover, AD patients have more severe atherosclerosis in large cerebral arteries at the base of the brain (circle of Willis) than age-matched controls without AD [6].

AD is the most common form of dementia and is often characterized by deposition of amyloid  $\beta$ -peptide in the blood vessels (amyloid angiopathy). Cerebral micro vessels are reduced in number and cerebrovascular function is also altered in AD. Resting CBF is reduced and the increase in CBF produced by activation (neurovascular coupling) is attenuated [7]. The cerebrovascular dysfunction often precedes the onset of cognitive impairment suggesting a role in the mechanisms of dementia [1]. Iadecola et al. [1] pose a hypothetical time-course of the interplay between vascular dysregulation, neuropathological alterations and decline in brain function in AD. In the latent phase vascular dysregulation is already apparent when patients are asymptomatic. During the prodromal phase neuropathological alterations begin to manifest and cognitive function begins to decline. At this time, cognitive alterations are likely to result from amyloid  $\beta$ -peptide ( $A\beta$ ) induced neuronal dysfunction and vascular dysregulation. As the disease progresses, the neuropathological changes evolve. Cerebrovascular disease deteriorates in parallel with cognitive function, reflecting in addition to  $A\beta$  induced vascular effects, the deleterious cerebrovascular effects of synaptic loss and vascular amyloid. In the late phase of the disease, brain function and vascular regulation are maximally compromised.

Cerebral autoregulation (CA) is one of the fundamental properties of the cerebral circulation through which CBF is maintained relatively constant despite variations in mean arterial pressure (MAP) within a certain range. To maintain flow in the autoregulated range of MAP, cerebral resistance vessels undergo vasoconstriction during hypertension and vasodilatation during hypotension. Therefore, failure of vasoconstriction and/or vasodilatation may result in CA disruption rendering the brain more susceptible to fluctuations in MAP.

Recently, results were published from a study describing specific abnormalities in AD in particular increased vessel flow resistance [8]. Cerebral blood flow was severely compromised during dynamic squat-stand procedures, and this was interpreted as reduced capability to counteract blood pressure changes in patients with early AD. To our knowledge, dynamic cerebral autoregulation (dCA) has not been studied in patients with mild cognitive impairment (MCI) and compared to AD and controls (C). MCI describes the transitional phase between normal aging and dementia. Patients with MCI are at increased risk for developing AD. Maybe impaired cerebral autoregulation can be a marker of developing AD in patients with MCI. Because vascular dysfunction might be a precursor of developing dementia it seems worthwhile to investigate parameters of vascular function in these groups.

A common approach to quantify the dynamics of cerebral autoregulation [9-11] is transfer function analysis (TFA) of the presumed linear control system with arterial blood pressure (ABP) as the input and cerebral blood flow velocity (CBFV) as the output signal. Data analysis methods such as TFA are descriptive techniques quantifying the relation between ABP and CBFV without any assumption of the underlying physiology. To gain more insight in the results of this analysis with respect to physiological parameters a windkessel model (WKM) proposed by Zhang et al.[12] can be fitted. In this way three parameters representing arterial vessel resistance ( $R_a$ ), peripheral vessel resistance ( $R_p$ ) and vessel compliance ( $C_p$ ) can be estimated.

The objective of this study was to investigate TFA quantified cerebral autoregulation using spontaneous blood pressure variations in subjects with AD type dementia, MCI/prodromal AD and healthy controls. We hypothesized that dCA is impaired in AD patients compared to healthy controls. Additionally, we hypothesized that in MCI, as a possible prodromal phase of AD, cerebral autoregulation shows reduced capacity. The model approach possibly can be used to identify specific physiological changes.

### **3.2 Patients & Methods**

In this study 17 AD patients, 19 MCI patients and 20 matched healthy controls subjects (C) were investigated. The groups were matched for age, sex and level of education. Patients with AD and MCI were selected from the Memory Clinic of the Maastricht University Medical Centre (MUMC). Control subjects were recruited from an existing cohort of elderly and through colleagues and personal acquaintances. The Institutional Review Board of the MUMC approved the study and all subjects gave written informed consent.

AD patients were diagnosed according to the DSM-IV criteria for dementia [13], and NINCDS-ADRDA criteria [14]. Nineteen MCI patients were included. Sixteen of these subjects (84%) fulfilled the MCI criteria of Petersen et al.[15], defined as a subjective cognitive complaint, objectified by an impaired cognitive performance; no significant impairments in daily living and no dementia. According to this definition, 11 subjects (69%) had amnesic MCI, operationalized as a score below -1.5 standard deviation on the memory domain), and 5 subjects (31%) had non-amnesic MCI, defined as a score below -1.5 standard deviation on the non-memory domain (more details are described

below). Three subjects were clinically representative for the MCI syndrome, but did not reach the threshold of -1.5 SD on the cognitive tests. Exclusion criteria were any somatic, psychiatric or neurological disorder that may have caused the cognitive impairment. In addition, patients were excluded if diagnosed with Vascular Dementia, according to NINDS/AIREN criteria [16]. Also patients with diabetes and/or cardiovascular disease were excluded. Subjects with a stenosis of the common or internal carotid artery or the middle cerebral artery (MCA) of more than 50%, as detected by extracranial and/or transcranial colour-coded duplex, were excluded as were subjects without a temporal bone window.

The electrocardiogram (ECG) and non-invasive ABP were measured using a Task Force Monitor (CN Systems, Austria). A transcranial Doppler system (Multidop X4, DWL, Sipplingen, Germany) was used to measure CBFV in the main stem of both the right and left MCA. Two 2 MHz probes were held in position by a special frame. Patients were in supine position with their eyes open during all 15-minute recordings and were breathing spontaneously. Based on analysis of available MRI images of AD (n=17) and MCI (n=15) patients scores were obtained for medial temporal lobe atrophy (MTA)[17], general cortical atrophy (GCA), age-related white matter changes (ARWMC) and Fazekas score [18]. All subjects underwent a neuropsychological assessment. The measured cognitive domains included general cognitive functioning (Mini Mental State Examination, MMSE) [19], memory (immediate and delayed recall of the Auditory Verbal Learning Test [20] or the story of the Rivermead Behavioral Memory Test [21], speed of information processing (Trail Making Test, part A [22]; Stroop, card I and II [23]; and Symbol Digit Modality Test [24]), executive functioning (Trail Making Test, part B; Stroop, card III), and verbal fluency (fluency animals, 60 seconds) [25].

#### **Data analysis**

Raw data from the Task Force Monitor were exported to an in-house made acquisition and analysis software package (AFOnew version 2.48, IDEE Maastricht®, the Netherlands). An automatic algorithm detected the ECG R-waves and determined the subsequent diastolic, mean and systolic blood pressure and corresponding end diastolic, mean and peak systolic CBFV. Artefacts were removed manually by linear interpolation. The beat-to-beat values of ABP and CBFV were exported to Matlab and resampled at 5 Hz using spline interpolation [10]. ABP and CBFV were normalized with respect to the mean. This resulted in zero-mean signals suited for spectral analysis to estimate the transfer function. Estimation of the transfer function was performed as previously described [26]. Phase and gain were evaluated for different frequency bands of autoregulation namely Total (0.04-0.11 Hz), very low frequency VLF (0.04-0.06 Hz), 01 (0.1 Hz), low frequency LF (0.06-0.11 Hz). In order to compare the results (addition JC in abbreviations) reported by Claassen et al.[8] with ours, we also computed the different CA parameters for the frequency bands VLFJC (0.02-0.07 Hz), LFJC (0.07-0.2 Hz) and HFJC (0.2-0.35 Hz). To be strict in acceptance of data, the coherence threshold applied is three times the previously described theoretically derived value [27]. With 15 minute recordings this means only recordings with a coherence of at least 0.18 were included. Recordings were excluded from further analysis, if nowhere in the frequency range below 0.25 Hz a coherence of 0.18 was reached. From fitting the first 5 seconds of the

step response function the autoregulation index (ARI) was determined in the same way as described previously [27].

#### Model description of dCA data

The layout of the WKM is shown in figure 1. It consists of two resistors and one capacitor. Resistor  $R_a$  represents flow resistance for arterioles distal to the MCA.  $R_p$  represents more peripheral resistance in the microcirculation.  $C_p$  represents compliance of the microcirculation. The transfer function from pressure ABP to flow CBF can be described in the Laplace domain with equation 1:

$$H = \frac{CBF}{ABP} = \frac{C_p R_p s + 1}{C_p R_p R_a s + R_p + R_a} \quad (1)$$

where  $H$  is the transfer function between arterial blood pressure ( $ABP$ ) and cerebral blood flow ( $CBF$ ).  $C_p$  is peripheral compliance,  $R_p$  is peripheral resistance,  $R_a$  is arterial resistance and  $s$  is the Laplace transform variable. Although the model parameters  $C_p$ ,  $R_p$  and  $R_a$  are time-invariant system parameters, the transfer function of the model in equation 1 describes behaviour in response to blood pressure changes that can be related to the estimated transfer function of dCA calculated through cross spectral analysis.

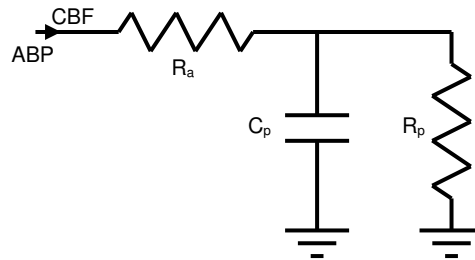


Figure 1 Windkessel model consisting of arterial resistance  $R_a$ , peripheral resistance  $R_p$  and peripheral compliance  $C_p$  with pressure  $ABP$  representing arterial blood pressure and  $CBF$  cerebral blood flow.

To fit the WKM and convert the measured flow velocity into a flow for the model ( $CBFV \rightarrow CBF$ )  $CBFV$  has to be multiplied by a cross sectional area  $A$ . Therefore, an internal MCA diameter of 3 mm was assumed [28], resulting in  $A$  of  $\pi (1.5)^2 = 0.0707 \text{ cm}^2$ . This assumption obviously introduces noise in the results since not everyone will have a MCA caliber of 3 mm. To estimate WKM parameters  $R_a$ ,  $R_p$  and  $C_p$ , an error function is minimized iteratively using the “fsolve” function in Matlab with a Levenberg-Marquardt algorithm.

$$\begin{aligned}
\varepsilon_k &= |H_{TFA}(f_i)| - |H_{WKM}(f_i)|, \quad k=1..9, \quad i=3..11 \\
\varepsilon_k &= \text{angle}\{H_{TFA}(f_i)\} - \text{angle}\{H_{WKM}(f_i)\}, \quad k=10..18, \quad i=3..11 \\
\varepsilon_k &= A \cdot (R_a + R_p) - CVR_i, \quad k=19
\end{aligned} \tag{2}$$

The error function consists of the set of expressions in equation 2 that represent the differences of: 1) TFA and WKM gain in the frequency band from 0.06-0.2 Hz 2) TFA and WKM phase in the frequency band from 0.06-0.2 Hz and 3) CVRi and (Ra+Rp)\*A. Consequently, for both gain and phase eight data points (in the frequency range 0.06-0.20 Hz) from the calculated transfer function are compared with corresponding frequency WKM values. For CVRi it consists of a single value difference. The fit error was calculated as the sum of squares of the error function components expressed in equation 3.

$$\varepsilon_{fit} = \sum_{k=1}^{19} \varepsilon_k^2 \tag{3}$$

### Statistical analysis

Statistical analyses were performed using the Statistical Package for Social Sciences (SPSS) version 16.0 for Windows. Between group data were statistically compared using multifactor ANOVA (Sidak correction). Confounders were only included if significant correlation existed with the parameter studied. In this case multifactor ANOVA was repeated with correction for the confounders. If during the course of the study MCI patients convert into Alzheimer's disease according to the diagnosis criteria, the results for these converters will be analysed separately.

### 3.3 Results

In two AD cases coherence was below the threshold of 0.18 at all frequencies up to 0.25 Hz and these patients were excluded from the results, thus leaving 15 AD patients. General subject characteristics are shown in table 1. Age and sex matching between the groups was adequate since there were no significant differences. The MMSE was significantly lower in AD compared to both MCI and C. Blood pressure values (systolic sBP, diastolic dBP and mean mBP) did not differ between the groups. Mean cerebral blood flow velocity (mCBFV) data from right and left MCA were pooled as there were no significant right-left differences. In AD mCBFV was significantly lower compared to C and tended to be lower compared to MCI (p=0.068). CVRi was significantly higher in AD compared to both MCI and C.

Table 1 General characteristics of subjects with AD, MCI and controls. MMSE =mini mental state evaluation, MTA = medial temporal lobe atrophy, sBP, dBP, mBP = systolic, diastolic, mean blood pressure, mCBFV = mean cerebral blood flow velocity, CVRi = cerebrovascular resistivity index

	AD (n=15)	MCI (n=19)	C (n=20)	
Male/female	8/7	11/8	10/10	NS
Age [year]	72 (2) [58-87]	70 (2) [58-80]	70 (1) [59-78]	NS
Level of Education [%]				
Lower	53	37	45	NS
Middle	33	16	35	NS
Higher	13	47	20	NS
MMSE	19.8 (1.2) [12-27]	27.6 (0.3) [24-30]	29.0 (0.3) [26-30]	AD-MCI p<0.001 AD-C p<0.001
MTA > 2 [%]	80	33	no data	p=0.011*
End-tidal CO <sub>2</sub> [%]	6.0 (0.4)	6.3 (0.2)	5.3 (0.1)	MCI-C p=0.006
sBP [mmHg]	134 (4) [116-156]	133 (2) [116-150]	133 (3) [107-158]	NS
dBP [mmHg]	89 (2) [78-101]	86 (2) [70-105]	88 (2) [61-104]	NS
mBP [mmHg]	104 (2) [90-119]	101 (2) [88-117]	103 (3) [76-119]	NS
mCBFV [cm/s]	37.3 (2.3) [26-54]	46.6 (2.8) [27-77]	51.0 (2.8) [32-82]	AD-C p=0.003
CVRi [mmHgs/cm]	2.9 (0.2)	2.3 (0.1)	2.1 (0.1)	AD-C p=0.002 AD-MCI p=0.02

All data are presented as mean (SEM) [min max].

n=number of subjects, p-values of multifactor Anova with Sidak correction

\* p-value of Mann-Whitney test

#### dCA linear transfer function results

Table 2 shows a summary of dCA parameters. Figure 2 shows the group averaged gain and figure 3 the group averaged phase plots. None of the dCA parameters showed significant differences between the groups. Also all other parameters including the dCA parameters in the specific frequency bands used by Claassen et al [8], did not reveal significant group differences.

Table 2 dCA parameters of AD, MCI and controls. ARI = autoregulatory index

	AD (n=15)	MCI (n=19)	C (n=20)
CoherenceVLF	0.25 (0.03)	0.27 (0.03)	0.28 (0.03)
CoherenceLF	0.47 (0.07)	0.53 (0.04)	0.53 (0.03)
CoherenceTotal	0.38 (0.05)	0.42 (0.03)	0.43 (0.03)
GainVLF [%/%]	0.85 (0.07)	0.96 (0.08)	1.03 (0.10)
GainLF [%/%]	1.32 (0.12)	1.51 (0.09)	1.58 (0.11)
GainTotal [%/%]	1.13 (0.08)	1.29 (0.08)	1.36 (0.09)
PhaseVLF [rad]	0.85 (0.13)	0.66 (0.06)	0.78 (0.11)
PhaseLF [rad]	1.00 (0.09)	0.94 (0.06)	0.84 (0.05)
PhaseTotal [rad]	0.94 (0.09)	0.83 (0.05)	0.81 (0.06)
ARI	6.1 (0.2)	5.8 (0.2)	5.5 (0.2)

All data are presented as mean (SEM). n=number of subjects.

No significant differences with multifactor Anova with Sidak correction

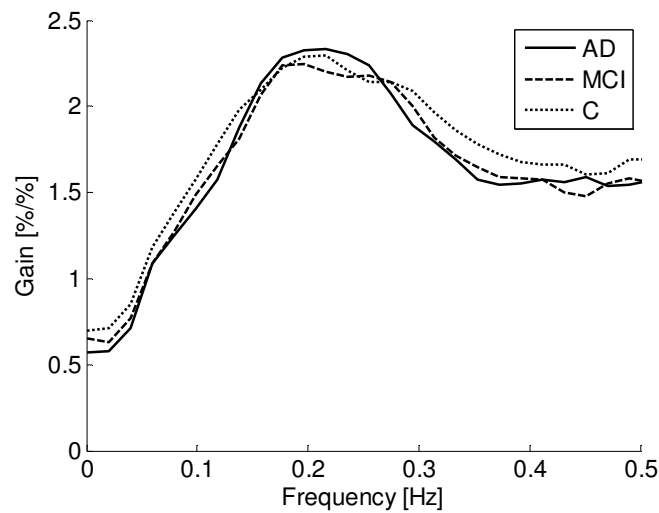


Figure 2 Group average gain spectrum for AD (solid), MCI (dashed) and C (dotted).



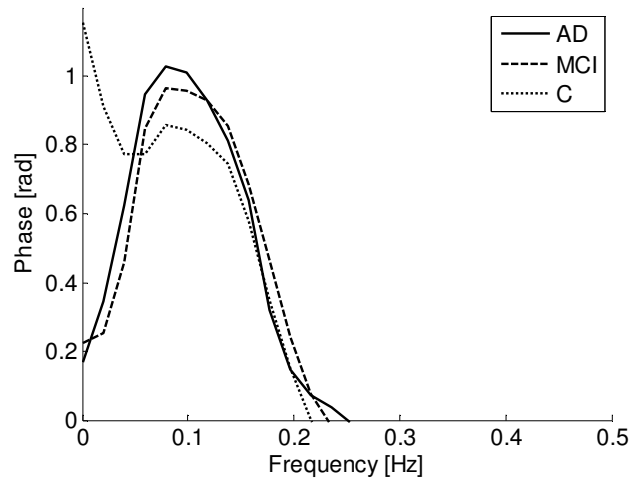


Figure 3 Group average phase spectrum for AD (solid), MCI (dashed) and C (dotted).

### Model description

Estimation of the WKM parameters was successful in all recordings. Table 3 summarizes the three model parameters for the three groups. Peripheral resistance  $R_p$  was significantly increased in AD compared to C. MCI was in between AD and C without significant differences to either of them. Entering the WKM parameters from table 3 in equation 1, gain and phase can be calculated respectively as the modulus and argument of the transfer function  $H$ . Plots of gain and phase versus frequency are shown in figure 4 and 5 showing no significant difference between groups.

Table 3 Windkessel model parameters of subjects with AD, MCI and controls

	AD (n=15)	MCI (n=19)	C (n=20)	
Ra [mmHg/ml]	5.6 (0.7) [2-10]	4.9 (0.4) [2-9]	5.2 (0.5) [0-11]	NS
Rp [mmHg/ml]	36 (3) [21-59]	29 (2) [16-52]	26 (2) [14-48]	AD-C p=0.004
Cp [ml/mmHg]	0.24 (0.02) [.12-.44]	0.25 (0.02) [.13-.47]	0.29 (0.04) [.13-.98]	NS
Fit error $\epsilon_{fit}$	2.1 (0.5) [0.4-7]	1.3 (0.3) [0.04-5]	1.7 (0.5) [.3-10]	NS

All data are presented as mean (SEM) [min max]. n=number of subjects.

P-values of multifactor Anova with Sidak correction

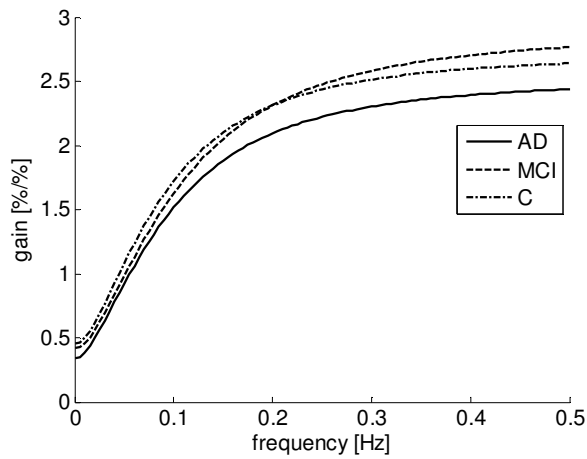


Figure 4 Gain plots for WKM group averaged parameters for AD (solid), MCI (dashed) and C (dotted).

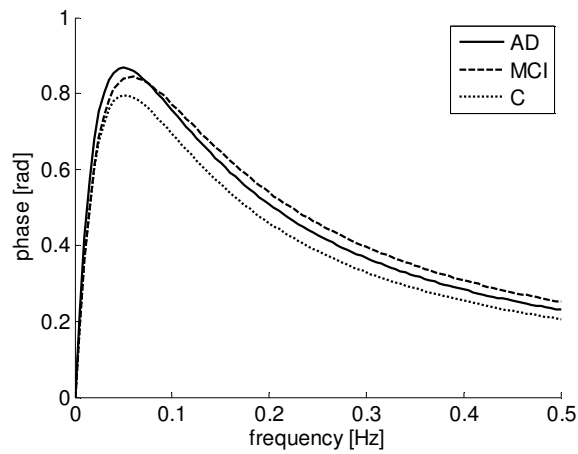


Figure 5 Phase plot for WKM group averaged parameters for AD (solid), MCI (dashed) and C (dotted)

### Correlations

Significant correlations between autoregulation parameters and subject characteristics are shown in table 4. To see if covariates exist for autoregulation parameters and to investigate dependencies between parameters bivariate correlations were calculated between general subject characteristics and autoregulation parameters. For continuous parameters (e.g. blood pressures) Pearson's correlation coefficient was calculated and for MRI parameters with only a few levels Spearman's correlation coefficient was calculated. In 4 MCI cases no MRI data was present. Comparing groups incorporating significant covariates did not show additional significant differences between groups nor did it abolish pre-existing significant differences.

Table 4 Significant Pearson (for sBP, dBP and mBP = systolic, diastolic and mean blood pressure) and Spearman (for GCA = general cortical atrophy, MTA = medial temporal lobe atrophy and MTA right) correlation coefficients between autoregulation parameters and general subject characteristics

	sBP	dBP	mBP	GCA	MTA	MTA right
	n=54	n=54	n=54	n=30	n=30	n=30
GainLF [%/%]						
GainTotal [%/%]						
PhaseVLF [rad]	0.28 *					
PhaseLF [rad]	0.37 **	0.31 *	0.35 **			
PhaseTotal [rad]	0.41 **	0.29 *	0.36 **			
ARI	0.29 *		0.28 *			
CVRi [mmHgs/cm]	0.28 *	0.36 **		0.38 *	0.43 *	0.49 **
Ra [mmHgs/ml]				0.41 *	0.46 *	0.49 **
Rp [mmHgs/ml]	0.30 *	0.37 **	0.36 **			
Cp [ml/mmHg]						0.38 *

\* p<0.05, \*\* p <0.001

#### Conversion of MCI into AD

Since the beginning of the study five of the MCI patients have converted into AD. Post hoc we analysed if certain parameters could predict this conversion. We tested all parameters using a Mann-Whitney test for the converted (n=5) and non-converted (n=14) MCI patients. Only mCBFV ( $35 \pm 5$  vs.  $51 \pm 11$  cm/s,  $p < 0.01$ ) and CVRi were significantly different ( $2.8 \pm 0.6$  vs. mean  $2.1 \pm 0.5$  mmHgs/cm,  $p < 0.05$ ) for converted versus non-converted MCI patients.

### 3.4 Discussion and conclusions

In this study we found reduced mCBFV and correspondingly elevated CVRi in AD patients compared to matched controls. Also compared to MCI CVRi is significantly elevated in AD. It has been argued that reduction in CBF in AD could be explained by loss of brain tissue due to the neurodegenerative processes, or by a reduction in brain metabolic demand that parallels cognitive decline [29]. We found increased medial temporal lobe atrophy in AD compared to MCI, which could support the relation between loss of brain tissue and reduced cerebral blood flow. Also, recent fMRI data in MCI and AD are beginning to reveal relationships between abnormalities of functional activity in the medial temporal lobe memory system and in functionally connected brain regions [30]. Since inclusion of AD and MCI subjects in our study was from an existing cohort of the Memory Clinic in our hospital, MRI data was sometimes acquired at an earlier stage compared to the autoregulation tests. Only in nine subjects auto-

regulation tests were performed within one year from the MRI acquisition date. While disease progresses this could have blurred the correlation between atrophy and auto-regulation data.

From the group of MCI patients, during the course of this study, five converted to AD. The results for this subgroup compared to the non-converted MCI patients showed mCBFV to be significantly lower and CVRi to be significantly higher. Although the number of converters is small this strongly suggests the value of these parameters in the diagnosis of AD. It could therefore be worthwhile to evaluate the value of screening elderly and specifically MCI patients for these parameters.

No significant differences were found between the groups for dCA. This is in correspondence with findings of Claassen et al.[8] for spontaneous fluctuations of blood pressure. However, they did show differences in gain during squat-stand maneuvers. They also showed increased spectral power in blood pressure and CBFV during these maneuvers. It could therefore be necessary to induce stronger challenges to the control of cerebral blood flow for changes in cerebral autoregulation to become apparent. By inducing stronger challenges such as squat-stand manoeuvres maybe also differences between MCI and C might appear. New extensive and long term prospective research is needed to investigate this theory and to study the development from MCI into AD in relation to dCA parameters.

Although we included roughly twice the amount of subjects as Claassen et al. [8] did, the study might be underpowered to show differences in autoregulation parameters with spontaneous blood pressure variations in supine rest. Using the results from this study the group size needed to show significant differences between AD and C could be estimated. A sample size analysis for GainLF shows that two to three times as many subjects are needed to show possible significant differences ( $p < 0.05$ ) between AD and C with 80 % power.

The windkessel model parameters that were fitted with the transfer function results show that the differences between AD, MCI and C groups are specific for the peripheral vasculature, since the arterial resistance  $R_a$  did not differ between the groups. The peripheral resistance  $R_p$  is increased in AD compared to controls. This is in accordance with the increased CVRi we found. Bateman et al. [31] also found increased resistance in AD using MRI to quantify cerebral haemodynamics. They also found compliance to be significantly lower (about 20 %) in AD compared to controls. We found compliance in AD to be 17 % lower than in controls, which was not significant. Our results therefore do not provide evidence for additional benefit of using the windkessel model over simply determining CVRi. CVRi is much easier to determine and could prove its value in the multidimensional diagnosis of AD. With a correlation between CVRi and  $R_p$  of 0.97 the parameters show to be almost identical.

The autoregulation parameters phase and ARI have positive correlations with blood pressure parameters, whereas autoregulation gain does not correlate with blood pressure. Apart from autoregulation, vascular compliance also elicits flow phase lead with respect to pressure due to fundamental hemodynamic behaviour of elastic tubes. As Zhang et al. showed, in the WKM for low values of  $C_p$  a positive correlation with phase exists and for high values of  $C_p$  it is negatively correlated with phase [12]. We found no correlation between  $C_p$  and blood pressure and therefore the correlation between

phase, ARI and blood pressure seems to be determined by direct influence of blood pressure. So, the higher blood pressure the faster autoregulation performs showing cerebral autoregulation seems to adjust adequately to higher levels of blood pressure. CVRi and  $R_p$  also positively correlate with blood pressure. For CVRi this can be easily explained by the formula used to calculate it.  $R_p$ , which is the only windkessel model parameter that significantly differs between AD and C, is strongly correlated with CVRi and therefore seems to reflect best the differences in CVRi among these groups also indicating that vascular pathology manifests predominantly in the smaller arterioles. CVRi and the windkessel parameters  $R_a$  and  $C_p$  positively correlate specifically with right medial temporal lobe atrophy, whereas CVRi and  $R_a$  also correlate with the MTA average, but less strong. This side specific correlation is difficult to explain, but could indicate lateralisation of pathological cognitive function.

Of course the autoregulation parameters evaluated in this study will never be a single diagnostic parameter identifying which MCI patient will develop Alzheimer's disease and which one doesn't, but these parameters could help in determining the influence of vascular components in the disease spectrum of cognitive disorders and together with other factors could disentangle the complex relationship between cerebral blood flow and cognition. A multidisciplinary approach is needed to study vascular cognitive impairment [32]. We also performed extensive duplex and neuropsychological investigations. These results will be published in successive papers.

### **Limitations**

TCD measures only relative velocity instead of absolute flow due to the unknown vessel diameter and insonation angle. Therefore, the assumed diameter of 3 mm for the WKM parameters increases noise and could mask differences in e.g. compliance.

The small number of patients in this study could limit the power to show significant differences. For the autoregulation parameter GainLF gain a post hoc analysis showed that at least twice the number of subjects would be needed to show a significant difference for this parameter. Since the recruitment was from an existing cohort of both AD and MCI the MRI data were not always acquired within the same time frame as the autoregulation measurement were performed. In only 9 patients the MRI was acquired maximally one year before the autoregulation test. This means that the condition of the cerebrovascular system could have been worsened with respect to the MRI results.

Medication can influence the relation between disease groups and their cerebrovascular results. Therefore, use of psychopharmacological medication was an exclusion criterion. Medication use was asked and almost every AD patient used a cholinesterase inhibitor. Due to ethical reasons this could not be stopped for the present study. A few AD patients (12%) and MCI patients (32%) used statins, which could influence autoregulation performance.

### **Conclusion**

This is the first study comparing cerebral autoregulation in three subject groups namely AD, MCI and matched controls in which distinct changes in cerebral hemodynamics in patients with AD were observed. Increased cerebrovascular resistance is found, possibly due to enhanced vasoconstriction in AD. CVRi values for MCI showed to be in be-

tween AD and controls but not significantly different from controls. In MCI decreased mCBFV and increased CVRi might be prognostic factors for developing AD. CVRi shows to be an easy to determine parameter and could be of value in the multidimensional diagnosis of AD.

Linear transfer function analysis of cerebral autoregulation may be used as a tool to characterise the cerebrovascular dynamics in AD and particularly in MCI patients, but probably the control of cerebral blood flow needs to be more strongly provoked by inducing greater blood pressure variability. Regarding the latter, future studies should evaluate the predictive power of such measurements with regard to the development of MCI into AD.

### **Acknowledgements**

Research supported by: Internationale Stichting Alzheimer Onderzoek (ISAO) grant # 06518 to JR.

The authors thank Prof. R.B. Panerai (University of Leicester, UK) for his valuable contributions to the manuscript.

## References

- [1] Iadecola C (2004) Neurovascular regulation in the normal brain and in Alzheimer's disease. *Nat Rev Neurosci* **5**, 347-360.
- [2] Niwa K, Kazama K, Younkin L, Younkin SG, Carlson GA, Iadecola C (2002) Cerebrovascular autoregulation is profoundly impaired in mice overexpressing amyloid precursor protein. *Am J Physiol Heart Circ Physiol* **283**, H315-323.
- [3] Rosengarten B, Paulsen S, Molnar S, Kaschel R, Gallhofer B, Kaps M (2006) Acetylcholine esterase inhibitor donepezil improves dynamic cerebrovascular regulation in Alzheimer patients. *J Neurol* **253**, 58-64.
- [4] de la Torre JC (2002) Vascular Basis of Alzheimer's Pathogenesis. *Annals of the New York Academy of Sciences* **977**, 196-215.
- [5] Snowdon DA (2003) Healthy aging and dementia: findings from the Nun Study. *Ann Intern Med* **139**, 450-454.
- [6] Roher AE, Esh C, Kokjohn TA, Kalback W, Luehrs DC, Seward JD, Sue LI, Beach TG (2003) Circle of Willis Atherosclerosis Is a Risk Factor for Sporadic Alzheimer's Disease. *Arteriosclerosis, Thrombosis, and Vascular Biology* **23**, 2055-2062.
- [7] Smith EE, Vijayappa M, Lima F, Delgado P, Wendell L, Rosand J, Greenberg SM (2008) Impaired visual evoked flow velocity response in cerebral amyloid angiopathy. *Neurology* **71**, 1424-1430.
- [8] Claassen JA, Diaz-Arrastia R, Martin-Cook K, Levine BD, Zhang R (2009) Altered cerebral hemodynamics in early Alzheimer disease: a pilot study using transcranial Doppler. *J Alzheimers Dis* **17**, 621-629.
- [9] Blaber AP, Bondar RL, Stein F, Dunphy PT, Moradshahi P, Kassam MS, Freeman R (1997) Transfer function analysis of cerebral autoregulation dynamics in autonomic failure patients. *Stroke* **28**, 1686-1692.
- [10] Panerai RB, Dawson SL, Potter JF (1999) Linear and nonlinear analysis of human dynamic cerebral autoregulation. *Am J Physiol* **277**, H1089-1099.
- [11] Zhang R, Zuckerman JH, Giller CA, Levine BD (1998) Transfer function analysis of dynamic cerebral autoregulation in humans. *Am J Physiol* **274**, H233-241.
- [12] Zhang R, Behbehani K, Levine BD (2009) Dynamic pressure-flow relationship of the cerebral circulation during acute increase in arterial pressure. *J Physiol* **587**, 2567-2577.
- [13] Association AP ed. (1994) *Diagnostic and Statistical Manual of Mental Disorders*, American Psychiatric Association, Washington, DC.
- [14] McKhann G, Drachman D, Folstein M, Katzman R, Price D, Stadlan EM (1984) Clinical diagnosis of Alzheimer's disease: report of the NINCDS-ADRDA Work Group under the auspices of Department of Health and Human Services Task Force on Alzheimer's Disease. *Neurology* **34**, 939-944.
- [15] Petersen RC, Smith GE, Waring SC, Ivnik RJ, Tangalos EG, Kokmen E (1999) Mild cognitive impairment: clinical characterization and outcome. *Arch Neurol* **56**, 303-308.
- [16] Roman GC, Tatemichi TK, Erkinjuntti T, Cummings JL, Masdeu JC, Garcia JH, Amaducci L, Orgogozo JM, Brun A, Hofman A, et al. (1993) Vascular dementia: diagnostic criteria for research studies. Report of the NINDS-AIREN International Workshop. *Neurology* **43**, 250-260.
- [17] Scheltens P, Leys D, Barkhof F, Huglo D, Weinstein HC, Vermersch P, Kuiper M, Steinling M, Wolters EC, Valk J (1992) Atrophy of medial temporal lobes on MRI in "probable" Alzheimer's disease and normal ageing: diagnostic value and neuropsychological correlates. *J Neurol Neurosurg Psychiatry* **55**, 967-972.

- [18] Fazekas F, Chawluk JB, Alavi A, Hurtig HI, Zimmerman RA (1987) MR signal abnormalities at 1.5 T in Alzheimer's dementia and normal aging. *AJR Am J Roentgenol* **149**, 351-356.
- [19] Folstein MF, Folstein SE, McHugh PR (1975) "Mini-mental state". A practical method for grading the cognitive state of patients for the clinician. *J Psychiatr Res* **12**, 189-198.
- [20] Van Der Elst WIM, Van Boxtel MPJ, Van Breukelen GJP, Jolles J (2005) Rey's verbal learning test: Normative data for 1855 healthy participants aged 24-81 years and the influence of age, sex, education, and mode of presentation. *Journal of the International Neuropsychological Society* **11**, 290-302.
- [21] van Balen HHG, Wimmers MFHG eds. (1993) *Rivermead Behavioural Memory Test: Normeringsgegevens voor Nederland en Vlaanderen.*, Swets & Zeitlinger, Lisse.
- [22] Reitan RM (1958) Validity of the trail making test as an indicator of organic brain damage. *Perceptual and Motor Skills* **8**, 271-276.
- [23] Van der Elst W, Van Boxtel MPJ, Van Breukelen GJP, Jolles J (2006) The Stroop Color-Word Test. *Assessment* **13**, 62-79.
- [24] Smith A ed. (1973) *Symbol Digit Modalities Test*, Western Psychological Services, Los Angeles, California.
- [25] Van Der Elst WIM, Van Boxtel MPJ, Van Breukelen GJP, Jolles J (2006) Normative data for the Animal, Profession and Letter M Naming verbal fluency tests for Dutch speaking participants and the effects of age, education, and sex. *Journal of the International Neuropsychological Society* **12**, 80-89.
- [26] Gommer ED, Staals J, van Oostenbrugge RJ, Lodder J, Mess WH, Reulen JP (2008) Dynamic cerebral autoregulation and cerebrovascular reactivity: a comparative study in lacunar infarct patients. *Physiol Meas* **29**, 1293-1303.
- [27] Gommer E, Shijaku E, Mess W, Reulen J (2010) Dynamic cerebral autoregulation: different signal processing methods without influence on results and reproducibility. *Medical and Biological Engineering and Computing*, 1-8.
- [28] Newell DW, Aaslid R (1992) *Transcranial Doppler*, Raven Press, New York.
- [29] Shih WJ, Ashford JW, Coupal JJ, Ryo YU, Stipp VV, Magoun SL, Gross K (1999) Consecutive brain SPECT surface three-dimensional displays show progression of cerebral cortical abnormalities in Alzheimer's disease. *Clin Nucl Med* **24**, 773-777.
- [30] Dickerson BC, Sperling RA (2008) Functional abnormalities of the medial temporal lobe memory system in mild cognitive impairment and Alzheimer's disease: Insights from functional MRI studies. *Neuropsychologia* **46**, 1624-1635.
- [31] Bateman GA, Levi CR, Schofield P, Wang Y, Lovett EC (2006) Quantitative measurement of cerebral haemodynamics in early vascular dementia and Alzheimer's disease. *Journal of Clinical Neuroscience* **13**, 563-568.
- [32] Marshall RS, Lazar RM (2011) Pumps, Aqueducts, and Drought Management: Vascular Physiology in Vascular Cognitive Impairment. *Stroke* **42**, 221-226.





# CHAPTER 4

## Neurovascular Coupling after Experience of Preeclampsia or Eclampsia.

Based on:

Martens EGHJ, Peeters LLH, Gommer ED, Mess WH, van de Vosse FN, Lima Passos V, Reulen JPH. *The visually-evoked cerebral blood flow response in women with a recent history of pre-eclampsia and/or eclampsia*. *Ultrasound in Medicine and Biology* 2009 Jan; 35(1):1-7.

## Abstract

Several studies provide evidence for altered cerebral hemodynamics during (pre)eclampsia. Whether (pre)eclampsia has a persistent negative impact on cerebral hemodynamics possibly contributing to an elevated risk of premature stroke, is unknown. The aims of this study were 1. To refine and apply a control system-based method previously introduced by Rosengarten to quantify the visually-evoked blood flow response of the posterior cerebral artery (PCA), and 2. To test the hypothesis with this method that cerebral hemodynamics in women with a recent history of (pre)-eclampsia is abnormal relative to that in parous controls. Hereto, we recorded cerebral blood flow velocity (CBFV) in the PCA by transcranial Doppler sonography during cyclic visual stimulation in 15 former preeclamptics (PE), 13 former eclamptics (E) and 13 controls (C). The typical CBFV response was fitted with the step response of a 2<sup>nd</sup>-order-linear model enabling quantification by parameters K (gain),  $\zeta$  (damping),  $\omega$  (natural frequency),  $T_v$  (rate time), and  $T_d$  (time delay). The method refinement introduced here consisted of response filtering before quantification and of considering individual instead of group averaged response patterns. Application of this refinement reduced the fitting errors ( $1.4 \pm 1.2$  vs.  $3.2 \pm 1.8$ ,  $p < 0.01$ ). Inter-group differences in model parameters were not found. Although statistically not significant, a trend was observed that critical damping ( $\zeta > 1$ ) occurred more frequently in the combined PE+E group than in C (7 of 28 vs. 1 of 13,  $p = 0.16$ ). Critical damping ( $\zeta > 1$ ) reflects an abnormal response, which is either compensated for by a rise in rate time ("intermediate";  $\zeta > 1$ ;  $T_v > 20$ ) or remains uncompensated ("sluggish";  $\zeta > 1$ ;  $T_v < 20$ ). Critical damping increased significantly ( $p = 0.039$ ) with (pre-)eclampsia-to-test-interval in patients with abnormal responses ( $\zeta > 1$ ), suggesting (pre)eclampsia might induce diminishing cerebral hemodynamic function over time. Based on a system-analytical classification approach, the study data provide evidence for individual CBFV responses to be abnormal in former (pre)-eclamptics compared to controls. Further study is needed to reveal how the abnormal CBFV response classification reflects cerebrovascular dysfunction.

## 4.1 Introduction

Formerly (pre)eclamptic women have a five times higher chance to die from cerebral hemorrhage [4] and three to nine year shorter life expectancy [1] than women who had uneventful pregnancies only. Whether this predisposition of former patients is related to a common denominator such as e.g. abnormal cerebral hemodynamics is unclear.

Preeclampsia is a hypertensive pregnancy complication triggered by endothelial dysfunction. The syndrome is defined by the concomitant presence of pregnancy-induced hypertension and de-novo pathologic proteinuria [13]. Abnormal renal, hepatic and clotting function often accompany the disorder, with occasionally also the presence of neurological symptoms such as visual disturbances and headache [6]. The development of seizures or coma unrelated to other cerebral conditions indicates progression of preeclampsia to “eclampsia”, the most severe complication of preeclampsia. (Pre)eclampsia has been shown to affect the cerebral perfusion [8, 16]. The cerebral circulation during (pre)eclampsia is often evaluated using Transcranial Doppler Ultrasonography (TCD). This technique is widely used to estimate the cerebral perfusion, as it is noninvasive, cost-effective and has a better time-resolution than, e.g. fMRI or PET [5]. Several TCD studies provide evidence for altered cerebral hemodynamics [2, 8, 9, 16] and impaired cerebral autoregulation [7] during (pre)eclampsia.

Although symptoms of preeclampsia, like visual disturbances such as seeing flash lights, and other cerebral perfusion-related complaints (e.g. headache) usually disappear postpartum, it is conceivable that the preeclampsia-related endothelial damage persists subclinically for a prolonged period. Functional evaluation of visual neurovascular coupling (NVC), which represents the control mechanism that adjusts the local blood flow to the metabolic demand of the visual cortex, provides an estimate of the cerebral hemodynamics and indirectly, of the cerebral endothelial function.

The objectives of this study were 1. To refine and apply a 2<sup>nd</sup>-order linear-model-based method to quantify the visually-evoked blood flow response of the posterior cerebral artery (PCA), and 2. To use this method for testing the hypothesis that cerebral hemodynamics in women with a recent history of (pre)eclampsia is abnormal relative to that in parous controls. To this end, we estimated the NVC function at least 3 months postpartum in 2 groups of either healthy formerly preeclamptic or eclamptic women who fully recovered from their complicated pregnancy, and compared the results which those obtained in a reference group of healthy parous controls.

## 4.2 Patients and methods

### Patients

We assessed the NVC in three groups, i.e. two patient groups of former preeclamptics (PE, n=15) and formerly eclamptics (E, n=13), respectively, and a reference group of healthy parous controls (C, n=13). The controls were matched with the patient groups for age, BMI and time elapsed between delivery and measurement session. The study was approved by the Institutional Review Board and all participating subjects gave written informed consent. Former preeclamptic and eclamptic women were obtained

from the database of the Department of Obstetrics and Gynecology of the University Hospital Maastricht. The inclusion criteria for the pre-eclamptic group were a recent history (elapsed time: 0.25-6 years) of a pregnancy complicated by preeclampsia, defined as *de-novo* hypertension (>140/90 mmHg) and pathological proteinuria after 20<sup>th</sup> week of pregnancy [13]. Women enrolled in the eclampsia group had a recent history of a pregnancy (elapsed time: 0.25-6 years) complicated by eclampsia, defined as the *de-novo* development of seizures during pregnancy. We only included subjects older than 18 years at the time of pregnancy in any of the study groups. Controls had an uncomplicated pregnancy in their recent history, and were matched with the patient groups with respect to age, BMI and the length of the period between delivery and measurement (birth-to-test-interval). Women with a history of chronic hypertension, a renal, metabolic, neurological or cerebrovascular disorder, the use of statins, or the presence of a new pregnancy, were excluded from this study. In addition, women were only evaluated after resumption of the menstrual cycle and discontinuation of breast feeding. Table 1 lists the demographic and clinical features (mean and standard deviation) of the two patient subgroups and the controls.

### Flow recording method

TCD measurements were performed using a Multidop X 4 Doppler device (® DWL, Sipplingen, Germany). A 2MHz probe was mounted on a headband and cerebral blood flow velocity (CBFV) was measured in the P2 segment of the PCA. From the envelope of the cerebral blood flow velocity (CBFV) signal, we used the beat-to-beat peak systolic CBFV-values for analysis. The Doppler device was coupled to the measurement computer, the Task Force Monitor (® CNSystems, Graz, Austria) enabling concomitant recording of CBFV, ECG and arterial finger blood pressure.

### Visual stimulus paradigm

Data were recorded during repetitive cycles of visual stimulation using a colored cartoon video on an LCD-screen. Each cycle consisted of 40 seconds visual stimulus “on” and 20 seconds visual stimulus “off” (black screen). Switching between these visual-stimulus phases was signaled by an audible tone. Subjects were instructed to close their eyes during the stimulus-off periods. This blocked stimulus paradigm was applied for approximately 10 minutes until at least 10 usable (i.e. artifact-free by visual inspection) cycles for every subject were recorded.

### Data processing

Peak-systolic CBFV was used for analysis to minimize artifacts and to make optimal use of signal quality [10]. Since non-equidistant beat-to-beat data were used as input, first linear interpolation and resampling (with 5 Hz) were applied to obtain equidistant data points with sufficient time resolution (0.2 sec). Absolute CBFV values were transformed into relative CBFV changes using equation (1):

$$\Delta V = \frac{V - V_{\text{baseline}}}{V_{\text{baseline}}} \times 100\% \quad (1)$$

where  $\Delta V$  represents the % change in CBFV relative to baseline,  $V$  the peak systolic blood flow velocity during the stimulation cycle and  $V_{\text{baseline}}$  the mean peak systolic baseline blood flow velocity during the 10 seconds rest period preceding stimulation. The TCD data of 10 visual stimulation cycles were stimulus-locked averaged to obtain a characteristic PCA CBFV response for each subject.

### Response quantification

We considered the PCA NVC-response as a so-called “step response of a 2<sup>nd</sup>-order-linear system” as proposed by Rosengarten [11] for the description of dynamic NVC responses. Fitting this step response enables quantification of the measured PCA NVC response by a specific set of system parameters. This quantification method was previously used by Tiecks [15] to describe cerebral autoregulation and later adapted to neurovascular coupling by Rosengarten [10, 11]. The model used here can be described in the Laplace domain with the following transfer function:

$$H(s) = \frac{K(1 + T_v s)}{\frac{s^2}{\omega^2} + 2\frac{\zeta}{\omega}s + 1} e^{-T_d s} \quad (2)$$

where  $K$  represents the gain,  $\omega$  the natural frequency,  $T_v$  the rate time,  $\zeta$  the damping and  $T_d$  the time delay. In terms of the response,  $K$  specifies the mean % CBFV difference between the “stimulus-off” and “stimulus-on” periods, whereas  $\omega$  characterizes the oscillation of the control system as if it were undamped.  $T_v$  modulates the initial flow response and  $\zeta$  describes the damping of the system. In literature parameter  $\zeta$  is also referred to as attenuation or damping ratio, however in this publication the term damping is used consistently. Finally,  $T_d$  is the time delay between stimulus onset and flow response start.

### Refinement

So far, the method explained here is consistent with procedures previously reported. However, we changed two aspects of this method. First, we filtered the characteristic NVC response before fitting it with the model, using an advanced time-variant low-pass filtering procedure based on a technique known as smoothness-priors (SP). Previously, this technique has been applied successfully for high-pass filtering or detrending of physiological signals [14]. Here, we employed low pass filtering with a time-varying cut-off frequency of 0.2 Hz ( $\lambda = 25$ ), which resulted in removal of high frequencies and still provided an optimal track of the low frequency NVC response. To avoid interference of SP-filtering, the low pass cut-off frequency  $f$  (0.2Hz) was chosen far outside the range ( $>$  mean + 10 standard deviations) of reported literature values for the NVC response natural frequency  $\omega$  ( $0.23 \pm 0.06$  rad/s corresponding to  $f = 0.04 \pm 0.01$  Hz; Rosengarten 2001a). Second, we evaluated individual rather than group-averaged responses.

Hereto, every individual SP-filtered response was fitted with the system transfer function according to equation (2) using the least square error technique. We performed all data analysis using the mathematical software program Matlab (® The Mathworks Inc., Natick, MA, USA). Figure 4.1 illustrates a typical response and accessory fitted step response.

### Statistics

We compared the system parameters between groups using the non-parametric Kruskal-Wallis test using a cut-off value of 0.05 to indicate a statistically significant difference. Where applicable, we additionally compared group medians with one another using the Mann-Whitney-U test or group incidences using the Fisher Exact Test. The influence of SP-filtering on the fitting errors was tested with the Wilcoxon signed ranks test. A linear regression analysis was conducted to investigate the effect of potential explanatory variables on the system parameters.

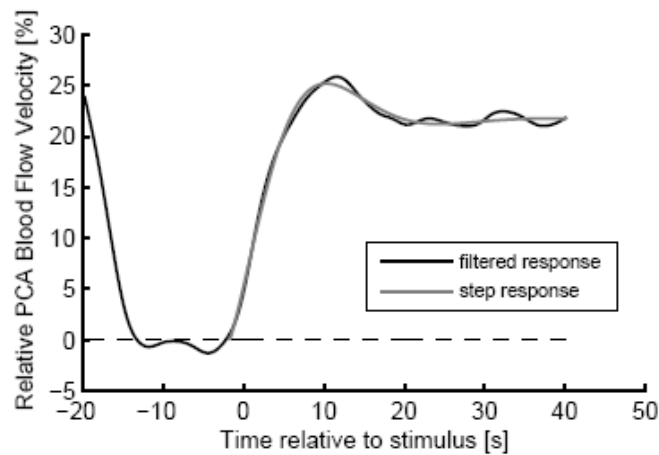


Figure 4.1. Example of smoothed response (filtered response) and its model-fitted step response (step response)

### 4.3 Results

The methodological refinement of filtering the characteristic responses before fitting them with the model resulted in smoothed response curves, which still track the trend of their original response accurately. A representative example is shown in figure 4.2. In all cases pre-analysis filtering reduced the fitting error ( $1.4 \pm 1.2$  instead of  $3.2 \pm 1.8$ , Wilcoxon signed ranks test,  $p < 0.01$ ) between the fitted step response and the measured response. The second adjustment in our approach, i.e. considering individual

rather than group-averaged responses, enabled us to detect incidence differences between groups.

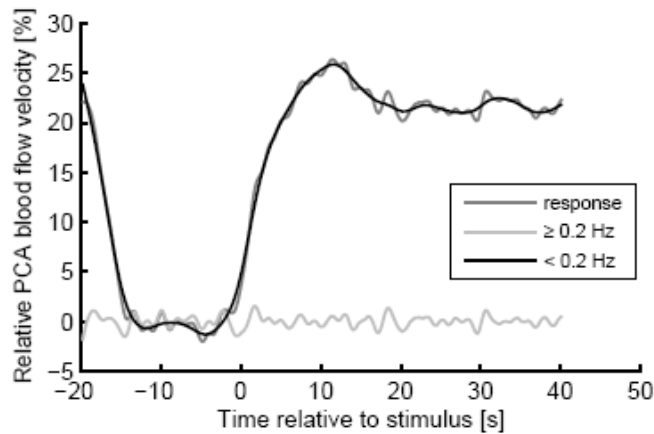


Figure 4.2. Example of a measured response with its high-frequency signal content separated from its low-frequency signal content by SP-filtering. The low-frequency signal content represents the trend of the original response.

Table 1 lists the demographic characteristics of all participants subdivided over two patients - and one control group. Both patient groups differed from the control group by a shorter gestation, a lower birth weight, and a lower parity, but were comparable with the control group with respect to age, BMI and time elapsed between delivery and the NVC measurement.

Table 1. Demographics and outcome of preceding pregnancy of the participants in the two patient subgroups (PE and E) and control group (C). \*  $p < 0.05$

	<b>C (N = 13)</b>	<b>PE (N = 15)</b>	<b>E (N = 13)</b>
age (years)	33 ± 3	31 ± 4	33 ± 3
BMI during testing (kg/m <sup>2</sup> )	24 ± 3	24 ± 3	26 ± 3
Interval birth to test (months)	24 ± 14	19 ± 12	29 ± 19
Primipara during testing	23% (3/13)	60% (9/15)	46% (6/13)
Gest. age at birth (weeks)	39 ± 1	30 ± 2*	32 ± 5*
Neonatal weight (g)	3383 ± 368	1051 ± 315*	1812 ± 1055*

A typical normal NVC response curve is characterized by an initial fast upstroke, a transient modest overshoot which then stabilizes (or saturates) at a higher plateau (fig.



4.1). After filtering of the response curve, we fitted for each participant the NVC response with the step response of a 2<sup>nd</sup> order transfer function (fig. 7.1) to obtain 5 model parameters defining their individual NVC response curve. The obtained values for the model parameters are listed per group in Table 2.

Table 2. Hemodynamic outcomes and model parameter values averaged over the subject group (C, PE, E).

MODEL PARAMETERS	C (N=13)	PE (N=15)	E (N=13)
Gain K	28 ± 7	24 ± 9	24 ± 6
Damping $\zeta$	0.6 ± 0.2	0.7 ± 0.4	0.7 ± 0.3
Natural frequency $\omega$ (rad/s)	0.23 ± 0.08	0.21 ± 0.08	0.25 ± 0.11
Rate time $T_v$ (s)	4.8 ± 7.8	11.0 ± 16.7	5.8 ± 6.6
Time delay $T_d$ (s)	0.4 ± 0.4	0.4 ± 0.4	0.6 ± 0.6
Fit error (%)	1.9 ± 1.8	1.1 ± 0.6	1.3 ± 0.7

Damping parameter  $\zeta$  and rate-time parameter  $T_v$  describe the dynamic behavior of the NVC response. In case of a normal response with both overshoot and saturation, these parameters were noted to be < 1 and < 20, respectively. In 12 of 13 controls, 11 of 15 former preeclampsics and 10 of 13 former eclampsics, we encountered a normal NVC response curve. Conversely, deviant response behavior (absence of overshoot or absence of saturation) was accompanied with a  $\zeta$  higher than 1, which is known from control system theory to indicate critically overdamping. Such an abnormal response was observed 3 times more often in former patients (7 of 28) than in controls (1 of 13) (Fisher Exact Test,  $p = 0.16$ ).

By taking the rate time  $T_v$  into account, the 8 critically overdamped response curves could be further differentiated in intermediate ( $T_v > 20$ ) responses, corresponding to curves which lack of saturation, and sluggish responses ( $T_v < 20$ ), representing responses without an overshoot. This led to a subdivision of the critically overdamped curves in a group of 5 intermediate responders (3 PE, 1 E, 1C) and 3 sluggish responders (1 PE, 2 E). Plotting the combinations of dynamic model parameters  $\zeta$  and  $T_v$  for all 41 subjects illustrates how the two critically-overdamped response types, i.e. intermediate and sluggish, are distributed in our study population (fig. 7.3). The three displayed sections in this plot were obtained by adding two standard deviations (Table 2) to the mean value of each parameter for the control group. This resulted in a limit of 1 [0.6 + 2 \* 0.2] for  $\zeta$ , and 20 [4.8 + 2 \* 7.8] for  $T_v$ . Section I ( $\zeta < 1$ ;  $T_v < 20$ ) contains the normal responders ( $n=33$ ), section II the 5 intermediate responders ( $\zeta > 1$ ;  $T_v < 20$ ) and section III the 3 sluggish responders ( $\zeta > 1$ ;  $T_v > 20$ ). The section-averaged responses, i.e. the responses resulting from averaging all responses per section, are shown in figure 4.4. In contrast to the section-averaged responses, the group-averaged responses, averaged

per patient group (PE, E or C), show no dissimilarities. All of them have a typical normal course with a modest overshoot and subsequent saturation.

It is conceivable that changes in model parameters and in particular damping  $\zeta$  and slope  $T_v$  may be related to other (patho)physiological factors. For this reason we evaluated  $\zeta$  and  $T_v$  behavior versus age and PE/E-to-test-interval. Damping  $\zeta$  increased significantly ( $p=0.039$ ) with PE/E-to-test-interval in the PE+E patients with abnormal responses ( $\zeta>1$ ), while in the controls no relation was found with the post-pregnancy period.

Finally, we compared the mean model parameters and additional physiological measures of both patient groups with those in the control group (Table 2). Arterial blood pressure, heart rate, CBFV and the mean values for the model parameters in neither of the two patient groups differed significantly from the corresponding values in the control group.

#### 4.4 Discussion

In this study we defined the NVC response curve on the basis of 5 model parameters, which were generated by fitting a 2<sup>nd</sup> order linear model to experimentally obtained NVC-responses. By separating the slow response of interest from superimposed higher unwanted frequencies, we successfully applied a novel signal analytical technique - called smoothness priors (SP) - to NVC responses. Considering both the balance between accurate tracking of the original response and adequate noise reduction in relation to literature values for NVC natural frequency  $\omega$ , a cut-off frequency of 0.2 Hz (corresponding to  $\lambda = 25$ ) was chosen for SP-filtering. Since the range of natural frequencies found in this study, ( $\omega = 0.25 \pm 0.11$  rad/s or  $f = 0.04 \pm 0.02$  Hz ; eclampsia group), does not overlap the applied low pass filter frequency of 0.2 Hz no relevant interference from SP-filtering on the low pass NVC response is present. Therefore, the 0.2 Hz cut-off frequency choice is justified. After SP-filtering, we obtained a smoothed NVC response for each participating subject, which was then fitted with the step response of the model to obtain a specific set of quantitative parameters. SP-filtering resulted in reduced fitting errors between the original response and fitted step response. In agreement with a recent study by Rosengarten [12], we found that the presence of the differentiating term in the model ( $T_v$ s) plays a crucial role in reducing the fit error.

As opposed to the approach of comparing the group-averaged NVC response between patient groups, we classified the individual NVC response curves into 3 categories (fig. 4.3) based on visual recognized differences and on the values of the 2 model parameters  $\zeta$  and  $T_v$ . In the model expression of the normal response curve (fig 1), damping parameter  $\zeta$  and rate-time parameter  $T_v$  are always  $< 1$  and  $< 20$ , resp. In the limited literature describing NVC response parameters, the normal value for  $\zeta$  and  $T_v$  are  $< 1$  and  $< 13$ , resp. [10]. In this study the upper limit for a normal  $\zeta$  was similar, but the one for  $T_v$  was higher (20 vs. 13). Using - together with a  $\zeta < 1$  - a cut-off value of 13 for a normal  $T_v$  would not have altered our current classification (fig. 4.3).

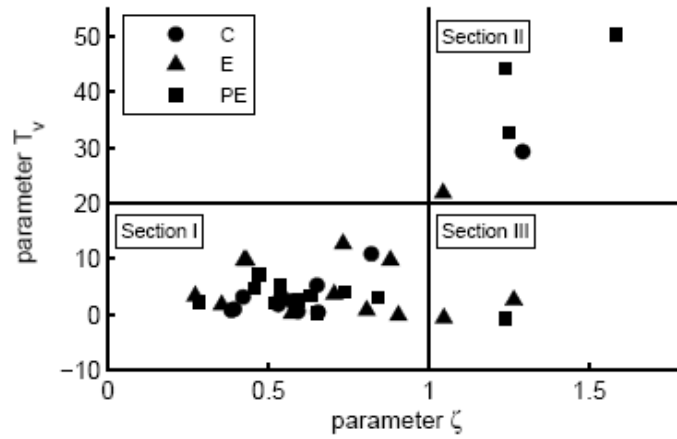


Figure 4.3. Classification of the responses based on model parameters rate time  $T_v$  and damping  $\zeta$ . Damping  $\zeta > 1$  reflects critically overdamping and differentiates - with parameter  $T_v$  - between the three observed response types.

When considering the group-averaged responses of the PE, E and C-group, differences between the groups can neither be detected by visual recognition nor by model parameter values. In contrast, evaluating the responses on an individual base disclosed different response types (fig. 4.4) as well as different incidences of these response types in patients relative to controls. This information is filtered and by that eliminated in case of group-averaging.

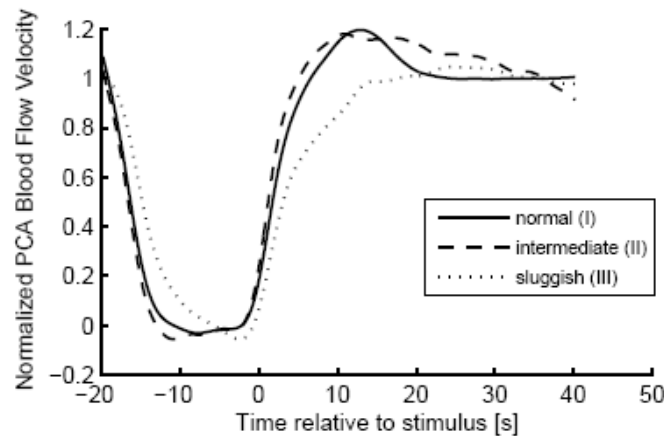


Figure 4.4. The section-averaged responses normalized on the mean value of the last 10 seconds of stimulation: normal (section I,  $n=33$ ), intermediate (section II,  $n=5$ ) and sluggish (section III,  $n=3$ ).

As mentioned before, we identified normal (fig 4.3 sec I, fig 7.4) and critically-overdamped ( $\zeta > 1$ ) responses, the latter either being compensated (intermediate) or uncompensated (sluggish) (fig 4.3 sec II, sec III resp. and fig 4.4). The intermediate response, observed in 5 of 8 subjects (3 PE, 1 E, 1C), differs from normal by failure of the overshoot to return to the new plateau within the stimulation period. The sluggish response, observed in the other 3 subjects (1 PE, 2 E) differs from normal by the complete absence of an overshoot and late saturation.

A major point of discussion is the value and interpretation of this control system approach with regard to (patho-)physiology of cerebrovascular NVC reactivity. Neurovascular coupling adjusts cerebral blood flow to cerebral metabolic activity. It is a complex mechanism of neuronal and vascular interactions [3]. Simplification and description of such a mechanism by an analytical model approach might enable the development of new insights.

The presentation of the visual stimulus is considered to be a step input for this control mechanism and the corresponding PCA flow its step output reaction. The interjacent input-output system, which includes the (micro)vasculature of the reacting visual cortical areas, is modeled as a second order transfer function incorporating parameters gain  $K$ , natural frequency  $\omega$ , damping  $\zeta$  and rate time  $T_v$ . This approach, however, allows no conclusions about the possible underlying physiological mechanisms of the neurovascular coupling. A major aspect of NVC is feedback control. This feedback control system should have the transfer function properties given by equation (2). A second order model incorporating both feedback and adherence to this requirement is schematically shown in fig. 4.5. It consists of a first-order vascular plant which is controlled by proportional-plus-integral control. In this model the error signal between the actual NVC output signal and the step input is processed by Proportional (Gain) and Integrative action (PI control), the sum of which is input for a first order plant (FOP). FOP represents the properties of the (micro)vasculature of the reacting visual cortical areas. Integral control action for this system eventually eliminates the error between input and output and raises the order of the system by one, thus resulting in a second order system that can oscillate.

Because of this PI-control the system is capable of producing larger overshoots but also faster rise times compared to a system without PI-control, in particular for damping values exceeding 1. It also illustrates the common misconception that  $\zeta > 1$  necessarily indicates a response to be sluggish.

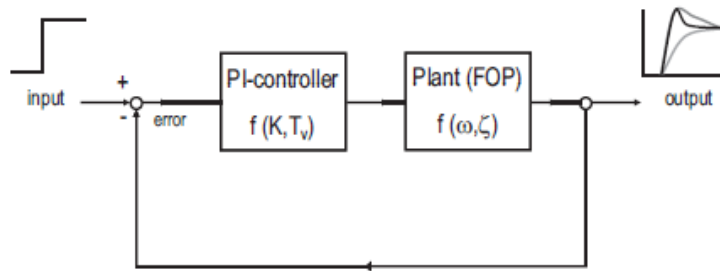


Figure 4.5. Schematic design of a control system representing the transfer functions of eq. 2. In this design the control system consists of an integrating proportional (PI)-controller, a FOP and an output-to-input feedback loop. FOP is a function of parameters  $\omega$  and  $\zeta$  notated as  $f(\omega, \zeta)$ . Similarly, PI is a function of  $K$  and  $T_v$ .

The finding of the two abnormal responses can possibly be explained in terms of this control system. The intermediate response is by its own an adequate response which attains the required blood flow reasonably fast, but in terms of model interpretation it could be an intermediate stage between normal and abnormal. It seems that the more the system becomes damped the larger the drive is to elicit a compensatory rise in  $T_v$  to accelerate the system's response to attain an adequate blood flow in time. How this differentiating action operates on vessels or neuronal level is unclear and should be subjected to further investigation. When a compensatory rise in  $T_v$  does not occur, the overdamped response will attain a sufficient blood flow much later than normal, giving rise to the sluggish response. As  $\zeta$  may vary as a function of vessel stiffness, an elevated  $\zeta$  may indicate cerebrovascular dysfunction secondary to a reduced vascular compliance.

In most subjects enrolled in this study the NVC response curve was normal (C 92%, PE 73 %, E 77 %), with 5 cases displaying an intermediate and 3 cases a sluggish response. Considering all critically overdamped responses to be abnormal, 7 of 8 abnormal responses occurred in former patients, disproportionally more than in controls. This difference, however, is less obvious after subdividing former patients into two subgroups. This may be due to loss of power as a result of diminishing group sizes. Notably, on the other hand, preeclampsia is a pregnancy disorder defined by clinical symptoms rather than causality, a feature causing more heterogeneity in subsequent group comparisons. We also questioned whether changes in model parameters and in particular damping  $\zeta$  and slope  $T_v$  may be related to other (patho)physiological factors and found that damping  $\zeta$  increased significantly ( $p=0.039$ ), not as may be expected with age, but with PE/E-to-test-interval in the PE+E patients with abnormal responses ( $\zeta > 1$ ). In the controls no relation was found with post-pregnancy-period. This finding supports the idea that the occurrence of PE or E may in some way trigger deterioration of cerebral function over post PE/E time or strengthen the already pre PE/E present diminished cerebral function in the period post PE/E. This addresses to but does not answer the question whether (pre-)eclampsia is just a marker of lifelong existing endothelial dysfunction or the cause of endothelial dysfunction. However, the possibility that cerebrovascular alterations, i.e. increased damping, induced by preeclampsia could be only a temporary effect can

not be excluded. Monitoring cerebrovascular hemodynamics of formerly preeclamptics on a longer time base e.g. in their middle ages, may provide more conclusive evidence on the time course of endothelial function. This issue is still topic of debate in the preeclamptic research field.

Vascular compliance is the most important determinant of the dynamic behavior of the visually-evoked responses. Different pathogenetic pathways in the subclinical period that precedes manifest (pre)eclampsia and the HELLP syndrome eventually merge into a relatively homogeneous clinical symptomatology [13]. The initiation of some of these pathogenetic pathways may be facilitated in the presence of an underlying vascular disorder. Therefore, it is conceivable that some former patients share vascular pathology that involves systemic vascular and cerebrovascular dysfunction. Measurement of NVC function possibly helps to discriminate between patients who in the future will or will not become symptomatic.

In summary, although abnormal NVC responses were found to cluster in former (pre)eclamptic patients, irrespective of whether they experienced eclampsia or preeclampsia, most of these former patients displayed a normal NVC response. An abnormal NVC response may be associated with reduced arterial compliance, but experimental evidence has not been provided yet. Our findings emphasize the importance of quantitative analysis of individual NVC responses in addition to group-averaged responses. In the future, NVC feedback control properties should be studied in more detail. Modeling of transfer function and its verification with new measurements and finally interpretation and translation of model parameters into the physiology and pathology of NVC deserve major attention.

## References

- [1] Arnadottir GA, Geirsson RT, Arngrimsson R, Jonsdottir LS, Olafsson O. Cardiovascular death in women who had hypertension in pregnancy: case-control study. *BJOG* 2005;112: 286-92
- [2] Belfort MA, Varner MW, Dizon-Townwon DS, Grunewald C, Nisell H. Cerebral perfusion pressure, and not cerebral blood flow, may be the critical determinant of intracranial injury in preeclampsia: A new hypothesis. *Am J Obstet Gynecol* 2002; 187(3): 626-634
- [3] Iadecola C. Neurovascular regulation in the normal brain and in Alzheimer's disease. *Nat Rev Neurosci* 2004; 5(5): 347-360
- [4] Irgens HU, Reisaeter L, Irgens LM, Lie RT. Long term mortality of mothers and fathers after preeclampsia: population based cohort study. *BMJ* 2001; 323: 1213-1217
- [5] Lohmann H, Ringelstein EB, Knecht S. Functional transcranial Doppler sonography. *Front Neurol Neurosci*. 2006; 21:251-260
- [6] Noris M, Perico N, Remuzzi G. Mechanisms of disease: pre-eclampsia. *Nat Clin Pract Nephrol*. 2005; 1 (2): 98-114
- [7] Oehm E, Reinhard M, Keck C, Els T, Spreer J, Hetzel A. Impaired dynamic cerebral autoregulation in eclampsia. *Ultrasound Obstet Gynecol* 2003; 22: 395-398
- [8] Riskin-Mashiah S, Belfort MA. Preeclampsia is associated with global cerebral hemodynamic changes. *J Soc Gynecol Investig* 2005; 12 (4): 253-256
- [9] Riskin-Mashiah S, Belfort MA, Saade GR, Herd JA. Cerebrovascular reactivity in normal pregnancy and preeclampsia. *Obstet Gynecol* 2001; 98(5): 827-832
- [10] Rosengarten B, Aldinger C, Kaufmann A, Kaps M. Comparison of visually evoked peak systolic and end diastolic blood flow velocity using a control system approach. *Ultrasound Med Biol*. 2001; 27(11):1499-1503.
- [11] Rosengarten B, Huwendiek O, Kaps M. Neurovascular coupling in terms of a control system: validation of a second-order linear system model. *Ultrasound Med Biol*. 2001; 27(5): 631-635.
- [12] Rosengarten B, Lutz H, Kaps M. The neurovascular coupling bears properties of a feed-forward and feedback regulative mechanism. *Ultrasound Med Biol* 2008;34(1):1– 6.
- [13] Sibai B, Dekker G, Kupferminc M. Preeclampsia. *Lancet* 2005; 365: 785-799
- [14] Tarvainen MP, Ranta-aho PO, Karjalainen PA. An advanced detrending method with application to HRV analysis. *IEEE Trans Biomed Eng*. 2002; 49(2): 172-175.
- [15] Tiecks FP, Lam AM, Aaslid R, Newell DW. Comparison of static and dynamic cerebral autoregulation measurements. *Stroke* 1995; 26(6): 1014-1019.
- [16] Zunker P, Happe S, Georgiadis AL, Louwen F, Georgiadis D, Ringelstein EB, Holzgreve W. Maternal cerebral hemodynamics in pregnancy-related hypertension. A prospective transcranial Doppler study. *Ultrasound Obstet Gynecol* 2000; 16: 179-187

# CHAPTER 5

## Neurovascular Coupling of Alzheimer and Mild Cognitively Impaired Patients: influence of reliability and blood pressure

Based on:

Martens EGHJ, Gommer ED, Bogaarts JG, Shijaku E, Ramakers IHGB, Aalten P, Verhey F, Mess WH, Reulen JPH. *Parameter reliability and blood pressure dynamics in assessment of neurovascular coupling of Alzheimer and cognitively impaired patient*. Submitted (2012)



## Abstract

Visually-evoked blood flow responses (VEFRs) measured by transcranial Doppler ultrasonography reveal information about neurovascular coupling. In general, VEFRs are analyzed by control system fitting. This study aims to compare a revised VEFR-analysis procedure incorporating parameter reliability and blood pressure dynamics, to the standard procedure.

To account for blood pressure dynamics the standard model (RG) has been extended (RGe). Both procedures are applied to VEFRs of 15 Alzheimer patients (AD), 17 mild cognitively impaired patients, and 18 controls.

Reliability consideration resulted in 40% VEFR exclusion mainly due to the models' inability to fit aberrant responses. Irrespective of this, a significantly increased damping was found in AD for RG but not for RGe fitting.

Accounting for blood pressure dynamics reverses study conclusions from altered into normal neurovascular coupling in AD, but they are unaffected by reliability consideration. Nevertheless, reliability consideration decreases parameter variability considerably. Therefore, both aspects should be included in VEFR-analysis.

## 5.1 Introduction

Visually-evoked blood flow responses (VEFRs), measured by transcranial Doppler ultrasonography (TCD), are commonly used to assess local cerebral blood flow regulation i.e. neurovascular coupling (NVC). The VEFR is the increase in blood flow velocity in the P2 segment of the posterior cerebral artery (PCA-P2) in response to a visual stimulus e.g. a cartoon, relative to baseline when eyes are closed. VEFRs can be analyzed either by identification of characteristic features or by transfer function analysis describing them by control system parameters [1, 2]. Two important aspects are, however, not included in VEFR analysis: first, the reliability of computed model parameters and second, the possible influence of blood pressure variation on the measured VEFR.

Reliability of VEFR parameters has been evaluated previously in a test-retest set-up and quantified by Cronbach's alpha [3]. Re-test errors were largest for initial rise time  $T_v$  and damping  $\zeta$  but single measurement reliability was not addressed. In this paper, we introduce a measure for reliability of model parameter values applicable to single measurements.

The second aspect regards possible influence of blood pressure variation on VEFR. Cerebrovascular control involves a complex interaction of a multitude of processes influencing vascular smooth muscle tone [4]. Cerebral autoregulation (CA), i.e. the mechanism which aims to maintain a stable blood flow despite blood pressure variations, may interfere with neurovascular coupling. Visual stimulation may evoke blood pressure variations, possibly activating the CA mechanism leading to flow variation. Interference between dynamic CA and neurovascular coupling is conceivable since both mechanisms act on the level of small arteriolar resistance vessels and have characteristic time constants in the same range ( $\sim 10$ s).

Several studies already contributed to the disentanglement of the neurovascular coupling - CA relationship. For example, the interaction between system hemodynamics and cerebral blood flow responses has previously been demonstrated for attentional processing [5] and for cognitive and motor activation [6, 7]. Very recently, Panerai and co-workers [8] introduced an autoregressive moving average model enabling identification of physiological signals contributing to a stimulus evoked blood flow response other than the stimulus itself. They evaluated motor-induced flow responses and revealed that blood pressure variation accounted for about 20% of the CBFV response variation. Their finding emphasizes the need to correct for blood pressure influence. Independently of the work of Panerai and co-workers of which we were not aware until recently, we also developed a model to enable correction for blood pressure dynamics based on a control system approach. Contributions to flow induced by blood pressure changes should be filtered to obtain the 'real' VEFR representing purely neurovascular coupling action.

The relevance of these two aspects in VEFR analysis was evaluated in this study in a cohort of Alzheimer patients, patients with mild cognitive impairment (MCI), and controls (HC). This cohort is selected because of accumulating neurobiological evidence for disturbed NVC in an early stage of Alzheimer pathology [9]. Alzheimer's disease (AD) is characterized by deposition of A $\beta$  amyloid in neurons and blood vessels (amyloid angiopathy) and alterations in phosphorylated neurofilaments, also called neurofibrillary

tangles. The emerging view is that AD is initiated by vascular factors which precede the neurodegenerative process [10]. The larger cerebral vessels of AD patients show a substantial increase in severity of atherosclerosis [9] whereas smaller arteries are affected through manifestation of cerebral amyloid angiopathy [10]. These structural changes may alter vascular wall properties such as stiffness and by that flow resistance and compliance. Cerebrovascular dysregulation is hypothesized to be evident before the onset of clinical AD symptoms [9], implying that it should be detectable in the prodromal stage, i.e. in MCI patients.

Several studies have compared VEFRs of AD and HC. One study found no difference in reactivity to visual stimulation [11], whereas a recent study showed a significantly decreased reactivity in AD [12]. Other studies reported increased VEFR damping in AD, suggesting increased vascular stiffness [13, 14]. VEFR damping improved in a dose dependent manner under treatment of acetylcholine-esterase inhibitors, indicating functional deficit in AD cerebrovasculature and that decreased VEFRs and A $\beta$ -induced morphological lesions might be related.

This study aims for a revised VEFR analysis procedure in which parameter reliability and blood pressure dynamics are considered. Study outcomes regarding NVC of AD, MCI and HC based on the revised procedure are compared to outcomes obtained by the standard procedure.

## 5.2 Patients and Methods

### Patients

VEFRs have been assessed in a group of Alzheimer patients (AD), a group of amnesic Mild Cognitive Impairment patients (aMCI) and a group of healthy controls (HC). The controls were matched with the patient groups for age, gender and educational level (table 1). The study was approved by the Institutional Review Board of the Maastricht University Medical Centre. AD-patients were only eligible for participation if they had a reliable informant. All participants gave written informed consent before the start of the study. Patients were recruited from the multidisciplinary memory clinic of the Maastricht University Medical Centre. AD patients were diagnosed according to the DSM-IV criteria for dementia [15] and NINCDS-ADRDA criteria [16]. Specific exclusion criteria for AD were diagnosis of Vascular Dementia according to NINDS/AIREN criteria [17]. aMCI patients were enrolled when they met the criteria of Petersen [18] for aMCI, including a subjective and objective memory impairment, no significant impairments in daily functioning and no dementia. An additional exclusion criterion for the patients was the presence of micro-vascular pathology detected on MRI images according to the Fazekas scale [19]. Exclusion criteria for all groups were living in a nursing home at the start of the study, alcohol and/or drug abuse, diabetes and/or heart disease and/or cerebrovascular diseases. All subjects underwent duplex investigation to exclude subjects with a possible stenosis (> 50%) of the carotid or basal intracranial arteries or subjects without a temporal “doppler” window. VEFRs of 15 AD, 17 aMCI and 18 HC were included in data-analysis.

Table 5. General demographic data of subject groups. All data are presented as mean (standard deviation) [min max]. ) n=number of subjects, p-values of One-way Anova, Sidak correction

	AD (n=15)	MCI (n=17)	HC (n=18)	
Male/female	7/8	11/6	7/11	
Age [year]	72 (1.7) [63-87]	69 (1.7) [58-79]	70 (1.6) [58-78]	
MMSE	19.8 (1.5) [8-28]	27.7 (0.4) [24-30]	28.9 (0.3) [26-30]	AD-MCI p<0.001 AD-C p<0.001
sBP [mmHg]	137 (3) [123-154]	133 (3) [120-147]	134 (3) [108-151]	
dBP [mmHg]	90 (1) [79-98]	85 (2) [71-104]	87 (3) [63-105]	
mBP [mmHg]	105 (2) [94-116]	101 (2) [88-116]	103 (3) [79-120]	
mCBFV [cm/s]	33.8 (3.0) [18-53]	37.8 (3.1) [22-60]	37.5 (2.1) [25-53]	

Demographic characteristics of the three groups are listed in table 1. Age was not significantly different between groups. The scores on the Mini-Mental State Examination (MMSE) [20], a test to assess general cognitive functioning, were significantly lower for AD compared to aMCI or HC. Systolic, mean and diastolic blood pressure (S/M/D BP) and cerebral blood flow velocity (CBFV) in the PCA-P2 during baseline, i.e. resting supine for at least 5 minutes, were similar for all groups.

### **VEFR acquisition**

TCD measurements were performed using a Multidop X4 Doppler device (® DWL Compumedics, Sipplingen, Germany). A 2MHz probe was mounted on a headband and CBFV was measured in the left PCA-P2 and right middle cerebral artery (MCA). The Doppler device was coupled to a data acquiring computer, (Task Force Monitor, ® CNSystems, Graz, Austria) enabling simultaneous recording of CBFV, ECG and beat-to-beat arterial finger BP. Data were recorded during repetitive visual stimulation cycles of 40s 'on' /20s 'off' using a colour cartoon video on an LCD-screen in a dimly lit room. This block stimulus was applied until at least 10 artefact-free 'on-off' cycles were recorded.

Mean CBFV and BP data were used for analysis. Absolute CBFV values were transformed into relative CBFV changes according to:

$$\Delta_V = \frac{V - V_0}{V_0} \times 100\% \quad (1)$$

where  $\Delta_V$  represents the % change in CBFV relative to baseline,  $V$  the mean CBFV during stimulation, and  $V_0$  the baseline CBFV during 10 seconds rest period preceding stimulation. The TCD data of 10 cycles were on-stimulus-locked averaged to obtain a characteristic VEFR.

### **VEFR quantification**

#### ***Time domain analysis***

Figure 1 shows a typical example of a VEFR. Amplitude/time-characteristics, i.e. the maximum relative velocity change during stimulation,  $\Delta_{V,max}$  (averaged over an epoch of 2s around the maximum velocity),  $t_{max}$  (time point corresponding to the maximum velocity) and  $\Delta_{V,end}$  (the mean relative velocity change of the last 10s), were determined for all VEFRs.

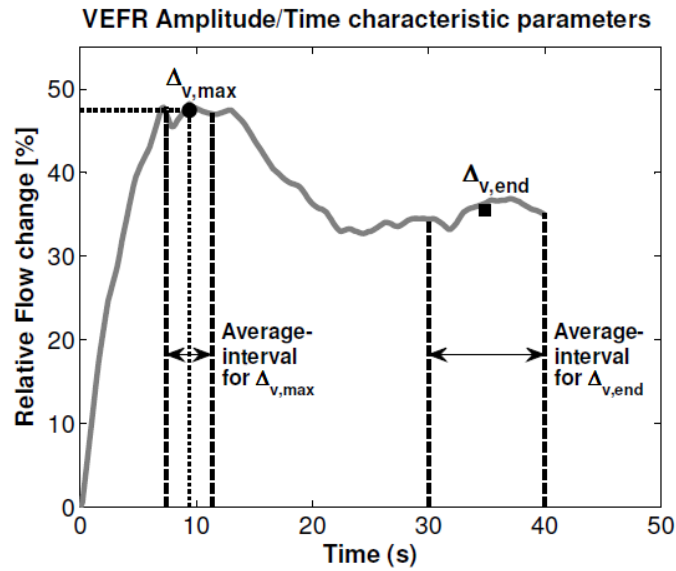


Figure 1. VEFR with amplitude-time characteristic parameters  $\Delta_{v,max}$ ,  $t_{max}$ ,  $\Delta_{v,end}$

#### Transfer function analysis: RG

To describe VEFR behaviour, two transfer function models i.e. RG and RGe were used as shown in figure 2. The concept for this method was introduced for describing cerebral autoregulation [20] and later adapted for NVC by Rosengarten [1, 2]. His model, denoted as RG, (figure 2 top) can be described in the Laplace domain as

$$H_{NVC}(s) = \frac{K(1 + T_v s)}{\frac{s^2}{\omega_0^2} + 2\zeta \frac{s}{\omega_0} + 1} \quad (1)$$

where gain  $K$  specifies the % CBFV difference between stimulus-on and -off period and  $\omega_0$  characterizes the natural oscillation frequency of the control system as if it was undamped.  $T_v$  represents the initial rise time that modulates the initial flow response and  $\zeta$  the system's damping.

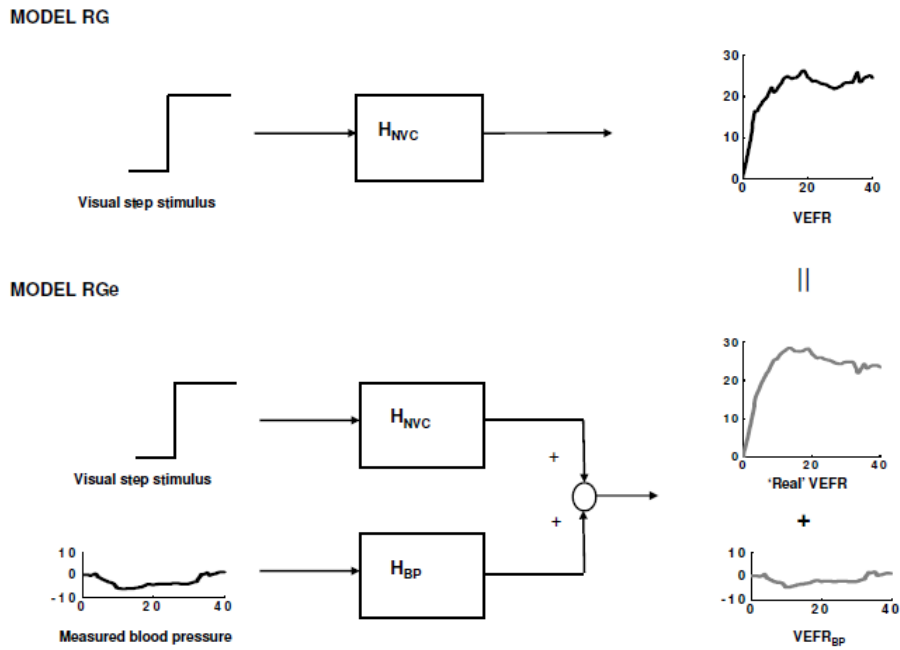


Figure 2. Rosengarten (RG) and extended Rosengarten model (RGe) to describe VEFR behaviour. The RG-model considers the VEFR as the output of a visual step stimulus of control system  $H_{NVC}$ . The RGe-model assumes the VEFR to be the sum of the visual step stimulus induced flow response of  $H_{NVC}$  ( $VEFR_{BP}$ ) and the blood pressure induced velocity response of dynamic cerebral autoregulation control system  $H_{BP}$  ( $FR_{BP}$ ).

### Transfer function analysis: RGe

RGe (figure 2 bottom) is an extension of RG to account for the contribution of BP variations to the VEFR. Figure 3 (top) shows an example of a beat-to-beat BP signal continuously recorded during a stimulation session. BP changes occur not only spontaneously but also time locked to the start of the stimulus (vertical dashed lines), resulting in a grand average net BP signal after stimulus-locked averaging (fig 3 bottom). Our working hypothesis is that such a stimulus-evoked BP response will lead to a BP induced flow response under control of cerebral autoregulation consequently contributing to the overall VEFR.

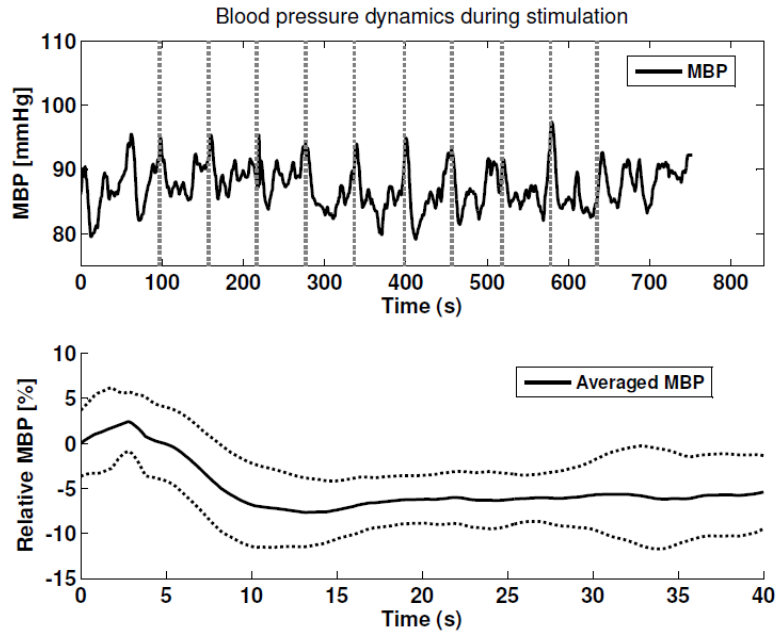


Figure 3. Example of a mean blood pressure measurement (MBP) during visual block stimulation (top) and the resulting visually-evoked blood pressure response after stimulus-locked averaging and standard deviations (bottom)

RGe considers the VEFR as the sum of the step response of RG ( $H_{NVC}$ ) and a BP induced flow velocity response ( $FR_{BP}$ ) occurring simultaneously and described by the dynamic CA pressure – flow transfer function ( $H_{BP}$ ). The  $H_{BP}$  part of RGe was adopted from Tiecks [21] and is equal to:

$$H_{BP}(s) = G_{CA} \left( 1 - \frac{K_{CA}}{\frac{s^2}{\omega_{0,CA}^2} + 2\zeta_{CA} \frac{s}{\omega_{0,CA}} + 1} \right) \quad (3)$$

where  $\omega_{0,CA}$  represents the time constant,  $\zeta_{CA}$  the damping and  $K_{CA}$  the gain of the CA system and  $G_{CA}$  an overall proportional gain (see figure 4).  $G_{CA}$  characterizes the amplification between the initial BP change and resulting CBFV change, whereas  $K_{CA}$  indicates to what extent the CA system is able to regulate CBFV back to its original value. Parameters  $\omega_{0,CA}$  and  $\zeta_{CA}$  describe response dynamics with  $\omega_{0,CA}$  the natural oscillation



time when  $H_{BP}$  would be undamped and  $\zeta_{CA}$  the extent to which this characteristic oscillation is damped.

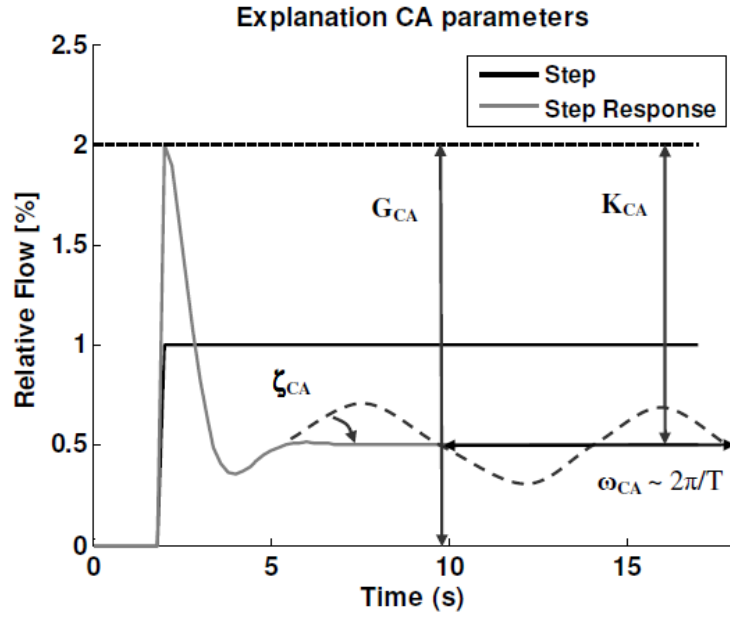


**Figure 4.** Step response characteristics of  $H_{BP}$  to illustrate meaning of parameters  $\omega_{CA}$ ,  $\zeta_{CA}$ ,  $G_{CA}$  and  $K_{CA}$ .

#### **VEFR model fitting and parameter precision**

The least square difference technique was used to minimize the curve fit difference between VEFR and model fit over the 'on' period. The mean square difference,  $\varepsilon_V^2$ , is calculated as follows:

$$\varepsilon_V^2 = \frac{1}{N} \cdot \sum_{i=1}^N (\Delta_{V_{i,m}} - \Delta_{V_i})^2 \quad (4)$$

with  $N$  the number of data points i.e. 200 (40s resampled with 5Hz),  $\Delta_{V_i}$  a VEFR data point and  $\Delta_{V_{i,m}}$  the corresponding optimal RG/RGe output. All data analysis was performed using the mathematical software Matlab (®The Mathworks Inc., Natick MA, USA).

To account for reliability of RG and RGe parameters, 95% confidence boundaries were calculated and the confidence interval width was used as reliability measure. The calculation is based on the Jacobian ( $J$ ) which expresses the change in the fit function value due to a change in the parameter value:

$$J = \frac{\partial \Delta_{V_i^*}}{\partial p_j} \quad (5)$$

with  $p_j$  the  $j$ th parameter of the total set. Given  $J$  and  $\varepsilon_V^2$ , the covariance matrix  $\Phi$  can be calculated [22]:

$$\Phi = \varepsilon_V^2 \cdot (J \cdot J^T)^{-1} \quad (6)$$

Parameter confidence limits were estimated from  $\Phi$  assuming a student's t inverse cumulative distribution function. Based on a 95% confidence level and 3 and 7 degrees of freedom for RG and RGe respectively, the statistical t-score,  $t$ , can be determined. With  $S$  the diagonal elements of  $\Phi$ , confidence boundaries  $C_b$  for a parameter  $x$  are given by:

$$C_b = x \pm t \cdot \sqrt{S_x} \quad (7)$$

$t \cdot \sqrt{S_x}$  represents half the width of the 95% confidence interval of parameter  $x$ .

Expression of this term relative to  $x$  yields:

$$C_i = \frac{t \cdot \sqrt{S}}{x} \cdot 100\% \quad (8)$$

$C_i$  is used as a measure for parameter estimation reliability. A criterion has to be set for the maximum  $C_i$  value for which a parameter value is judged to be reliable. For a  $C_i$  value of 100%, the estimated parameter value equals its spread resulting in a value of 0 for the low  $C_b, x - t \cdot \sqrt{S_x}$ .

This implies that the parameter may have no contribution in the model description. To exclude this possibility, the cut-off for  $C_i$  has been fixed on 100%. Only responses having  $C_i < 100\%$  for **all**  $H_{NVC}$  parameters are included in statistical analysis.

#### **VEFR behaviour: $T_v$ - $\zeta$ dynamics**

VEFR behavior will also be evaluated using  $T_v$  -  $\zeta$  plots. In our previous study [23], we identified 3 VEFR types with a different time shape i.e. normal, intermediate and slug-

gish. Normal VEFRs typically have an early overshoot and late saturation and  $T_v < 20$  and  $\zeta < 1$ . Aberrant VEFRs lack either one of these features resulting in critically overdamped behavior ( $\zeta > 1$ ). Intermediate VEFRs, lacking saturation, are accompanied by large  $T_v$ 's ( $> 20$ ), whereas sluggish VEFRs, lacking overshoot, by  $T_v$ 's  $< 20$ .

### **Statistics**

The Software Package for Social Sciences (SPSS Statistics version 17.0) has been used for statistical analyses. One-way Anova with Sidak correction has been applied to compare group demographics and Mann-Whitney-U test for amplitude-time characteristics and model parameters. A p-value  $< 0.05$  was regarded as significant.

### 5.3 Results

#### VEFR analysis WITHOUT BP consideration

##### Amplitude-time characteristics

Group-averaged amplitude/time-parameters values and standard deviations are listed in table 2a. No significant differences were found between groups. Group-averaged VEFRs have similar time courses (figure 5a).

Table 2. Group-averaged VEFR amplitude/time parameter values for measured VEFRs (A) based on all data (All) or data meeting the 100%-reliability criterion (Reliable) i.e. AD [n=8], MCI [n=10], HC [n=12]. Similarly, values are shown for blood pressure corrected VEFRs (B) i.e. AD [n=7], MCI [n=14], HC [n=13]

A. Measured VEFRs						
Data	$\Delta_{V,max}$ [%]		$t_{max}$ [s]		$\Delta_{V,end}$ [%]	
	All	Reliable	All	Reliable	All	Reliable
AD	37 ± 9	36 ± 8	20 ± 9	19 ± 9	30 ± 10	27 ± 10
MCI	33 ± 9	35 ± 9	18 ± 8	17 ± 9	26 ± 8	28 ± 8
HC	34 ± 13	34 ± 13	19 ± 9	15 ± 6	28 ± 14	26 ± 13
B. Blood pressure corrected VEFRs (by RGe-model)						
Data	$\Delta_{V,max}$ [%]		$t_{max}$ [s]		$\Delta_{V,end}$ [%]	
	All	Reliable	All	Reliable	All	Reliable
AD	37 ± 9	40 ± 9	17 ± 8	19 ± 10	30 ± 10	31 ± 12
MCI	34 ± 9	35 ± 9	18 ± 8	17 ± 8	26 ± 9	27 ± 9
HC	35 ± 14	35 ± 15	19 ± 9	17 ± 8	28 ± 15	28 ± 15

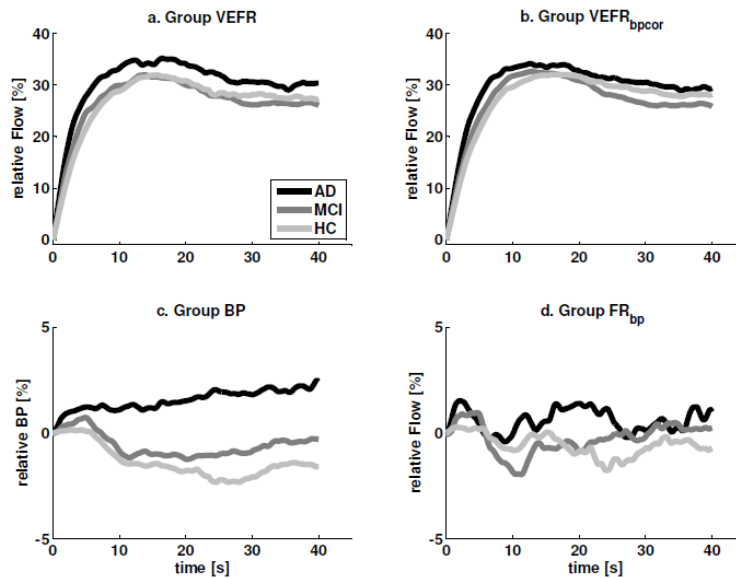
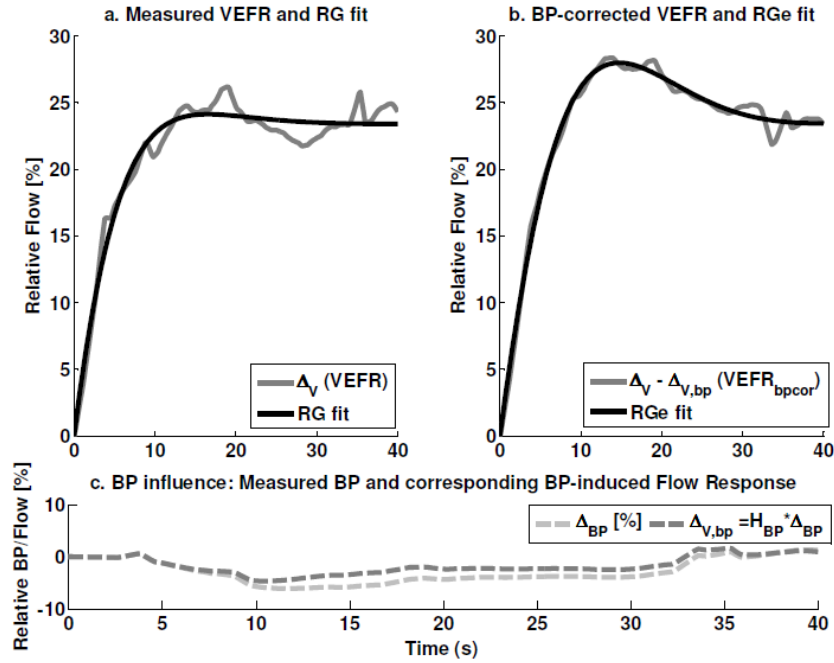


Figure 5. Group-averaged VEFR (a), BP corrected VEFs or VEFR<sub>BPCor</sub> (b), group-averaged BP response during visual stimulation (c), group-averaged BP - induced flow response or FR<sub>BP</sub> (d).

### RG fitting and reliability consideration

Figure 6a shows an VEFR example and its RG-fit. Median group RG parameter values and 25-75% percentiles are presented in table 3a. Damping  $\zeta$  is significantly increased in AD compared to HC.

Reliability consideration, i.e.  $C_i < 100\%$  for all 4 parameters, reduced the number of VEFR included in statistical analysis to 8/15 (AD: 53%), 10/17 (aMCI: 59%) and 12/18 (HC: 67%) in HC. Re-analysis of this subset did not yield significant differences between groups. Only  $\zeta$  is still significantly increased in AD compared to HC (0.84 vs. 0.63,  $p=0.031$ ). Group median parameter values and 25-75 percentiles are listed in table 3b.



**Figure 6.** a. Example of measured VEFR (gray) and its RG fit (black), b. resulting 'real' VEFR i.e. output of  $H_{nvc}$  part of RGe with step input (gray) and its RGe fit (black), c. corresponding measured BP response (dark gray) and resulting  $FR_{BP}$  i.e. output of  $H_{BP}$  part of RGe with BP as input (light gray).

Table 3. Medians (25<sup>th</sup>-75<sup>th</sup> percentiles) of parameter values based on RG model (top) and RGe model (bottom) for all data (A and C) and data meeting reliability criterion (B and D)

<b>RG – MODEL</b>			
<b>A. All Data</b>			
	<b>HC (n=18)</b>	<b>MCI (n=17)</b>	<b>AD (n=15)</b>
$\omega$	0.18 (0.15-0.26)	0.21 (0.11-0.27)	0.15 (0.14-0.33)
$\zeta$	0.71 (0.54-1.2)	0.83 (0.72-1.4)	1.2 (0.84-1.6)*
$T_v$	7.2 (2.7-10.8)	6.0 (3.6-30.5)	10.9 (2.1-203)
<b>K</b>	23.8 (14.2-37.0)	22.2 (16.9-27.4)	23.2 (11.6-29.2)
<b>B. Reliable Data</b>			
	<b>HC (n=12)</b>	<b>MCI (n=10)</b>	<b>AD (n=8)</b>
$\omega$	0.18 (0.15-0.22)	0.21 (0.14-0.22)	0.15 (0.14-0.25)
$\zeta$	0.63 (0.41-0.77)	0.77 (0.68-0.85)	0.84 (0.76-1.4) **
$T_v$	7.2 (3.4-8.7)	6.1 (5.6-17.0)	10.3 (5.3-33.7)
<b>K</b>	22.3 (14.9-35.4)	22.8 (20.4-29.2)	25.2 (19.5-35.0)
<b>RGe – MODEL</b>			
<b>C. All Data</b>			
	<b>HC [n=18]</b>	<b>MCI [n=17]</b>	<b>AD [n=15]</b>
$\omega_{BP}$	0.16 (0.13-0.26)	0.17 (0.14-0.20)	0.16 (0.09-0.31)
$\zeta_{BP}$	0.73 (0.58-1.3)	0.72 (0.63-0.86)	1.0 (0.75-1.6)
$T_{vBP}$	7.3 (1.6-19.7)	9.6 (6.4-17.1)	11.0 (1.9-43.2)
<b>K<sub>BP</sub></b>	23.9 (15.6-34.8)	22.7 (19.5-27.2)	24.8 (14.4-27.4)
<b>D. Reliable data</b>			
	<b>HC [n=13]</b>	<b>MCI [n=14]</b>	<b>AD [n=7]</b>
$\omega_{BP}$	0.16 (0.14-0.25)	0.17 (0.14-0.20)	0.21 (0.15-0.35)
$\zeta_{BP}$	0.63 (0.49-1.2)	0.66 (0.63-0.76)	0.76 (0.71- 1.0)
$T_{vBP}$	6.8 (2.7-9.7)	8.8 (6.4-15.7)	9.2 (1.7-14.7)
<b>K<sub>BP</sub></b>	25.5 (17.1-37.5)	23.2 (20.2-30.0)	25.9 (25.1-37.1)

**VEFR behaviour:  $T_v$  -  $\zeta$  dynamics**

Dynamic VEFR behavior may be classified by parameters  $T_v$  and  $\zeta$  [23]. Three classes of  $T_v$  -  $\zeta$  combinations were identified corresponding to three different VEFR types. First, the “normal” response (type I) with typically  $0 < \zeta < 1$  and  $T_v < 20$ . The other 2 types showed so-called critically damped behavior with  $\zeta > 1$  and were sub classified into intermediate ( $\zeta > 1$  and  $T_v > 20$ , type II ) and sluggish responses ( $\zeta > 1$  and  $T_v < 20$ , type III).

Figure 7 shows  $T_v$  and  $\zeta$  values of AD, aMCI and HC in a logarithmic plot normalized on reference values  $T_{v0}=20$  and  $\zeta_0=1$  and marked according to their reliability. All three aforementioned VEFR types are present in all three groups. Normal VEFRs are generally accompanied by reliable  $T_v$  and  $\zeta$ , whereas the type II and III often have unreliable  $T_v$  and/or  $\zeta$ .

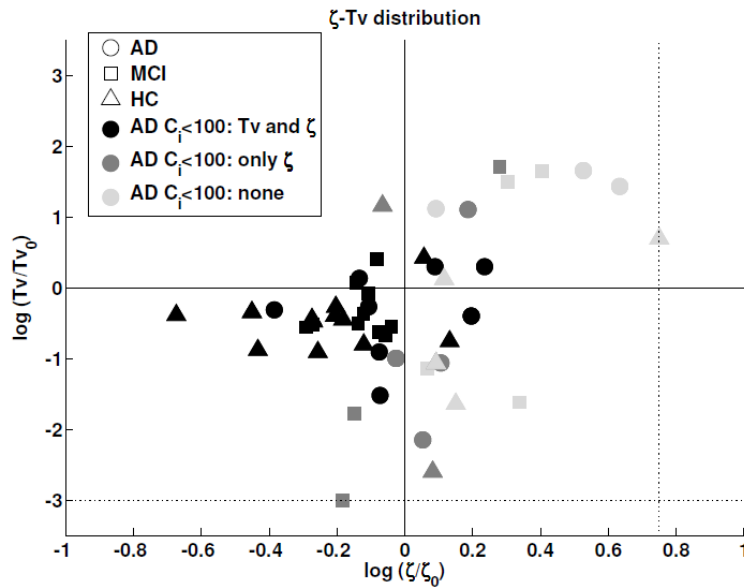


Figure 7. log-log plot of  $T_v$  -  $\zeta$  combinations in the three study groups. Reliability according to 100% criterion i.e.  $C_i < 100\%$  is regarded reliable. Parameter combinations in which both parameters are reliable are marked by a black filled symbol, only one of them reliable by a grey filled symbol, and both parameters unreliable with a white or open symbol (circle for AD, square for aMCI and triangle for HC group). The graph has been clipped for  $\log(\zeta / \zeta_0)$  on a value of 0.75 and for  $\log(T_v / T_{v0})$  on -3 (dashed lines), outliers are displayed on this clip value.

**Amplitude-time characteristics for VEFRs with reliable RG parameters**

Repetition of time-domain analysis for VEFRs with a reliable RG parameter set showed no significant group differences. Mean values and standard deviations are shown in table 2a.

### **VEFR analysis WITH BP dynamics consideration**

Group-averaged stimulus locked BP responses were determined and are shown in figure 5c. In AD, a BP increase is visible as opposed to a decrease in aMCI and HC. The VEFRs were corrected for BP influence by application of RGe (subtraction of  $FR_{bp}$ , figure 2b) obtaining BP corrected VEFRs as shown in figure 5b ( $VEFR_{BPCOR}$ ). BP-induced flow responses,  $FR_{bp}$ , are shown (fig 5d).

#### ***Amplitude-time characteristics***

Group-averaged amplitude-time parameter values and standard deviations of BP corrected VEFRs are listed in table 2b. No significant differences are found between groups.

#### ***RGe fitting and reliability consideration***

An example of a BP-corrected VEFR and its RGe-fit is shown in figure 6b and corresponding BP and  $FR_{bp}$  in figure 6c. Group-averaged RGe parameters of the  $H_{NVC}$  part are shown in table 3c. No significant difference was found for  $\zeta_{bp}$  or other parameters.

Also RGe parameter values were checked on their reliability. The number of VEFRs accompanied by 4 reliable model parameters was 7/15 (47%) for AD, 14/17 (82%) for aMCI and 13/18 (72%) for HC. Group medians and 25/75 percentiles for the reliable responses are listed in table 3d. Group comparison of this subset again revealed no significant differences.

#### ***VEFR behaviour: $T_{v,bp}$ - $\zeta_{bp}$ dynamics***

Comparison of  $T_{v,bp}$  and  $\zeta_{bp}$  values to  $T_v$  and  $\zeta$  values show that some subjects changed from quadrant and/or reliability status due to BP correction. However, these individual shifts did not show a consistent tendency towards a specific quadrant or reliability status.

#### ***Amplitude-time characteristics VEFRs with reliable RGe parameters***

Repetition of time-domain analysis for VEFRs with reliable RGe parameter values showed no significant differences between groups. Mean values and standard deviations are shown in table 2b.



## 5.4 Discussion

### Main findings

Group-averaged VEFRs show a similar time course with similar amplitude-time-characteristics for AD, aMCI and HC. Application of RG revealed a significantly increased damping in AD compared to HC, whereas for RGe no significant differences in  $H_{NVC}$  parameters were observed. Findings remained unaffected by reliability consideration.

### Reliability

About 40% and 33% of the VEFRs analysed by respectively RG and RGe had at least one unreliable parameter value. Although reliability consideration did not affect (non-parametric) statistical outcomes, it has important consequences for the parameter distribution. For  $T_{v,bp}$ , for example, group means decrease substantially after reliability consideration, i.e. AD 169 to 10 and HC 62 to 9s. Also,  $\zeta$  and  $T_v$  ranges become considerably narrowed (figure 8a and b), enhancing the confidence by which a measurement can be allocated to one group or the other.

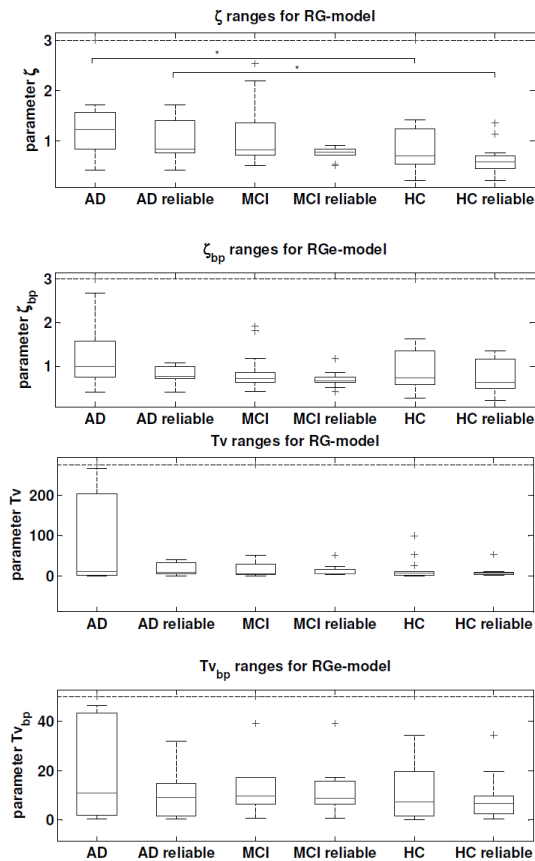


Figure 8. Effect of reliability consideration on parameter ranges of  $\zeta$  and  $\zeta_{bp}$  (a) and of  $T_v$  and  $T_{v,bp}$  (b). The graphs have been clipped for  $\zeta$  and  $\zeta_{bp}$  on a value of 3 and for  $T_v$  and  $T_{v,bp}$  on 60 (dashed lines), extreme values are displayed on the clip value.

In particular VEFRs with extreme parameter values become excluded. Remarkably,  $T_v - \zeta$  combinations are in general unreliable when  $T_v$  attains extreme values (see figure 7). Roughly, 2 cases are distinguishable: unreliable  $T_v - \zeta$  values lie either in the upper right quadrant where  $T_v$  is large, i.e.  $\log(T_v/T_{v0}) > 0$  and  $T_v > 20$  (intermediate behaviour), or below the horizontal line where  $\log(T_v/T_{v0}) < -1$  or  $T_v < 2$  (subgroup of sluggish behaviour). Thus, aberrant VEFRs seem prone to be accompanied by RG fits with unreliable parameter values.

Unreliability may result from the least squares search in the fitting procedure in which model limits may be approached. To model the non-saturation of intermediate VEFRs, a fast initial upstroke has to be combined with a very slow oscillation. The fitting routine is forced to make a trade-off between these contradictory requirements resulting in unreliable parameter values. The subgroup of sluggish VEFRs have in common that they saturate very fast. The course of these fits, i.e. model outputs, resembles the step input, suggesting a linear input-output relation. This can be obtained in case  $H_{NVC}$  would reduce to  $K$ , which applies either when  $T_v \rightarrow 0$  and  $\omega_0 \rightarrow \infty$  or when  $T_v$  equals  $2\zeta/\omega_0$  and  $\omega_0 \rightarrow \infty$  (see eq. 1). Based on obtained parameter values the second case does not apply, implying that the first case is valid i.e. the model approaches its limits.

To prevent unreliability of model parameters, it is crucial to determine whether aberrant VEFRs result from procedural aspects or reflect physiological behavior. Optimization of the experimental set-up may improve measurement accuracy and reduce VEFR variance. Examples of optimization measures are prolongation of stimulus-on period to prevent non-saturation and EOG recording to determine precisely the moment at which the stimulus is 'on' to minimize trigger jitter due to uncertainty around the exact moment of eyes opening. If aberrant VEFRs are physiological, the models used in this study may not be completely adequate to describe their behavior. It would make sense to incorporate the functioning and influence of other physiological systems on VEFR establishment. The most obvious physiological systems and their measurable output are baroreflex (heart rate) and ventilation/ pH balance ( $CO_2$ ).

#### **BP variation**

The difference in study outcomes for RG and RGe implies that either BP responses or CA action might differ between AD and HC. Figure 5c shows a visually-evoked BP increase in AD in contrast to a marked decrease in aMCI and HC. Inspection of individual BP responses showed that AD BP responds to visual stimulation by an increase or no change, aMCI by no change or decrease and HC mainly by decrease. For better understanding of these relationships, mechanisms underlying BP responses deserve closer consideration. A BP response may result directly from visual stimulation or indirectly by triggering of mechanisms with a general influence on BP. The possible presence of a non-specific general effect of visual stimulation e.g. arousal, attention or vigilance has also been suggested to explain the observed small MCA flow increase during visual stimulation by some authors [24,25]. Our findings support that BP predominantly responds to visual stimulation, but more conclusive evidence about its responsiveness in different conditions regarding e.g. vascular reserves, emotional or behavioral status is required. Preliminary findings of an ongoing study in our cohort reveal a significantly

decreased baroreflex sensitivity in AD favoring a vascular origin (collaboration JC Claassen group, UMC St Radboud Nijmegen, not published yet).

Also, individual variability in BP fluctuations in general, i.e. not related to group, may explain the difference in study outcomes for RG and RGe. BP fluctuations during visual stimulation trigger CA action resulting in a subject-specific  $FR_{BP}$  i.e. BP correction effect. Individual variations can be ascribed to multiple sources of variance because of the complex interplay of different physiological systems.

Mean BP and CBFV values were used to compare RG and RGe outputs for investigation of blood pressure influence on VEFRs. It can be argued, however, that systolic CBFV responsiveness seems less dependent on blood pressure than diastolic or mean CBFV responsiveness to visual stimulation or orthostatic/blood pressure induced changes [26, 27]. On the other hand, static and dynamic cerebral autoregulation are defined as CBF(V) changes following a change in mean arterial blood pressure or cerebral perfusion pressure [28, 29, 30]. To elucidate whether a different blood pressure contribution is found for peak-systolic sampled in contrast to time-averaged sampled (i.e. mean) beat-to-beat values, we compared RG and RGe model outputs of a large study cohort [n=72] consisting of subjects with diverse age and pathology based on systolic and mean values. Fit errors between VEFRs and RGe outputs appeared to be significantly lower compared to those for RG outputs both for mean ( $0.8 \pm 0.6$  vs.  $2.4 \pm 2.8$ ,  $p < 0.001$ ) and systolic values ( $1.5 \pm 1.2$  vs.  $2.2 \pm 2.6$ ,  $p < 0.001$ ) [33]. Although the effect was more pronounced for mean than systolic values, this suggests that blood pressure variations should be accounted for irrespective of the chosen sampling time point within the heart cycle.

#### **Choice of blood pressure correction procedure**

Very recently, Panerai and coworkers [8] identified and removed the influence of BP and end-tidal  $CO_2$  to motor induced changes in CBFV. They state that this additional post-processing step should lead to more robust estimates of NVC and better understanding of its physiological covariates. Indeed, the study provides supporting evidence for the influence of circulatory peripheral changes on measures of NVC following sensorimotor manoeuvres [8]. These findings stress the relevance of this topic and prompt us to discuss Panerai's findings in the light of our study.

Although both the study of Panerai and co-workers [8] and our study were aimed at retrieving the unpolluted flow response originating directly from the stimulus to ensure pure NVC description, different approaches are chosen for realizing this. Panerai adopted a multivariate autoregressive moving average (ARMA) model with 3 inputs (stimulus,  $etCO_2$  and BP), whereas we employed a control system model with 2 inputs (stimulus, BP) to describe the CBFV output. We departed from current control system practice for development of a blood pressure correction procedure. Hereto, we modelled the influence of beat-to-beat BP variation on CBFV via the system of dynamic cerebral autoregulation. This means that we made assumptions regarding the relation between BP and CBFV but we based this on a well-accepted model for cerebral autoregulation introduced by Tiecks et al [21]. Panerai and co-workers on the other hand, did not restrict their model by such assumptions which enables quantification of the ratio of input to output variance. However, their approach does not allow for linkage of effects to control system parameter changes which would assist in hypotheses genera-

tion for (patho-)physiological explanation. Future comparison of blood pressure contribution as found by the model of Panerai and by our model might reveal the extent to which both models agree in blood pressure contribution identification giving rise to increased reliability.

### ***Physiology***

The significant increase in AD damping compared to HC (RG) disappeared when accounting for BP variation (RGe). Previously, significantly increased VEFR damping was found in non-medicated AD which normalized after cholinesterase inhibitor treatment with donepezil or rivastigmine [13, 14]. Cholinesterase inhibitors promote acetylcholine availability in the cholinergic pathways by inhibiting its breakdown [14]. Most of our AD received cholinesterase inhibitors, but showed nevertheless increased damping. This discrepancy may be due to differences between studies in patient characteristics e.g. use of other medication. Alternatively, neurovascular coupling may be unaffected in AD implying that the finding of increased damping by other studies may have resulted from neglecting BP influence. This explanation is supported by the spatial progression path of AD atrophy, which often starts in medial temporal lobes, spreads to posterior temporal and parietal lobes and eventually to frontal lobes [31]. Occipital lobes are unlikely to be affected in the disease stage of our population. Even in the tempo-parietal area of our AD group, CA integrity is preserved [32]. Peripheral resistance was significantly increased, but compliance was similar to HC. In view of this, neurovascular coupling is conceivably preserved in AD.

### **5.5 Conclusion**

This study shows that neglecting reliability and BP dynamics, can lead to misinterpretations when studying neurovascular coupling. Although reliability consideration did not affect study outcomes, it did decrease parameter variability substantially. Accounting for BP dynamics reverses study conclusions from altered to normal neurovascular coupling in AD. Both parameter reliability and BP dynamics should therefore be included in VEFR analysis. The individual variability in VEFRs and BP variations request an approach with a stronger link to physiology e.g. development of physiology-based models incorporating interacting physiological systems. This may reduce VEFR variance, increase parameter reliability and enable linkage of behavior to vascular properties. It would enable us to reveal the 'real' VEFR reflecting only neurovascular coupling action.

### ***Acknowledgements***

Research supported by Internationale Stichting Alzheimer Onderzoek (ISAO) grant # 06518 to JR.

## References

- [1] Rosengarten B, Huwendiek O, Kaps M, Neurovascular coupling and cerebral autoregulation can be described in terms of a control system. *Ultrasound in medicine & biology* 2001;27:189-93.
- [2] Rosengarten B, Huwendiek O, Kaps M, Neurovascular coupling in terms of a control system: validation of a second-order linear system model. *Ultrasound in medicine & biology* 2001;27:631-5.
- [3] Trillenber P, Eggers J, Steffen J, Seidel G, Reliability of modeling evoked flow responses. *Ultraschall Med* 2008;29:611-7.
- [4] Ainslie PN, Ogoh S, Regulation of cerebral blood flow in mammals during chronic hypoxia: a matter of balance. *Experimental physiology* 2009;95:251-62.
- [5] Duschek S, Heiss H, Schmidt MFH, Werner NS and Schuepback D. Interactions between systemic hemodynamics and cerebral blood flow during attentional processing. *Psychophysiology* 2010; iv:i-iii.
- [6] Moody M, Panera RG, Eames PJ, Potter JF. Cerebral and systemic hemodynamic changes during cognitive and motor activation paradigms. *Am J of Physiol Regul Integre Comp Physiol* 2005; 288:R1581-88.
- [7] Panerai RB, Moody M, Eames PJ, Poter JF. Cerebral blood flow velocity during mental activation: interpretation with different models of the passive pressure-velocity relationship. *Journal of Applied Physiology* 2005; 99: 2352-62.
- [8] Panerai RB, Salinet ASM, Robinson TG. Contribution of arterial blood pressure and PaCO<sub>2</sub> to the cerebrovascular responses to moto stimulation *Am J Physiol Heart Circ Physiol* 2012; 302: H459-66.
- [9] Iadecola C, Neurovascular regulation in the normal brain and in Alzheimer's disease. *Nature reviews* 2004;5:347-60.
- [10] de la Torre JC, Alzheimer disease as a vascular disorder: nosological evidence. *Stroke; a journal of cerebral circulation* 2002;33:1152-62.
- [11] Asil T, Uzuner N, Differentiation of vascular dementia and Alzheimer disease: a functional transcranial Doppler ultrasonographic study. *J Ultrasound Med* 2005;24:1065-70.
- [12] Gucuyener DO, Yenilmez C, Ayranci U, Ozdemir F, Uzuner N, Ozkan S, Kaptanoglu C, Ozdemir G, An analysis of changes in cerebral blood flood velocities in depressive pseudo-dementia and Alzheimer disease patients. *The neurologist* 2010;16:358-63.
- [13] Rosengarten B, Paulsen S, Burr O, Kaps M, Neurovascular coupling in Alzheimer patients: effect of acetylcholine-esterase inhibitors. *Neurobiology of aging* 2009;30:1918-23.
- [14] Rosengarten B, Paulsen S, Molnar S, Kaschel R, Gallhofer B, Kaps M, Acetylcholine esterase inhibitor donepezil improves dynamic cerebrovascular regulation in Alzheimer patients. *Journal of neurology* 2006;253:58-64.
- [15] Association A, ed, *Diagnostic and Statistical Manual of Mental Disorders*.. American Psychiatric Association, Washington, DC 1994.
- [16] McKhann G, Drachman D, Folstein M, Katzman R, Price D, Stadlan EM, Clinical diagnosis of Alzheimer's disease: report of the NINCDS-ADRDA Work Group under the auspices of Department of Health and Human Services Task Force on Alzheimer's Disease. *Neurology* 1984;34:939-44.
- [17] Roman GC, Tatemichi TK, Erkinjuntti T, Cummings JL, Masdeu JC, Garcia JH, Amaducci L, Orgogozo JM, Brun A, Hofman A, et al., Vascular dementia: diagnostic criteria for research studies. Report of the NINDS-AIREN International Workshop. *Neurology* 1993;43:250-60.

- [18] Petersen RC, Smith GE, Waring SC, Ivnik RJ, Tangalos EG, Kokmen E, Mild cognitive impairment: clinical characterization and outcome. *Archives of neurology* 1999;56:303-8.
- [19] Fazekas F, Chawluk JB, Alavi A, Hurtig HI, Zimmerman RA, MR signal abnormalities at 1.5 T in Alzheimer's dementia and normal aging. *Ajr* 1987;149:351-6.
- [20] Folstein MF, Folstein SE, McHugh PR, "Mini-mental state". A practical method for grading the cognitive state of patients for the clinician. *Journal of psychiatric research* 1975;12:189-98.
- [21] Tiecks FP, Lam AM, Aaslid R, Newell DW, Comparison of static and dynamic cerebral autoregulation measurements. *Stroke; a journal of cerebral circulation* 1995;26:1014-9.
- [22] Šimůnek J, Hopmans JW, Parameter Optimization and Nonlinear Fitting In: *Methods of Soil Analysis, Part 1*, Eds. J. H. Dane and G. C. Topp, Third edition, SSSA, Madison, WI, 2002;Physical Methods, Chapter 1.7:139-57.
- [23] Martens EG, Peeters LL, Gommer ED, Mess WH, van de Vosse FN, Passos VL, Reulen JP, The visually-evoked cerebral blood flow response in women with a recent history of preeclampsia and/or eclampsia. *Ultrasound in medicine & biology* 2009;35:1-7.
- [24] Aaslid R. Visually evoked dynamic blood flow response of the human cerebral circulation. *Stroke* 1987; 18:771-5.
- [25] Urban PP, Allardt A, Tettenbom B, Hopf HC, Pfennigsdorf S, Lieb W. Photoreactive flow changes in the posterior cerebral artery in control subjects and patients with occipital lobe infarction. *Stroke* 1995; 26:1817-9
- [26] Azevedo E, Rosengarten B, Santos R, Freitas J, Kaps M. Interplay of cerebral autoregulation and neurovascular coupling evaluated by functional TCD in different orthostatic positions. *J Neurol* 2007; 254:236–41.
- [27] Rosengarten B, Kaps M. Peak systolic velocity Doppler index reflects most appropriately the dynamic time course of intact cerebral autoregulation. *Cerebrovasc Dis* 2002; 13:230–234.
- [28] Panerai RB. Transcranial Doppler for evaluation of cerebral autoregulation. *Clin Auton Res* 2009; 19:197-211.
- [29] Paulson OB, Strandgaard S, Edvinsson L. Cerebral Autoregulation. *Cerebrovascular Brain Metab Rev* 1990; 2(2):161-192
- [30] Aaslid R, Lindegaard KF, Sorteberg W, Hornes H. Cerebral autoregulation dynamics in humans. *Stroke* 1989; 20:45-52.
- [31] Whitwell JI. Progression of atrophy in Alzheimer's disease and related disorders. *Neurotoxicity research* 2010; 18:339-46.
- [32] Gommer ED, Martens EGHJ, Aalten P, Shijaku E, Verhey RFJ, Mess WH, Ramakers IHGB, Reulen JPH. Dynamic cerebral autoregulation in subjects with Alzheimer's disease, mild cognitive impairment and controls: evidence for increased peripheral vascular resistance. *Journal of Alzheimer's disease* 2012; 30(4), in press.
- [33] Gommer ED, Bogaarts JG, Martens EGHJ, Mess WH, Reulen JPH. Visually evoked blood flow responses and interaction with dynamic cerebral autoregulation: correction for blood pressure variation 2012, submitted

# CHAPTER 6

## Physiology-Based Modeling of the Visually-Evoked Blood Flow Response

Partly based on:

Spronck B, Martens EGHJ, Gommer ED, Van de Vosse FN. *Cerebral blood flow fluctuations induced by autoregulation and neurovascular coupling described by a single physiological model*. Submitted (2012)



## Abstract

Control system analysis of visually-evoked blood flow responses (VEFRs) is often applied to quantitatively assess neurovascular coupling function. Although control system models enable description of VEFR behaviour by patient-specific model parameter values, they do only provide linkage of VEFR behaviour to control system properties but not to physiological properties. Previous investigations, however, emphasize the need for a model incorporating physiological features, especially since other physiological systems such as cerebral autoregulation may influence VEFR establishment. In this study, preliminary results are reported for the application of a newly developed lumped parameter model of the visual cortex vasculature to previously described three different VEFR types. In this new model, regulatory processes i.e. neurogenic, metabolic, myogenic and shear stress mechanisms, act on smooth muscle tone which inherently leads to adjustment of microcirculatory resistance and compliance. This allows the study of effects of (patho-)physiological changes on the VEFR. It may be concluded that the model provides an improved link between VEFR and physiology. In addition, the preliminary results show that our physiology-based model can describe the representatives of the three different VEFR types reasonably well obtaining physiologically plausible parameter values.

## 6.1 Introduction

Regulation of cerebral blood flow may be disturbed in several pathologies, e.g. hypertension and Alzheimer's disease [14, 18]. Underlying pathophysiological mechanisms are not elucidated yet. Function of cerebrovascular control mechanisms, such as cerebral autoregulation (CA) and neurovascular coupling (NVC), is usually assessed by determination of their input-output relationship i.e. transfer function analysis (TFA). CA transfer function is assessed by spectral cross-correlation between its input, measured finger blood pressure, and its output, cerebral blood flow velocity measured by transcranial Doppler ultrasonography (TCD), relative to spectral auto-correlation of its input [36]. For NVC assessment, the measured visually-evoked blood flow response (VEFR) is described by the step response output of a 2<sup>nd</sup> order control system model with a (visual stimulus) step as input [28, 29]. In this way, patient-specific parameter values are obtained as quantitative measures for their regulatory capacity e.g. gain and phase for CA and amongst others damping and initial rise time for NVC. An important limitation of TFA is, however, that it is purely descriptive without a well-defined relation to physiology. Application of a physiology-based mathematical model which is able to describe processes leading to vascular regulation by physic laws, would provide more insight in CA and NVC function both in normal and pathophysiological conditions.

The complexity of cerebrovascular control is reflected by the different processes and factors proposed to be involved [26]. Neural activation, pressure fluctuations compensated by myogenic action, metabolic changes and flow-induced changes in shear stress may all trigger different simultaneously acting mechanisms which together maintain local homeostasis and energy balance. A detailed description of processes, starting from molecular changes on cell-level to changes in smooth muscle tone on pial artery level, has been presented by Banaji et al [2]. Their model is intended as a virtually complete background relating the majority of factors involved in cerebrovascular control by phenomenological descriptions. Parameter ranges are, however, not provided, which hampers usability for our application.

Mathematical modeling can be applied to describe a system by its system properties on which physic laws are applicable such as mass conservation and momentum balance. Regarding cerebrovascular control, mathematical modeling has gained considerable attention in the field of functional imaging to explain fMRI Blood Oxygen Level Dependent (BOLD) responses. Buxton et al. [5] put a fundament by introducing their so-called 'balloon-model' in which mainly flow-volume relationships and oxygen dynamics have been included. Boas [4] has integrated this in a vascular network model consisting of an arterial, capillary and venous segment to investigate spatio-temporal aspects of the BOLD response. This has been extended to a lumped parameter model to describe the influence of CA on the BOLD-response [27]. Aforementioned models provide also only phenomenological descriptions i.e. they are not applicable to patient-specific data.

For the description of TCD velocity measurements, Ursino and Lodi [34] provided a solid base by the development of a multiple-element windkessel model of the brain circulation. They validated their model with physiological experimental data from literature and applied it to patient data obtained during neurosurgery. Olufsen et al. [25] used a simple three-element windkessel model, consisting of two resistors representing sys-

temic and peripheral resistance, and a capacitor to describe vascular compliance, in a different context i.e. to explain TCD measurements gathered during (gradual) change in orthostatic conditions. Although the authors could not ascribe their observations directly to physiological changes, the model provided them with a tool to test hypotheses of how the observed data could be explained in a physiologically plausible way. A similar lumped parameter model was recently used to study changes in the CA mechanism when blood pressure is increased stepwise [36]. This study revealed that transfer function phase shows bimodal behavior as a function of compliance which may explain why CA data evaluated by TFA show conflicting results.

Lumped parameter models have not been used so far to describe visually-evoked blood flow responses (VEFRs) reflecting NVC function. In previous studies, we investigated NVC function of former (pre)eclamptics [21] and Alzheimer patients by VEFR measurement [22]. In both studies, we found three types of VEFRs which were not exclusively related to pathological or healthy condition. These VEFR types include the so-called normal VEFR showing an overshoot in the first 20s of stimulation and saturation in the last 20s of stimulation, the intermediate VEFR lacking saturation in the last 20s and the sluggish VEFR without an overshoot in the first 20s. Recently, a lumped parameter model of the vasculature of the visual cortex including different processes to adapt smooth muscle tone has been designed in our group [32]. This lumped parameter model is based on Ursino's model consisting of an arterial segment (PCA), a microcirculatory segment including adjustable vascular properties (visual cortex vasculature) and a venous segment. The microcirculatory segment parameters, reflecting vascular resistance and compliance, can vary through changes in smooth muscle tone induced by different directly or indirectly activated physiological processes.

The aim of this study is to examine the ability of our lumped parameter model to describe the different VEFR types. In addition, the potential use of the model will be demonstrated by testing hypotheses regarding which combination of regulatory processes will yield the best fit for a particular VEFR type. To this end, we will first explore model settings to investigate whether VEFR behaviour can be described by physiologically defensible model parameter values. Then different combinations of possible underlying processes will be applied to gain more insight in their possible contributions to any of the VEFR types.

## 6.2 Methods

### Lumped parameter model

To study cerebral blood flow regulation, a lumped parameter model has been developed in our group, describing the P2 segment of the PCA and its distal vessels, up to the large cerebral veins [32]. The model consists of three lumped parts: the PCA, the arteriolar and microcirculation, and the venous circulation (see figure 1). The physics and physiological base underlying the model will be largely explained here, but we refer to [32] for the details. Also, fixed parameter values are specified in Table 1.

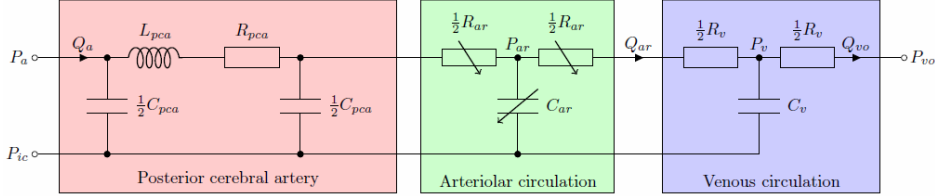


Figure 1: Lumped parameter model of the posterior cerebral artery and its distal arteriolar and venous beds.  $P_a$ ,  $P_{ic}$  and  $P_{vo}$  denote the arterial, intracranial and venous output blood pressure, respectively.  $P_{ar}$  and  $P_v$  are the central arteriolar and venous pressure, respectively.  $Q_a$  is the PCA inflow.  $Q_{ar}$  and  $Q_{vo}$  are venous in- and outflow, respectively.  $C_{pca}$ ,  $L_{pca}$  and  $R_{pca}$  represent PCA compliance, inertia and resistance, respectively.  $C_{ar}$  and  $R_{ar}$  are the arteriolar compliance and resistance, respectively.  $C_v$  and  $R_v$  denote the venous compliance and resistance, respectively. PCA is the posterior cerebral artery.

### Posterior cerebral artery

The PCA is modelled by an electrical analogue with parameters based on local geometrical and mechanical vessel properties. PCA resistance, i.e. its viscous resistance to blood flow, is represented by a resistor,  $R_{pca}$ , whereas PCA compliance, i.e. its blood storage capacity, is modelled by a capacitor,  $C_{pca}$ . The inertia of the blood, which can not be neglected in (larger) arteries as the PCA, is characterized by an inductor,  $L_{pca}$ . The total PCA compliance can be calculated assuming a thick-walled vessel with radius  $r_{pca}$ , wall thickness  $h_{pca}$ , length  $l_{pca}$  and elastic modulus  $E_{pca}$ :

$$C_{pca} = \frac{3 \cdot \pi \cdot r_{pca}^2 \cdot \left( \frac{r_{pca}}{h_{pca}} + 1 \right)^2}{E_{pca} \cdot \left( \frac{2 \cdot r_{pca}}{h_{pca}} + 1 \right)} \cdot l_{pca} \quad (1)$$

conform [18]. The PCA's inertia is given by

$$L_{pca} = \frac{\rho_{blood}}{\pi \cdot r_{pca}^2} \cdot l_{pca} \quad (2)$$

With  $\rho_{Blood}$  the density of the blood. The resistance is calculated assuming Poiseuille flow:

$$R_{pca} = \frac{8 \cdot \eta_{blood}}{\pi \cdot r_{pca}^4} \cdot l_{pca} \quad (3)$$

Here  $\eta_{Blood}$  is the dynamic viscosity of the blood. Values for constant model parameters, amongst others  $E_{pca}$ ,  $h_{pca}$ ,  $\rho_{blood}$  and  $\eta_{blood}$ , are listed in Table 1.

### Venous circulation

Also the venous circulation is described by its electrical analogue, consisting of a (split) resistor to account for its viscous resistance and a capacitor to model its volume storage capacity. The parameters of the venous system are based on data from literature. Venous capacitance is 0.025 ml/mmHg, reflecting a venous RC-time ( $R_v C_v$ ) of 0.4s [34]. Venous resistance is 0.26 mmHg\*min/ml, leading to a venous pressure drop of 14 mmHg [34] at baseline flow ( $Q_{BL}=53$  ml/min, [23]).

### Arteriolar circulation

The electrical analogue of the arteriolar circulation consists of a resistance and capacitance. They are modelled as variable parameters since they need to be adjustable via stimulus-induced changes in arteriolar radius to enable VEFR description. Arteriolar radius may change in case arteriolar pressure and hence, smooth muscle tension will change. The relation between arteriolar wall tension ( $T_{ar}$ ), arteriolar radius ( $r_{ar}$ ) and arteriolar pressure ( $P_{ar}$ ) can be described by Laplace's law cf. [34]. Total arteriolar vessel wall tension ( $T_{ar}$ ) can further assumed to be the sum of elastic ( $T_{ar,e}$ ), muscular ( $T_{ar,m}$ ) and viscous ( $T_{ar,v}$ ) tensions [34]:

$$T_{ar} = P_{ar} \cdot r_{ar} - P_{ic} (r_{ar} + h_{ar}) = T_{ar,e} + T_{ar,m} + T_{ar,v} \quad (4)$$

With  $P_{ic}$  the intracranial pressure. Elastic tension is defined as

$$T_{ar,e} = \sigma_{ar,e} \cdot h_{ar} = \left( \sigma_{ar,e,0} \cdot \left( \exp\left( K_{ar,\sigma} \cdot \frac{r_{ar} - r_{ar,0}}{r_{ar,0}} \right) - 1 \right) - \sigma_{ar,coll} \right) \cdot h_{ar} \quad (5)$$

With  $\sigma_{ar,e}$  and  $\sigma_{ar,coll}$  the elastic stress and collagen fiber stress respectively. Subscript 0 refers to unstressed condition. Values for  $\sigma_{ar,e}$ ,  $\sigma_{ar,coll}$ ,  $K_{ar}$  and  $h_{ar}$  are listed in Table 1. Muscular tension can be described by

$$T_{ar,m} = T_{ar,max} \cdot \exp\left(-\left|\frac{r_{ar} - r_{ar,m}}{r_{ar,t} - r_{ar,m}}\right|^{n_{ar,m}}\right) \quad (6)$$

With  $n_{ar,m}$  a constant parameter for smooth muscle tension modelling cf. [34]. Subscripts t and m refer to instantaneous and muscular component of defined parameters respectively. Again, values for constant model parameters  $r_{ar,m}$ ,  $r_{ar,t}$  and  $n_{ar,m}$  are listed in Table 1. The viscous tension is defined as

$$T_{ar,v} = \sigma_{ar,v} \cdot h_{ar} = \frac{\eta_{ar}}{r_{ar,0}} \cdot \frac{dr_{ar}}{dt} \cdot h_{ar} \quad (7)$$

With  $r_{ar,0}$  the radius in unstressed condition. Arteriolar wall thickness ( $h_{ar}$ ) in these equations is formulated by

$$h_{ar} = \sqrt{r_{ar}^2 + 2 \cdot r_{ar,0} \cdot h_{ar,0} + h_{ar,0}^2} - r_{ar} \quad (8)$$

With  $h_{ar,0}$  the wall thickness in unstressed condition. CBF is regulated by adjusting  $T_{ar,max}$  in (6), according to

$$T_{ar,max} = T_{ar,max,0} \cdot (1 + M_{vsm}) \quad (9)$$

$M_{vsm}$  is a measure of smooth muscle activation, which varies from -1 to 1, representing maximum vasodilation and -constriction, respectively.  $T_{ar,max,0}$  is constant (Table 1).

Arteriolar resistance ( $R_{ar}$ ) and volume ( $V_{ar}$ ) are assumed to scale with  $r_{ar}^{-4}$  and  $r_{ar}^{-2}$ , respectively:

$$R_{ar} = \frac{K_{R,ar}}{r_{ar}^4} \quad (10)$$

and

$$V_{ar} = K_{V,ar} \cdot r_{ar}^2 \quad (11)$$

$K_{R,ar}$  is chosen such that, for baseline arteriolar pressure and radius,  $R_{ar}$  leads to a baseline flow ( $Q_{BL}$ ).  $K_{V,ar}$  ensures that baseline capacitance corresponds to an arteriolar RC-time ( $R_{ar} * C_{ar}$ ) of 1s [27].

### 2.1.2 Regulation

CBF regulation is performed by varying  $M_{vsm}$  in (9), which in turn affects smooth muscle tension.  $M_{vsm}$  is coupled to  $M_{vsm,lin}$  via a sigmoidal function:

$$M_{vsm} = \frac{e^{2 \cdot M_{vsm,lin}} - 1}{e^{2 \cdot M_{vsm,lin}} + 1} \quad (12)$$

$M_{vsm,lin}$  is the summation of influences of myogenic ( $x_{myo}$ ), shear stress based ( $x_{shear}$ ), neurogenic ( $x_{neuro}$ ), and metabolic ( $x_{meta}$ ) regulation, multiplied by their respective gains ( $G_{myo}$ ,  $G_{shear}$ ,  $G_{neuro}$  and  $G_{meta}$ ):

$$M_{vsm,lin} = G_{myo} \cdot x_{myo} + G_{shear} \cdot x_{shear} + G_{neuro} \cdot x_{neuro} + G_{meta} \cdot x_{meta} \quad (13)$$

An overview of regulation is depicted in figure 3. In all four regulatory mechanisms, the regulatory state ( $x_{regulation}$ ) is coupled to the regulatory activation ( $A_{regulation}$ ) via first-order behaviour. An extra parameter,  $x_{initial}$ , may be used to correct the initial flow when it has not been measured in baseline condition e.g. with the subject's eyes open instead of eyes closed..

#### Myogenic regulation

Activation of myogenic regulation ( $A_{myo}$ ) is based on the deviation of the current arteriolar wall tension,  $T_{ar}$ , from a reference tension,  $T_{myo,0}$ , and is normalised by a normalisation tension,  $T_{myo,s}$  [6, 7, 31]:

$$A_{myo} = \frac{T_{ar} - T_{myo,0}}{T_{myo,s}} \quad (14)$$

$T_{myo,0}$  is chosen to be the tension at baseline pressure for  $M_{vsm} = 0$ .  $T_{myo,s}$  is a normalisation tension for obtaining a dimensionless  $A_{myo}$ , and is chosen to be 0.3 mmHg\*cm. For myogenic regulation, the coupling of the regulatory state to the regulatory activation equates to

$$\frac{dx_{myo}}{dt} = \frac{A_{myo} - x_{myo}}{\tau_{myo}} \quad (15)$$

where  $\tau_{myo}$  is the time constant governing myogenic regulation.

### Shear stress based regulation

Shear stress is caused by viscous friction of blood and the vessel wall. If viscosity-dominated (Poiseuille) flow is assumed, wall shear stress ( $\tau_w$ ) is quantified by

$$\tau_w = \frac{4 \cdot \eta \cdot Q}{\pi \cdot r^3} \quad (16)$$

in which  $Q$  and  $r$  are blood flow and vessel radius, respectively.

From (16), it can be inferred that shear stress scales with  $Q/r^3$ . Shear stress activation is therefore chosen as

$$A_{shear} = K_{shear} \cdot \frac{Q_{ar}}{r_{ar}^3} - 1 \quad (17)$$

$K_{shear}$  is chosen such that, at baseline,  $A_{shear} = 0$ .

$x_{shear}$  is coupled to  $A_{shear}$  via first-order time behaviour, analogous to (15).

### Neurogenic regulation

Neurogenic regulation, together with metabolic regulation, is assumed to be determined by the amount of visual cortex activation. For the sake of simplicity, neurogenic activation ( $A_{neuro}$ ) is assumed to change stepwise at eye-opening, cf. [28, 29]. Neurogenic regulation is then again described by a first-order response, analogous to (15).

### Metabolic regulation

Metabolic regulation is assumed to be mediated by venous  $CO_2$  [1, 12], a potent vasodilator [20]. It is assumed that the set of arterioles feeding the capillary bed are in close proximity to the venous return, a concept reviewed by [16].

Brain tissue  $CO_2$  concentration  $[CO_2]_t$  is assessed from the molar balance between  $CO_2$  production and  $CO_2$  disposal.  $[CO_2]_t$  represents a molar concentration. Tissue  $CO_2$  is produced by metabolism ( $M_{CO_2}$ ) and disposed by blood perfusing the tissue. This is formulated in the following equation:

$$\frac{[CO_2]_t}{dt} = \frac{1}{V} \cdot (M_{CO_2} - Q_{ar} \cdot ([CO_2]_v - [CO_2]_a)) \quad (18)$$

in which  $V$  is the brain volume perfused by one PCA and  $[CO_2]_v$  and  $[CO_2]_a$  are the venous and arterial  $CO_2$  concentrations, respectively.  $V$  represents the unilateral primary visual cortex volume.



Visual cortex stimulation influences metabolism as follows:

$$M_{CO_2} = M_{CO_2,0} \left( 1 + A_{neuro} \frac{f_Q - 1}{n_{QM}} \right) \quad (19)$$

In this equation,  $f_Q$  is the ratio between open eye and closed eye flows at baseline i.e. without visual stimulation.  $n_{QM}$  is a factor describing the ratio of percentual flow increase to percentual metabolism increase, which is chosen to be 2.2 [33].  $M_{CO_2,0}$  is assumed to be  $1.35 \cdot 10^{-7}$  mol/s [12].  $[CO_2]_a$  is assumed to be constant at 20.65 mmol/l [13].  $[CO_2]_v$  is assumed to be in equilibrium with  $[CO_2]_t$ , which is justified by the very fast diffusion of  $CO_2$  [15; p.504]. Note that for two dissolved gases to be in equilibrium, their partial pressures (not their concentrations) are to be equal [10].

$[CO_2]_t$  influences metabolic activation,  $A_{meta}$ , via

$$A_{meta} = G_{Ameta} ([CO_2]_t - [CO_2]_{t,sp}) \quad (20)$$

$[CO_2]_{t,sp}$  is defined as the steady-state solution of (18).  $G_{Ameta}$  is a scaling gain factor, which is chosen to be 0.59 l/mmol.  $x_{meta}$  is coupled to  $A_{meta}$  via first-order dynamics, analogous to (15).

#### **VEFR Fitting**

Measured visually evoked flow responses (VEFRs) showing behaviour representative for every category of VEFRs i.e. normal, intermediate or sluggish, were chosen for model testing. Since all time constants of the regulatory processes largely exceed the cyclic heart beat time base, use of VEFRs based on beat-to-beat values is justified. VEFRs and accompanying visually-evoked blood pressure responses (VEBPR) are shown in figure 2.

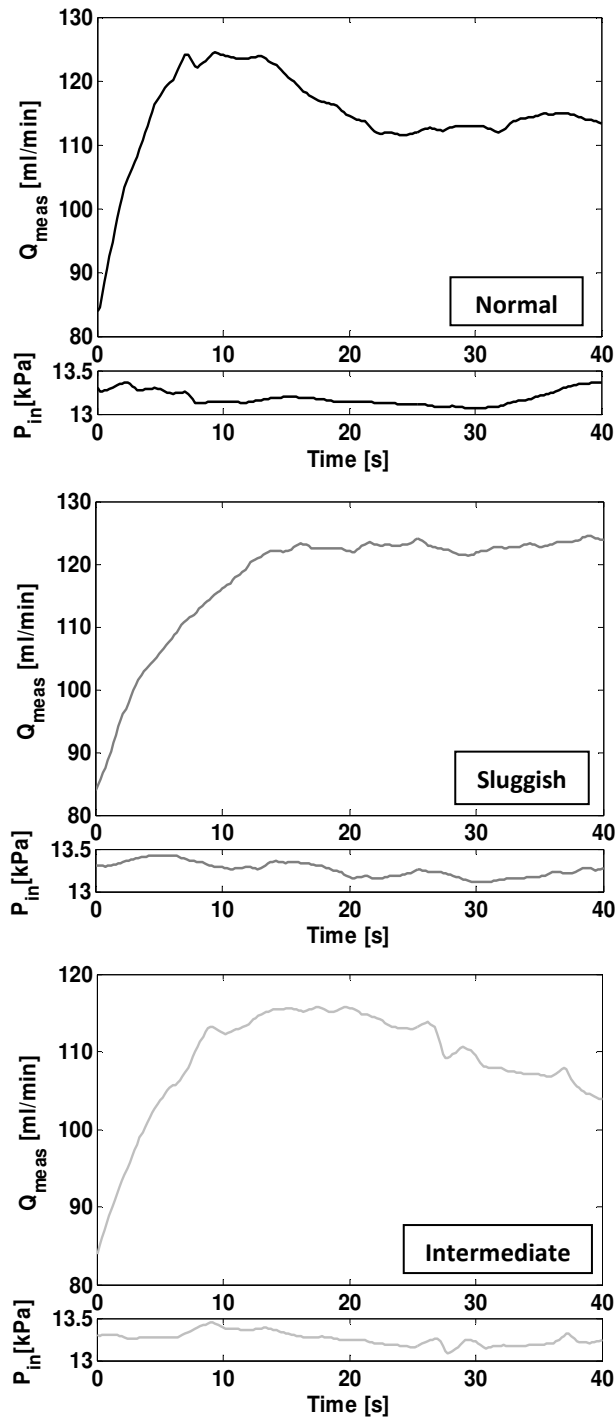


Figure 2. Representative VEFRs and accompanying VEBPR, i.e. target for model output fitting and model input, for normal (A), sluggish (B) and intermediate (C) type.

The VEBPR was used as model input. The VEFR was converted to flow assuming a PCA diameter of 2.1 mm and a circular cross-sectional area. The converted VEFR was then compared to the model arterial flow ( $Q_A$ ) i.e. modelled PCA flow. The sum of squares between measured and model flow was calculated and minimised by changing the activation parameters i.e. gains and time constants of regulatory processes. Fit quality could thus be assessed by examining the minimised root mean square error ( $E_{RMS}$ ), defined as

$$E_{RMS} = \sqrt{\frac{1}{N} \sum_{i=1}^N (Q_{meas}(i) - Q_a(i))^2} \quad (21)$$

Fitting was performed using the trust-region-reflective algorithm [8, 9], implemented in the MATLAB Optimization Toolbox function lsqnonlin. Fitting was initiated from multiple start points in parameter space using the MATLAB Global Optimization Toolbox function MultiStart.

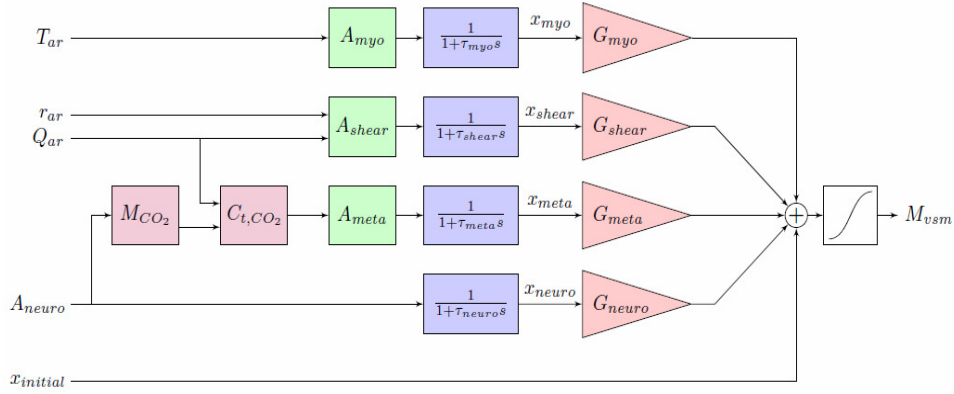


Figure 3: Flow chart showing the four modelled regulatory mechanisms (myogenic, shear stress based, metabolic, and neurogenic regulation).  $T_{AR}$ ,  $r_{AR}$  and  $Q_{AR}$  represent the arteriolar tension, radius and outflow, respectively.  $A_{NEURO}$ , neurogenic activity, parameter correcting for steady-state differences between fitted and measured flows.  $M_{CO_2}$ ,  $CO_2$  metabolism (19).  $[CO_2]_v$ , brain tissue  $CO_2$  concentration (18).  $A_{MYO}$ ,  $A_{SHEAR}$ , and  $A_{META}$ , myogenic, shear stress based, and metabolic activation (14, 17, and 20). For each mechanism, a blue box represents a first order low-pass filter (15), yielding a regulatory state variable, which is multiplied by a gain factor represented by a red triangle. Regulatory influences are then summed (13) and yield  $M_{VSM}$  via a sigmoidal function (12).  $CO_2$ , carbon dioxide.

Table 1: Constant model parameters. PCA, posterior cerebral artery.

Symbol	Value	Unit	Description	Reference
$\eta_{Blood}$	$4 \cdot 10^{-3}$	Pa*s	Dynamic blood viscosity	(Letcher 1981)
$\rho_{Blood}$	1.05	$g \cdot ml^{-1}$	Blood mass density	(Mulder 2011, Alastruey 2007)
$E_{pca}$	1.6	MPa	Young's modulus of PCA wall	
$R_{pca}$	1.05	mm	PCA inner radius	
$L_{pca}$	8.6	cm	PCA length	
$h_{pca}$	0.026	mm	PCA thickness	
$r_{ar,0}$	0.0075	cm	Vessel inner radius in the condition of unstressed wall	
$h_{ar,0}$	0.0025	cm	Wall thickness in the unstressed condition ( $r = r_0$ )	
$\sigma_{ar,e,0}$	11.19	mmHg	Constant parameter for elastic stress model	
$K_{ar,0}$	4.5	-		
$\sigma_{ar,coll}$	41.32	mmHg		
$T_{ar,max,0}$	1.50	mmHg * cm	Optimal smooth muscle tension in basal condition	
$r_{ar,m}$	0.0128	cm	Radius at which smooth muscle exerts maximal force	
$r_{ar,t}$	0.0174	cm	Constant parameter for smooth muscle tension model	
$n_{ar,m}$	1.75	-		
$\eta_{ar}$	47.8	mmHg	Wall viscosity	
$Q_{bl}$	53	ml/min	Baseline flow	(Moore 2007)
$P_{ic}$	10	mmHg	Intracranial pressure	(Payne 2006)
$P_{vo}$	14	mmHg	Venous output pressure	(Ursino 1998)

### Strategy

To gain insight in the behaviour and quality of the fitting procedure, first a few exploratory steps will be carried out. Assessment of parameter ranges is not obvious, especially not for the gains since there are no literature values available. Although ranges for time constants can be retrieved from literature, these are also rough estimations. Therefore, we start by evaluating the dependency of the output of the fitting routine on chosen parameter space and chosen initial values i.e. start points. First, the parameter space will be varied by choosing large (L) and small (S) ranges for the fitting parameters. The multi-start procedure will be applied i.e. the fitting routine is allowed to randomly choose 9 start points within the parameter space apart from the user-defined start point to obtain the output accompanied by the minimum root mean square error ( $E_{RMS}$ ). The fitting procedure will be applied to the normal response type. Obtained parameter values will be re-entered in the fitting procedure to test its dependency on initial value choice despite the use of the multi-start procedure.

In case the multi-start procedure will not provide a unique solution, a single start point procedure in the small parameter space will be applied as a 'best practice' alternative, also for the other VEFR representatives. The obtained output will again be re-entered as initial values in the fitting procedure to reveal its consistency.

After evaluation of the quality of the fitting procedure, the potential use of the model will be illustrated by testing hypotheses regarding description of the VEFR representatives:

- H1: The normal response is best described by neuronal and metabolic activation, since a fast and slower time-constant are required to describe the overshoot .
- H2: The intermediate response is best described by neuronal and shear activation, since a fast and slow time constant are required to describe its course.
- H3: The sluggish response can be described solely by activation of the neuronal process, since it has no overshoot and an exponential course.

To test the hypotheses, all three VEFR types will be fitted by solely the neurogenic process (2 degrees of freedom, i.e.  $\tau_{\text{neuro}}$  and  $G_{\text{neuro}}$ ) and by all three possible combinations of the neurogenic process and either one of the three other processes i.e. metabolic, myogenic or shear stress activation (4 degrees of freedom per combination). Of the 4 obtained fits for every VEFR type, the fit with the minimum root mean square error will be regarded as the best fit to describe a particular VEFR type.

## 6.3 Results

### Large/Small parameter spaces + multi-start procedure

Based on preliminary runs using infinite ranges, a large but reasonable parameter space has been determined. The large parameter space was defined by ranges for the gains of -100 - 0 or 0 - 100, with exception of the neuronal gain with a range -10 - 0, and ranges for all time constants of 0-60s (table 2A). Initial values for the large parameter space were chosen based on their expected order. The multi-start procedure was set on 10 start points, which implies that the user-defined initial values were used as 1 start point and that the other 9 start points were randomly selected within the parameter space.

For the set-up of the small parameter space, the parameter ranges were finetuned based on literature values in order to define conceivable values from a physiological perspective (table 2B). This resulted in time constants for the different processes in the order of  $\tau_{\text{neuro}} \sim 1-15\text{s} < \tau_{\text{myo}} \sim 5-13\text{s} < \tau_{\text{meta}} \sim 10-25\text{s} < \tau_{\text{shear}} \sim 25-60\text{s}$ . Gain boundaries were chosen to vary between 0 and their largest value obtained for the large boundaries plus  $\sim 25\%$ . The initial values for the time constants and gains were chosen to be exactly in the middle of the range, but again the multi-start procedure was applied.

The model fits and parameter values obtained are presented in figure 4. The graphs show the measured VEFR (green) and the obtained model-fit (blue). The accompanying table shows the fit parameter values. The results show that although the difference in fits for the large and small parameter spaces do not change dramatically, the parameter values differ considerably. Notably, several processes seem to compete with each other e.g. metabolic and shear time constants are  $\sim 55-60\text{s}$  in both the first and second run whereas the metabolic gain ( $G_{\text{meta}}$ ) increases and shear stress gain ( $G_{\text{shear}}$ ) decreases considerably in the second run as compared to the first.

### Initial values + single start procedure

Following our strategy, the fitting routine was repeated for the small parameter space using the single start procedure to ensure it started at the user-defined initial values. The obtained fit parameter values were then entered as initial values and the fitting procedure was repeated to test the sensitivity of the fitting routine for its initial values. Apart from the normal VEFR representative, this second exploratory step is also applied to the other VEFR types. The model fits and parameters obtained are shown in figure 5. In contrast to what is expected, the obtained parameter values do change somehow proving that outcomes depend on chosen initial values.

### Illustration of model use for hypothesis testing

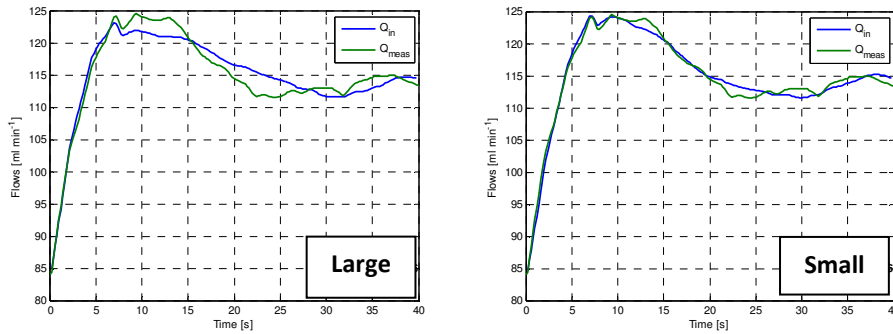
Then, the hypotheses were tested by fitting all VEFR types with solely the neurogenic process (2 degrees of freedom, i.e.  $\tau_{\text{neuro}}$  and  $G_{\text{neuro}}$ ) and with all three possible combinations of the neurogenic process and either one of the three other processes i.e. metabolic, myogenic or shear stress activation (4 degrees of freedom per combination). In this way, 4 fits were obtained for each of the three VEFR types. For every VEFR type, the best fit, i.e. lowest least square difference between VEFR and fit, and accompanying parameter values are shown in figure 6.

Notably, fits of almost similar goodness of fit as the best fits could be obtained when the time constant range of the second (additional) process was adapted to include the value obtained for the second process of the best fit. For the normal type, for example,

the best fit was obtained when the neurogenic process was combined with the metabolic process ( $\tau_{\text{meta}} \sim 15\text{s}$ ). A value of 15s was not included in the time constant ranges of the myogenic or shear stress process. When fitting the normal VEFR by the neurogenic process combined with these processes the boundary limits were attained (i.e. upper limit of 13s for myogenic process and lower limit of 20s for the shear stress process). Adjusting these limits to include 15s in their range showed that also a good fit could be attained for the neurogenic combined with the myogenic process. Similarly, the intermediate response could be best described by the neurogenic process combined with the shear stress mechanism ( $\tau_{\text{shear}} \sim 50\text{s}$ ). However, when the time constant ranges for myogenic or metabolic process were adapted to include 50s as well, they were both able to describe the intermediate response reasonably when combined with the neurogenic process. The sluggish response can be described solely by the neurogenic process, but also combined with metabolic activation a good fit was observed.

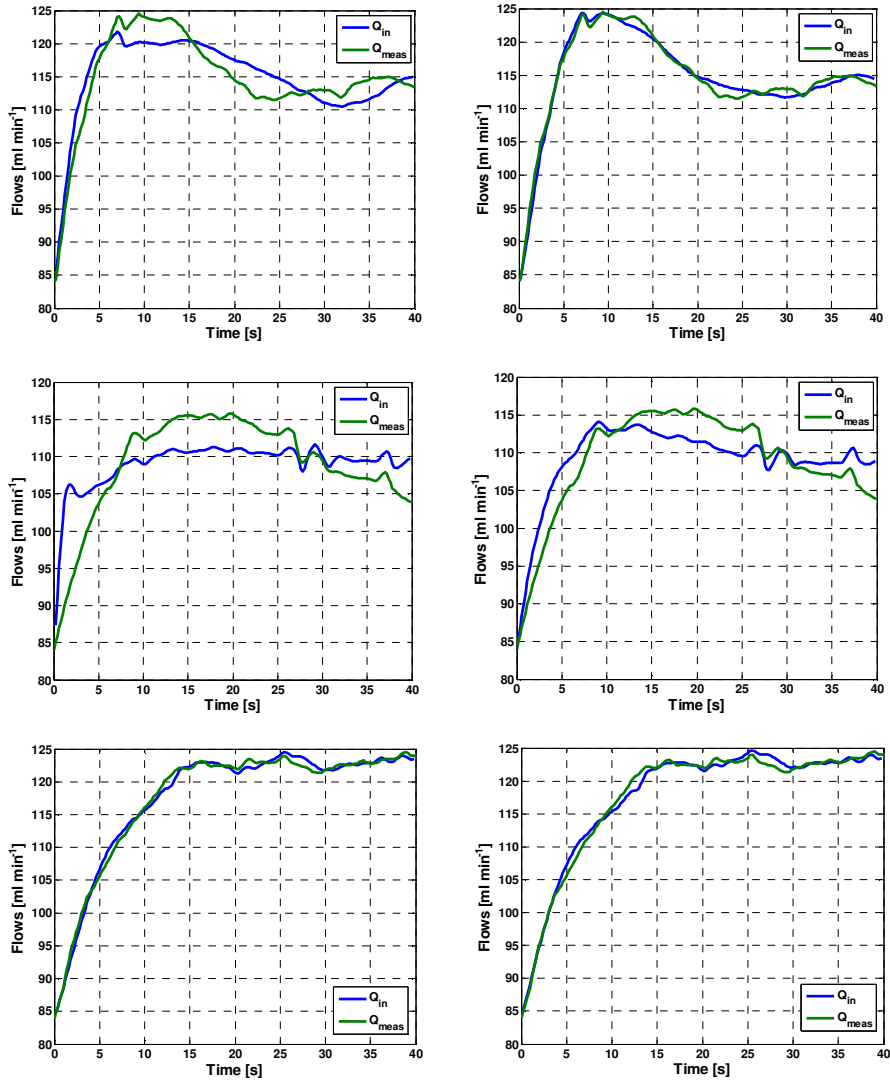
Table 2. Large (A) and small (B) parameter spaces defined by upper and lower parameter limits. Initial values were chosen by expected order (A) or halfway (B), respectively.

<b>A. LARGE</b>	$\tau_{\text{neuro}}$	$G_{\text{neuro}}$	$G_{\text{meta}}$	$\tau_{\text{meta}}$	$G_{\text{myo}}$	$\tau_{\text{myo}}$	$G_{\text{shear}}$	$\tau_{\text{shear}}$
<b>Initial values</b>	10	-0.1	-10	10	10	10	-10	10
<b>Lower Limit</b>	0	-10	-100	0	0	0	-100	0
<b>Upper Limit</b>	60	0	0	60	100	60	0	60
<b>B. SMALL</b>	$\tau_{\text{neuro}}$	$G_{\text{neuro}}$	$G_{\text{meta}}$	$\tau_{\text{meta}}$	$G_{\text{myo}}$	$\tau_{\text{myo}}$	$G_{\text{shear}}$	$\tau_{\text{shear}}$
<b>Initial values</b>	7.5	-2.5	-60	17.5	10	9	-35	40
<b>Lower Limit</b>	0	-5	-120	10	0	5	-70	20
<b>Upper Limit</b>	15	0	0	25	20	13	0	60



<b>MULTI-START</b>	$\tau_{\text{neuro}}$	$G_{\text{neuro}}$	$G_{\text{meta}}$	$\tau_{\text{meta}}$	$G_{\text{myo}}$	$\tau_{\text{myo}}$	$G_{\text{shear}}$	$\tau_{\text{shear}}$
<b>Normal L</b>	26.7	-2.5	-42.2	54.2	10.8	57.5	-26.0	<b>→ 60</b>
<b>Normal L RP</b>	28.8	-2.3	<b>-100 ←</b>	57.8	9.2	<b>→ 60</b>	-8.0	58.1
<b>Normal S</b>	10.2	-0.78	-42.6	19.3	0.67	12.8	<b>→ 0</b>	<b>→ 60</b>
<b>Normal S RP</b>	8.7	-0.92	<b>→ 0</b>	18.2	2.8	<b>→ 13</b>	-8.5	42.5

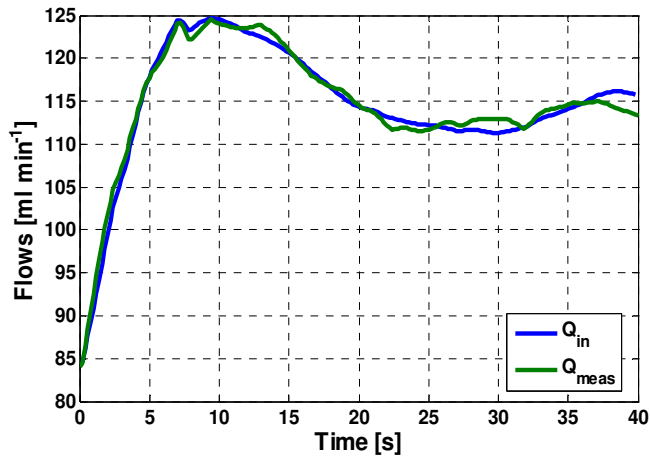
Figure 4. Dependency on parameter space (multiple start points in fitting routine). VEFR (green) and model-predicted flow (blue) for varying space sizes (left: L, right: S). Accompanying fit values for initial values as in table 2 and obtained values re-entered (RP).



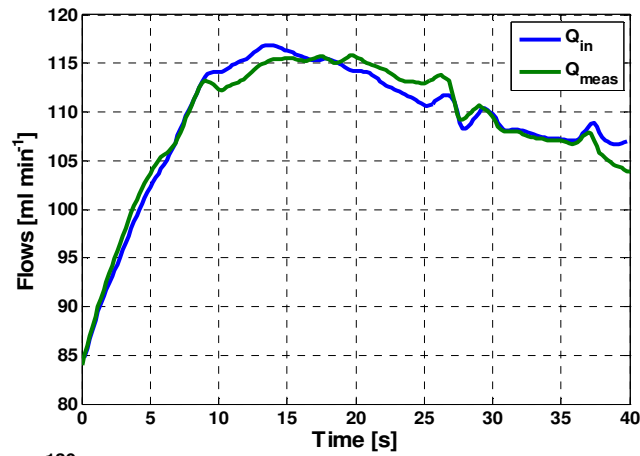
	$\tau_{neuro}$	$G_{neuro}$	$G_{meta}$	$\tau_{meta}$	$G_{myo}$	$\tau_{myo}$	$G_{neuro}$	$\tau_{shear}$
<b>Normal S</b>	11.7	-1.6	→ 0	24.5	1.8	5.9	-53.0	53.3
<b>Normal S RP</b>	11.7	-0.87	-56.6	21.8	0.45	9.1	→ 0	56.0
<b>Intermediate S</b>	11.2	-2.2	→ 0	21.8	8.8	6.4	-38.8	33.4
<b>Intermediate S RP</b>	→ 15	-1.3	-60	→ 25	1.9	5 ←	-14.8	23.0
<b>Sluggish S</b>	14.4	-0.71	-13.5	22.9	0.57	5 ←	-4.2	58.4
<b>Sluggish S RP</b>	→ 15	0.87	→ 0	15.6	1.1	5 ←	-11.3	43.8

Figure 5. Dependency on choice of initial values (single start point fitting routine). VEFRs (green) and predicted flows (blue) for parameter space  $S$ . Initial values as in table 2 and obtained values re-entered (RP). Fit values in red indicate approach of boundaries.

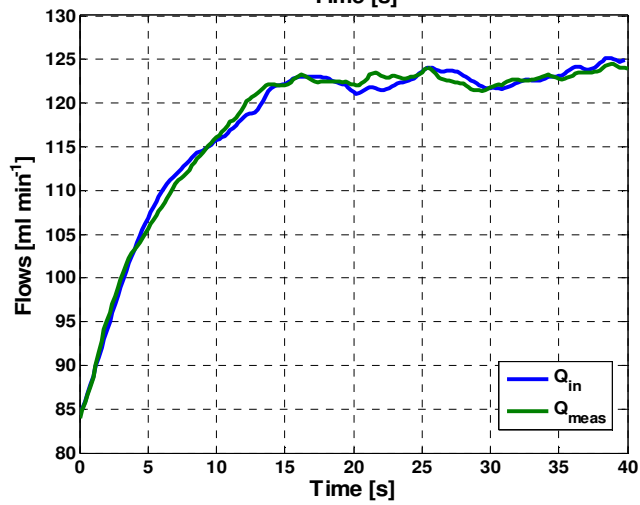




$\tau_{\text{neuro}}$	$G_{\text{neuro}}$
9.0	-0.66
$\tau_{\text{meta}}$	$G_{\text{meta}}$
14.9	-39.1



$\tau_{\text{neuro}}$	$G_{\text{neuro}}$
6.4	-0.33
$\tau_{\text{shear}}$	$G_{\text{shear}}$
52.9	-11.5



$\tau_{\text{neuro}}$	$G_{\text{neuro}}$
6.2	-0.72

Figure 6. Best model-predicted flows (blue) and model outcomes for VEFR types (green).

#### 6.4 Discussion

The main advantage of applying a lumped parameter model incorporating regulatory processes for VEFR description is that it provides parameter values with a physiological meaning. This may enable linkage of VEFR behavior to (patho-)physiological processes. Our model is based on previous models as proposed by Ursino and Lodi [34] to describe transcranial Doppler blood flow velocity recordings and introduced by Payne [27] for the understanding of fMRI BOLD responses. We integrated parts of these models with process descriptions representing different mechanisms capable of activating vascular smooth muscle tone. We aimed in first instance to describe physiology behind neurovascular coupling as complete and flexible as possible, since proposed physiological pathways for VEFR establishment are yet ambiguous regarding involved processes. This prompted us to design a model which allows testing of hypotheses about responsible mechanisms.

The model contains 4 different activation processes, which all act on smooth muscle tone of the arteriolar compartment. Both the neuronal and metabolic process can be activated by a (step) stimulus, whereas the myogenic and shear stress mechanisms are indirect mechanisms reacting on pressure and flow changes respectively. All mechanisms are capable of accomplishment of a change in vascular smooth muscle tone and in arteriolar diameter i.e. vasodilation or constriction. The metabolic and shear stress descriptions probably describe best the actual physiological mechanisms. Metabolic activation is based on the dynamic relation between  $\text{CO}_2$  production and removal, which is disturbed in case metabolism increases e.g. by a step stimulus. Also, the shear stress process may reflect physiology quite well by describing the increase in wall shear stress resulting from increased blood flow. Neuronal and myogenic processes are based on best current knowledge adopted from basic research.

Two parameter spaces were defined i.e. a large parameter space based on rough estimation and a small parameter space in which the ranges of the time constants of the 4 processes were based on literature values. Neuronal time-constants are reported in the order of 2-4s [27], whereas metabolic time constants are chosen in the order of 20s in other models [34]. Myogenic responses are also relatively fast as shown by reported time constants of 5-14s, whereas shear-induced processes involving NO for vasodilation will be relatively slow, i.e. a typical time constant of 60s is observed in other vascular beds [3, 11]. These values were used in the analyses and referred to as (part of) the small parameter space (S).

To test the feasibility of the model to describe VEFRs, we first made a few exploratory steps to test the quality of the fitting routine i.e. its dependency on parameter space and initial values. The first step of our strategy shows that for the large parameter space, the model-fit does match the VEFR fairly but not perfectly. As expected, a better description was attained when applying a smaller parameter space. In both cases a good match between VEFR and fit was expected, since the model has sufficient degrees of freedom to describe normal VEFR behavior i.e. overshoot and saturation. The limited match for the large parameter space and the spread in outcomes between the first run and repeated run (with outcome of first run entered as initial values), implies that the set of differential equation constituting the numerical problem has not an unique solution. This complicates the fit procedure since it may encounter a local minimum instead

of a global minimum. The findings suggest that the parameter space should be further finetuned to ensure a global minimum irrespective of which initial values are chosen by the fitting routine. Therefore it is highly recommendable to first apply a global sensitivity analysis to enable fine-tuning of the parameter space and possible parameter reduction since it will identify parameters which do not or barely influence model outcomes. Parameters which do not have an effect on the outcome may either be fixed to prevent overfitting.

As a second exploratory step, we applied the procedure using the small parameter space to all 3 VEFR types but now with a single start point to ensure that the fitting routine in all types starts from this user-defined start point (in contrast to multi-start use). Also here repetition of the run, using model outcomes obtained in the first run as initial values, leads to changes in model parameter outcomes. This confirms that the fitting procedure is sensitive to user-defined initial values also when a single fit procedure is used. Nevertheless, it can be concluded that our model is applicable for physiological description of VEFRs since the fits obtained match the normal and sluggish VEFR quite good, the intermediate VEFR reasonable and accompanying parameter values seem plausible from physiological perspective. However, again a global sensitivity analysis should be carried out to improve parameter reliability. Given the number of parameters involved and the relatively strong interaction between the different parameters, this would require an implementation of the fitting procedure on a massive parallel computer system.

Irrespective of the quality of the fitting routing, we demonstrated the capability of the model for hypotheses testing to show the model's potential use in the future. We tested different hypotheses with our model i.e. normal VEFR best described by combination of neuronal and metabolic process, intermediate VEFR by neuronal and shear stress mechanism and the sluggish response solely by neuronal activation. To this end, we used different combination of processes and compared the fits with respect to fit error between VEFR and fit. Since visual activation will activate the neurogenic process anyway, it may be combined with each of the three other processes to describe the VEFRs i.e. metabolic, myogenic or shear stress. Comparison of fits and parameter values for solely neurogenic action and those for neurogenic process combined with either one of the three other processes for all VEFR types, shows that only the sluggish VEFR can be described by solely neurogenic action as was expected regarding its time course. The normal VEFR can best be described by neurogenic action combined with a process of a time constant of 20s. Good fits were obtained both for neurogenic activation combined with myogenic and metabolic processes. Similarly for the intermediate response, it was demonstrated that it can best be described by neurogenic action combined with a process with a time constant of about 50s. This could be accomplished by the combination of neurogenic action with either one of the three other processes. Thus, new clinical experiments should be thought off to improve distinction between the three processes, in particular between myogenic and metabolic action. Since the myogenic response can not be selectively manipulated, strategies should be sought in selective metabolic suppression by pharmaceuticals or manipulative maneuvers to control its levels of activation e.g. by inducing hyper- or hypocapnia. VEFRs have previously been

acquired in condition of hypercapnia, showing a decreased initial rise and increased visually-evoked flow level [30].

***Possibilities and outlook***

This explorative study shows how a newly introduced physiological model may be explored to gain insight in model parameter ranges, computational limitations and the behavior of the different processes given various preconditions. A more systematic and thorough approach is required to assure that global instead of local minima are found and to gain more insight in the effect of (combinations of) parameter changes on the model outcome. A suitable tool for this purpose would be the Monte-Carlo approach. With this technique all model parameters are (randomly or selectively) varied over arbitrary predefined ranges in the parameter space. This reveals their influence on the model outcome i.e. the sensitivity of the model for a parameter change. It provides information on which parameters are the most influential to the model output and hence, need to be assessed with the most accuracy. This method has successfully been applied for a wave propagation model for vascular access [17].

Furthermore, application of the physiological model enables a mechanistic approach to unravel contributions of different processes thereby generating hypotheses for further research. Our exploratory study revealed for example that myogenic and metabolic processes are hard to differentiate via modeling. Strategic experimental set-ups can be designed to reveal their relative contributions in certain conditions. Dynamic interaction between testing hypotheses with the model and generation of new hypotheses for experiments provides a productive base for further research.

## References

- [1] Alzaidi SS. Computational Models of Cerebral Hemodynamics (PhD thesis). Canterbury: University of Canterbury, 2009.
- [2] Banaji M, Tachtsidis I, Delpy D, Baigent S. A physiological model of cerebral blood flow control. *Math Biosci* 194: 125–173, 2005.
- [3] Black MA, Cable NT, Thijssen DH, Green DJ. Importance of Measuring the Time Course of Flow-Mediated Dilatation in Humans. *Hypertension* 51: 203–210, 2008.
- [4] Boas DA, Jones SR, Devor A, Huppert TJ, Dale AM. A vascular anatomical network model of the spatiotemporal response to brain activation. *Neuroimage* 2008; 40:1116-29
- [5] Buxton RB, Uludag K, Dubowitz DJ, Liu TT. Modeling the hemodynamic response to brain activation. *Neuroimage* 23: S220–S233, 2004.
- [6] Carlson BE, Arciero JC, Secomb TW. Theoretical model of blood flow autoregulation: roles of myogenic, shear-dependent, and metabolic responses. *Am J Physiol Heart Circ Physiol* 295: H1572–H1579, 2008.
- [7] Carlson BE, Secomb TW. A Theoretical Model for the Myogenic Response Based on the Length-Tension Characteristics of Vascular Smooth Muscle. *Microcirculation* 12: 327–338, 2005.
- [8] Coleman TF, Li Y. On the convergence of interior-reflective Newton methods for nonlinear minimization subject to bounds. *Math Program* 67: 189–224, 1994.
- [9] Coleman TF, Li Y. An Interior Trust Region Approach for Nonlinear Minimization Subject to Bounds. *SIAM J Optimiz* 6: 418–445, 1996.
- [10] Colt JE. The computation and reporting of dissolved gas levels. *Water Res* 17: 841–849, 1983.
- [11] Corretti MC, Anderson TJ, Benjamin EJ, Celermajer D, Charbonneau F, Creager MA, Deanfield J, Drexler H, Gerhard-Herman M, Herrington D, Vallance P, Vita J, Vogel R. Guidelines for the ultrasound assessment of endothelial-dependent flow-mediated vasodilation of the brachial artery: A report of the International Brachial Artery Reactivity Task Force. *J Am Coll Cardiol* 39: 257–265, 2002.
- [12] David T, Alzaidi S, Farr H. Coupled autoregulation models in the cerebro-vasculature. *J Eng Math* 64:453 403–415, 2009.
- [13] Geers C, Gros G. Carbon dioxide transport and carbonic anhydrase in blood and muscle. *Physiol Rev* 80:471 681–715, 2000.
- [14] Girouard H, Iadecola C. Neurovascular coupling in the normal brain and in hypertension, stroke, and Alzheimer disease. *J Appl Physiol* 100: 328–335, 2006.
- [15] Guyton AC, Hall JE. *Textbook of Medical Physiology*. Philadelphia, Pennsylvania:W.B. Saunders, 2006, p. 504.
- [16] Hester, R. L. and Hammer, L. W. (2002). “Venular-arteriolar communication in the regulation of blood flow.” In: American Journal of Physiology - Regulatory, Integrative and Comparative Physiology 282.5, R1280–R1285.
- [17] Huberts W. Personalized computational modeling of vascular access creation. PhD-thesis, Eindhoven: Eindhoven University of Technology, 2012.
- [18] Iadecola C., *Neurovascular regulation in the normal brain and in Alzheimer's disease*. *Nat Rev Neurosci*, 2004. 5(5): p. 347-60.
- [19] Jager G. Electrical model of the human systemic arterial tree (PhD thesis). Rijksuniversiteit Utrecht, 1965.
- [20] Kontos H, Wei E, Raper A, Patterson J. Local mechanism of CO<sub>2</sub> action of cat pial arterioles. *Stroke* 8: 487 226–229, 1977.

- [21] Martens E, Peeters L, Gommer E, Mess W, van de Vosse F, Passos VL, Reulen J. The Visually-Evoked Cerebral Blood Flow Response in Women with a Recent History of Preeclampsia and/or Eclampsia. *Ultrasound Med Biol* 35: 1–7, 2009.
- [22] Martens EGHJ, Gommer ED, Bogaarts JG, Shijaku E, Ramakers IHGB, Aalten P, Verhey F, Mess WH, Reulen JPH. Parameter reliability and blood pressure dynamics in assessment of neurovascular coupling of Alzheimer and cognitively impaired patients. Submitted
- [23] Moore SM. Computational 3D Modelling of Hemodynamics in the Circle of Willis (PhD thesis). University of Canterbury, 2007.
- [24] Ngai AC, Winn HR. Estimation of shear and flow rates in pial arterioles during somatosensory stimulation. *Am J Physiol* 270: :1712-1717, 1996.
- [25] Olufsen MS, Nadim A, Lipsitz LA. Dynamics of cerebral blood flow regulation explained using a lumped parameter model. *Am J Physiol Regulatory Integrative Comp Physiol* 282:611-622, 2002.
- [26] Panerai RB, Dawson SL, Potter JF (1999) Linear and nonlinear analysis of human dynamic cerebral autoregulation. *Am J Physiol* **277**, H1089-1099.
- [27] Payne S. A model of the interaction between autoregulation and neural activation in the brain. *Math Biosci* 204: 260–281, 2006. (Corrigendum. *Math Biosci* 218: 72, 2009)
- [28] Rosengarten B, Huwendiek O, Kaps M, Neurovascular coupling and cerebral autoregulation can be described in terms of a control system. *Ultrasound in medicine & biology* 2001;27:189-93.
- [29] Rosengarten B, Huwendiek O, Kaps M, Neurovascular coupling in terms of a control system: validation of a second-order linear system model. *Ultrasound in medicine & biology* 2001;27:631-5.
- [30] Rosengarten B, Spiller A, Aldinger C., Kaps M, Control system analysis of visually evoked blood flow regulation in humans under normocapnia and hypercapnia. *European Journal of Ultrasound* 2003; 16:169-175.
- [31] Secomb TW. Theoretical Models for Regulation of Blood Flow. *Microcirculation* 15: 765–775, 2008.
- [32] Spronck B, Martens EGHJ, Gommer ED, Van de Vosse FN. Cerebral blood flow fluctuations induced by autoregulation and neurovascular coupling described by a single physiological model. Submitted
- [33] Uludag K, Dubowitz DJ, Yoder EJ, Restom K, Liu TT, Buxton RB. Coupling of cerebral blood flow and oxygen consumption during physiological activation and deactivation measured with fMRI. *Neuroimage* 23:544 148–155, 2004.
- [34] Ursino M, Lodi CA. Interaction among autoregulation, CO<sub>2</sub> reactivity, and intracranial pressure: a mathematical model. *Am J Physiol* 274: H1715–H1728, 1998.
- [35] Zhang R, Zuckerman JH, Giller CA, Levine BD (1998) Transfer function analysis of dynamic cerebral autoregulation in humans. *Am J Physiol* **274**, H233-241.
- [36] Zhang R, Behbehani K, Levine BD (2009) Dynamic pressure-flow relationship of the cerebral circulation during acute increase in arterial pressure. *J Physiol* 587, 2567-2577.



# **CHAPTER 7**

## **General Discussion**



## General discussion

The aim of the work presented in this thesis was to progress towards development of reliable and clinically relevant parameters for cerebral blood flow regulation assessment by use of ultrasonography. Quantitative assessment of cerebral blood flow and its regulation is of great clinical importance since cerebral hypoperfusion predisposes a variety of pathologies. Given the important advantages of ultrasonography, efforts have been focused on the description of ultrasonographic blood flow velocity measurements by reliable parameters preferably with a physiological interpretation.

### 7.1 Main Findings

In chapter 2, blood flow velocities (BFV) of patients with Alzheimer's disease (AD) are shown to be significantly lowered at proximal sites but preserved at distal sites as compared to BFV of mild cognitive impaired patients (MCI) or healthy controls (HC). This pattern holds for three trajectories i.e. the internal carotid arteries, the middle and posterior cerebral arteries. It can presumably be ascribed to reduced distal diameters resulting from AD pathology. In addition, MCI BFV appears to be similar to HC BFV in the extracranial and intracranial posterior circulation, whereas they are intermediate between AD and HC in the intracranial anterior circulation. This suggests that intracranial anterior vessels may be most suitable for early detection of pathological alterations. Thus, location-specific cerebrovascular BFV decline in AD and MCI is detectable using ultrasonography showing its potential as a screening tool for MCI.

In the same study cohort, dynamic cerebral autoregulation (DCA) has been studied and discussed in chapter 3. The cerebrovascular resistance index, CVRi, was significantly higher in AD compared to MCI and HC implying increased AD vessel stiffness. Also, CVRi is shown to be a potential biomarker for AD development of MCI. Moreover, windkessel model findings of a significantly elevated peripheral resistance parameter confirmed cerebrovascular resistance increase in AD.

To investigate neurovascular coupling assessment, visually-evoked blood flow responses (VEFRs) were examined first in a relative young study cohort i.e. formerly (pre-)eclamptic patients and controls as described in chapter 4. VEFRs were fitted with the step response of a 2nd order control system model to obtain patient-specific parameter values. Although inter-group differences in model parameters were not found, a trend was observed that critical damping ( $\zeta > 1$ ) occurred more frequently in former patients than in controls. Critical damping reflects an atypical VEFR, which is either uncompensated (sluggish,  $\zeta > 1$ ;  $T_v < 20$ ) or compensated by a rise in rate time (intermediate,  $\zeta > 1$ ;  $T_v > 20$ ). Further study is required to interpret these two VEFR types.

The standard VEFR analysis procedure as described in chapter 4, has been optimized by consideration of parameter reliability and blood pressure dynamics in chapter 5. These two VEFR-analysis procedures were applied to the AD study cohort. Reliability consideration resulted in about 40% VEFR exclusion, mainly due to the models' inability to fit critically damped responses but reduced parameter variability considerably. Regarding the influence of blood pressure variation, a significantly increased damping was found in AD for the standard but not for the revised model. This reversed conclusions from altered to normal neurovascular coupling in AD. Considering their influence on ob-

tained parameters, both aspects should be included in VEFR-analysis. Neurovascular coupling is unaffected in AD, which is conceivable given usual spatial-temporal AD pathology progression.

To enable linkage of VEFR behavior to physiological properties, a lumped parameter model of the visual cortex vasculature is introduced in chapter 6. Regulatory processes i.e. neurogenic, metabolic, myogenic and shear stress mechanisms, act on smooth muscle tone which inherently leads to adjustment of microcirculatory resistance and compliance. Preliminary results show that this newly introduced physiology-based model can describe a representatives of VEFR types reasonably well obtaining physiologically plausible parameter values.

## **7.2 Considerations for data acquisition**

### ***Use of transcranial Doppler ultrasonography (TCD)***

In this thesis, duplex and Transcranial Doppler (TCD) ultrasonography have been applied to assess cerebral blood flow and its regulation because of their major advantages over other imaging techniques such as non-invasiveness, cost-effectiveness and high temporal resolution. However, ultrasonography has some drawbacks which need to be considered when employing this technique.

Both duplex and TCD, depend on temporal window size and bone thickness to obtain sufficient ultrasound signal quality. In practice, this results not only in exclusion of about 10% of the population due to insufficient window quality, but also in less optimal signal quality in case of poor window quality. Mean spectral energies of 36.4 dB on average have been reported for subjects with normal window quality, whereas reduced values of 30.3 dB are found for subjects with poor window quality [9]. Its influence on DCA parameters has also been investigated by corrupting the normal insonation windows with aluminum foils obtaining spectral energies similar to poor window quality subject group. This causes a significant reduction in phase difference but magnitude is preserved. Use of ultrasound contrast agent via bolus injection is recommended to compensate for lowered signal quality [10]. In this work, however, 5Hz low-pass filtering of raw blood pressure and velocity data was applied for beat-to-beat detection combined with artifact removal to optimize signal quality for further analysis. Filtering and artifact removal work sufficiently well and preserve non-invasiveness.

Another consideration for ultrasonography use is that operator-dependency may introduce measurement inaccuracy. Inter-observer variability, expressed by interclass correlation coefficients (ICC), has been reported to be 0.9 for peak systolic and 0.8 for end diastolic velocity, whereas values of 0.81 to 0.97 are reported for peak systolic and 0.69—0.89 for end-diastolic intra-observer variability [12]. These findings suggest that measurements performed by well-experienced operators are very consistent. Since lack of regular practice is known to reduce measurement accuracy, it is advisable to stimulate clinical operators and investigators to keep up experience by regular practice. Ultrasonographic velocity recordings in this thesis have been measured by a limited number of operators who were all moderate to well-experienced in operating these techniques implying negligible influence on presented results.

In contrast to duplex ultrasonography, TCD recordings are not corrected for insonation angle. Insonation angles for the MCAs and PCAs are reported to be in the order of 30° [7] accounting for an underestimation of about 15-20% (cosine relationship) of the measured velocities. However, individual variability of insonation angles may be considerable, which emphasizes the need to account for it when investigating absolute cerebral blood flow (velocity). To cancel out the influence of insonation angle, only angle-corrected velocities or relative TCD velocity changes have been reported in this thesis as is also recommendable in general for use in clinical and research practice.

### **Quality Assurance**

#### Transcranial Doppler ultrasonography (TCD)

The research in this thesis revealed the diagnostic value of ultrasonographic BFV measurements for AD e.g. detectable location-specific BFV decline. Still, diagnostic value may be further improved by optimizing dataset quality via combination of Duplex ultrasonography (D-TCD) or 'blind' TCD (B-TCD) with other techniques. A major drawback of D-TCD /B-TCD is that velocities are measured, whereas we are interested in cerebral blood flow requiring also diameter and velocity profile information. With MR angiography (MRA) or Time-Of-Flight images (TOF) cerebrovascular diameter differences can be detected with a resolution of ~0.35mm corresponding to flow changes of minimally 3 ml/min for a BFV of 50 cm/s. Also, assumed velocity profiles should be evaluated especially for tortuous vessels or near bifurcations. Novel technics such as multigate Doppler [2] or particle image velocimetry may be applied to gain more insight in the velocity profile near the carotid bulb. This may not only help to explain lowered proximal ICA BFV in AD as compared to MCI or HC, but it will also improve flow estimation.

#### Visually-evoked blood flow response (VEFR)

Furthermore, the remarkable but consistent finding of atypical VEFR types emphasizes the need for a critical review of the experimental set-up. It is crucial for correct measurement interpretation to determine whether atypical VEFRs result from procedural aspects or reflect physiological behavior. Therefore, it is not only advisable to further optimize the experimental set-up to ensure optimal measurement accuracy, but also to include potential sources of physiological variation such as blood pressure and CO<sub>2</sub> in the data acquisition to enable quantitative correction for their effects.

Optimization measures for experimental set-up may involve electrooculography (EOG) measurement for precise eye opening and closure detection (exact on and off time detection to minimize trigger jitter in averaging of responses), assurance of optimal visual acuity and prolongation of stimulus duration to prevent non-saturation of VEFRs. In addition, quality measures and criteria should be standardized and routinely incorporated in post-processing steps. For DCA analysis, a statistical procedure has been introduced called surrogate analysis, which provides a kind of reliability criterion. Above its cut-off, pressure and flow data can be assumed to be correlated with sufficient confidence, so that gain and phase measures may be regarded as meaningful. Our newly introduced reliability parameter for VEFR-analysis has a similar function i.e. it is meant to select only parameter values for statistical analysis which are sufficiently reliable and meaningful. These quality measures should be further evaluated with the purpose to eventually become standard applied as a consensus between researchers in the field.

### 7.3 Considerations for modeling

#### *Quality of models*

Regarding the principles of ‘good modeling’, guidelines have been developed first for problem identification and specification and second for the three parts of the modeling process i.e. model development, evaluation and application [4]. Each of these iterative basic steps is accompanied by some modeling issues which should be considered.

For problem definition and specification, knowledge of the background of the modeled process is required also to make decisions regarding input requirements and desired output. For neurovascular coupling, there seems to be a gap between micro-level research in which processes involved in establishment of local vasodilation are central, and macro-level research where differentiation between VEFRs in normal and pathologic conditions is the main topic of investigation. The intermediate level consisting of spatial and temporal courses of neural signal spread and vasodilatory propagation appear to be underexposed in neurovascular coupling research. Schummers et al [11] used two-photon imaging of calcium signals in a ferret visual cortex to investigate the influence of tuned astrocytic responses to visual stimulation on hemodynamical signals. Similar studies should be designed to gain insight in the spatial and temporal organization of coupling between neuronal and hemodynamical responses via the tuning interference of astrocytes. This information could help in designing a lumped parameter model with more spatial and temporal detail e.g. the arteriolar compartment could possibly be split up in more parallel compartments to differentiate spatially between cortex areas which may interact via the activation processes underlying neurovascular coupling.

For model development, a consideration needs to be made between the required model complexity and the uncertainty in model output (see figure 7.1). When increasing the model complexity, model framework uncertainty becomes smaller since the number of parameters or degrees of freedom increases. However, data uncertainty will increase since the potential error coming from input data will grow. To obtain a minimum total uncertainty, an optimum between these two sources of uncertainty needs to be realized. Both newly introduced models, i.e. the RGe model and the physiology-based model, lead to a shift to the right on the uncertainty curves. They provide more degrees of freedom but lead to stricter accuracy requirements for the input data. As a first step towards physiology-based modeling, it was essential to incorporate all possibly important physiological processes underlying neurovascular coupling. The ultimate goal is, however, to describe the VEFR accurately by the minimum required parameters i.e. finding the best compromise between model framework and data uncertainty (fig 7.1). Therefore, as a second step the complexity of the model may be reduced by comparison of the contributions of processes or sensitivity analyses.

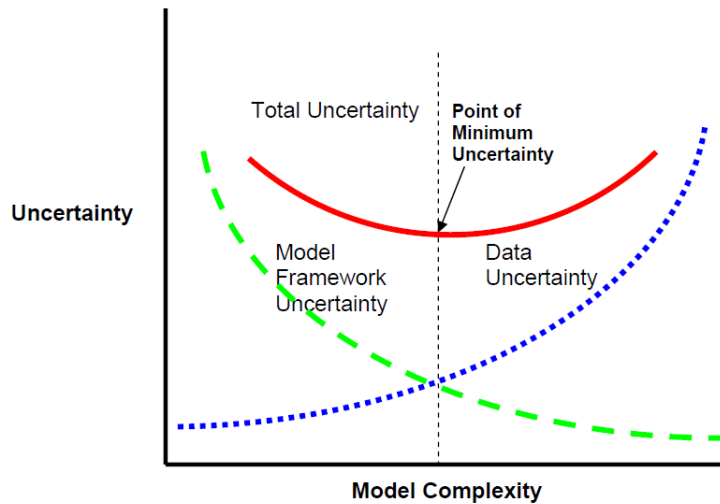


Figure 7.1 Relationship between model framework uncertainty and data uncertainty and their effect on total model uncertainty (in [4], adapted from Hanna [5])

A major issue for model evaluation is to assess the (relative) sensitivity of the model output for a change in a model input parameter. Model input parameters for which the model output is the most sensitive should be determined with the highest accuracy. Other parameters may be considered as less important and can possibly even be removed from the model, so that uncertainty in model outcome will decrease. This is a crucial step before the newly developed model can be applied in further research. It is highly recommendable to perform a global and local sensitivity analysis for the lumped parameter model similar to those previously applied for patient-specific wave-propagation models of the systemic arterial tree for the purpose of obtaining mechanical property values [8] and to predict outcomes after vascular access creation [6].

#### 7.4 Clinical Relevance

The research in this thesis revealed the diagnostic value of ultrasonographic BFV measurements for several pathologies i.e. AD, MCI, pre-eclampsia and eclampsia. Extensive duplex examination of intra- and extracranial BFV in MCI may reveal which (sites of) blood vessels are most susceptible for declined BFV and may predict conversion to AD. In addition, CVRi seems to be a good potential candidate for prediction for future conversion of MCI to AD. An optimal set-up for future study is to prospectively measure location-specific BFV with duplex ultrasonography, CVRi by simultaneous Doppler velocity and blood pressure recording, to perform cognitive tests and to acquire MRI images and MRA diameters for all MCI patients. Monitoring these MCI patients will reveal the predictive value of blood volume flow maps and resistance values for AD conversion. Moreover, other patient populations may benefit from this methodological approach. Cerebral hypoperfusion makes the brain vulnerable to and may predispose different pathological processes. Screening and diagnostic value of duplex ultrasonography may be structurally explored such as done for the relatively new MRI perfusion technique

arterial spin labeling [3]. Early detection of cerebrovascular hemodynamics may be beneficial for diseases such as stroke. Also cerebral hyperperfusion is potentially harmful for the brain. Migraine is associated with increased cerebral blood flow. The effect of acupuncture as therapeutic treatment has been investigated with promising results [1].

Both cerebral autoregulation and neurovascular coupling seem to be preserved in AD based on transfer function analysis. For neurovascular coupling, however, VEFR interpretation i.e. diagnostic value of model parameters is not unambiguous yet. Although a VEFR showing an overshoot and late saturation is reported being the normal response, it may be argued that it is not efficient to require an overshoot before attaining the required saturation level. From this point of view, the sluggish response, if fast enough, may be more efficient. Similar if the saturation level is the desired flow level, the intermediate type and fast sluggish type meet the required need. From this perspective, only the very slow sluggish responses are problematic. There may be a transition from one type to the other dependent on pathology, which would imply that monitoring of these patients would be beneficial. This is supported by the stimulus dependency of the VEFR course i.e. simpler stimuli do in general not lead to an overshoot in the VEFR. If neurovascular coupling functions well, a more complex stimulus would also not require an overshoot. Also, the response may be dependent on the precondition of the vessels i.e. level of vasodilation/constriction. Challenging conditions such as increasing stimulus complexity or pre-dilation level are easy applicable and may improve distinction of pathological from normal VEFR.

## 7.5 Conclusion

The work in this thesis was aimed to progress towards reliable and clinically employable parameters for assessment of cerebral blood flow regulation using ultrasonography. The current standard of control system analysis to assess local cerebral blood flow regulation has limitations regarding parameter reliability and VEFR interpretation. The application of a reliability parameter exposed control system limitations regarding reliable description of all three measured visually-evoked blood flow responses (VEFR) types. Both reliability and interpretation may be improved by optimization and control of data acquisition quality and by use of physiology-based models. The need for physiology-based models is further emphasized by the alteration of clinical study outcomes when blood pressure variation was taken into account in the control system model. Physiological mechanisms influencing VEFR establishment should be incorporated in such a model to possibly explain part of its variance. Application of a lumped parameter model of the visual cortex vasculature including regulatory adjustment of smooth muscle tone shows that it has similar ability to describe VEFRs than a control system model, providing physiologically meaningful parameter values for evaluation.

From a clinical perspective, it is shown in this thesis that blood flow velocity of Alzheimer patients is decreased at specific locations in the extracranial carotid arteries and throughout the intracranial circulation. Extracranial and intracranial posterior blood flow velocity of MCI patients is similar to controls, whereas intracranial anterior blood flow velocity is intermediate between Alzheimer patients and controls. In addition, global cerebral blood flow regulation of Alzheimer patients is preserved despite increased peripheral resistance. When accounting for blood pressure variations, local cerebral blood flow regulation in the occipital lobe is found to be preserved as well. Thus, it is recommendable to examine all future MCI patients on extra- and intracranial baseline blood flow velocity using Duplex ultrasonography and to determine their cerebrovascular resistance index by use of simultaneous recording of blood pressure. Follow-up of MCI patients will reveal the predictive value of these parameters for future AD development.

## References

- [1] Bäcker M, Sander D, Hammes M, Funke D, Deppe M, Conrad B, Tölle T. Altered cerebrovascular response pattern in interictal migraine during visual stimulation. *Cephalalgia* 21: 611–616, 2001.
- [2] Beulen, B. Toward simultaneous flow and pressure assessment in large arteries using non-invasive ultrasound. PhD-thesis 2009.
- [3] Deibler AR, Pollock JM, Kraft RA, Tan H, Burdette JH, Maldjian JA. Arterial Spin Labeling in routine clinical practice, part 2: hypoperfusion patterns. *Am J Neuroradiol.* 29:1235-1241, 2008
- [4] Council for Regulatory Environmental Modeling (CREM). Guidance on the development, evaluation and application of environmental models, 2009. ([www.epa.gov/crem/cremlib.html](http://www.epa.gov/crem/cremlib.html))
- [5] Hanna, SR. Air quality model evaluation and uncertainty. *JAPCA* 38:406-412, 1988
- [6] Huberts W. Personalized computational modeling of vascular access creation. PhD-thesis. Eindhoven: Eindhoven University of Technology, 2012.
- [7] Krejza J, Rudzinsky W, Pawlak MA, Tomaszewski M, Ichord R, Kwiatkowski J, Gor D, Melhem ER. Angle-corrected imaging transcranial Doppler sonography vs imaging and non-imaging transcranial Doppler sonography in children with sickle cell disease. *Am J Neuroradiol.* 28:1613:1618, 2008
- [8] Leguy, C. On the clinical estimation of the hemodynamical and mechanical properties of the arterial tree. PhD-thesis. Eindhoven: Eindhoven University of Technology, 2010 .
- [9] Lorenz MW, Gonzalez M, Lienerth C, Loesel N, Thoelen N, Sitzler M. Influence of temporal insonation window quality on the assessment of cerebral autoregulation with transcranial Doppler sonography, *Ultrasound in Med & Biol.* 33(10):1540-1545, 2007
- [10] Lorenz MW, Thoelen N, Loesel N, Lienerth C, Gonzalez M, Humpich M, Roelz W, Dvorak F, Sitzler M. Assessment of cerebral autoregulation with transcranial Doppler sonography in poor bone windows using constant infusion of an ultrasound contrast agent *Ultrasound in Med & Biol.* 34(3):345-353, 2008
- [11] Schummers J, Yu H, Sur M. Tuned responses of astrocytes and their influence on hemodynamic signals in the visual cortex. *Science* 320:1638-1643. 2008
- [12] Shen Q, Stuart, H, Venkatesh, B, Wallace J, Lipman J. Inter observer variability of the transcranial Doppler ultrasound technique: impact of lack of practice on the accuracy of measurement. *J of Clin Mon and Comp* 15(3-4):179-184, 1999





# Summary

## **Towards Clinical Assessment of Cerebral Blood Flow Regulation using Ultrasonography**

### *Model Applicability in Clinical Studies*

For preservation of its vital functions, the brain is largely dependent of a sufficient delivery of oxygen and nutrients. Blood flow to the brain is essentially regulated by 2 control mechanisms i.e. neurovascular coupling and cerebral autoregulation. Cerebral autoregulation aims for constant adequate blood supply by compensating for blood pressure variations by dilatation or narrowing of the cerebral microvasculature. Neurovascular coupling adjusts blood supply to the local metabolic need. Cerebral perfusion and blood flow regulation are compromised in several pathological conditions. Clinical examination of cerebral blood flow and its regulation may therefore provide helpful diagnostic, predictive and therapeutic information. The work in this thesis was aimed at putting a step forward towards development of reliable and clinically usable parameters for cerebral blood flow regulation assessment using ultrasonography.

Regarding early diagnostics, screening and monitoring of cerebral blood flow and its regulation, ultrasonography has major advantages over other imaging tools because of its non-invasiveness, cost-effectiveness, easy usability and its good time resolution. It allows examination of blood flow velocities at multiple locations throughout the extra- and intracranial circulation and evaluation of both control mechanisms by transfer function analysis. For evaluation of cerebral autoregulation, transcranial Doppler blood flow velocities in the large middle cerebral arteries have been recorded simultaneously with plethysmographic (finger) blood pressure. Gain and phase of the pressure-flow transfer function have been determined to obtain quantitative measures for cerebral autoregulation. Neurovascular coupling has been assessed by presenting a visual block stimulus to a subject and simultaneous measurement of the blood flow velocity in the artery exclusively supplying the visual cortex. The obtained visually-evoked blood flow response (VEFR) has been considered as the step response of a linear second order control system model providing patient-specific parameters such as gain and damping as quantitative measures for neurovascular coupling .

In **chapter 2**, a clinical study has been described in which extra- and intracranial blood flow velocities (BFVs), measured at multiple sites in the circulation, have been compared between Alzheimer patients (AD), patients with mild cognitive impairment (MCI) and healthy aging controls (HC). BFVs of AD were significantly lowered at proximal sites but preserved at distal sites for the internal carotid artery and middle and posterior cerebral arteries as compared to those of MCI or HC. This specific pattern can presumably be ascribed to reduced distal diameters resulting from AD pathology. MCI BFV were similar to HC BFV in the extracranial and intracranial posterior circula-

tion, whereas they were intermediate between AD and HC in the intracranial anterior circulation. This suggests that intracranial anterior vessels are most suitable for early detection of pathological alterations resulting from AD. The study findings further indicate that extensive ultrasonographic screening of intra- and extracranial arteries is useful for monitoring BFV decline in the MCI stage. Future follow-up of MCI patients may reveal the predictive value of location-specific BFV for conversion to AD.

In the same study cohort, dynamic cerebral autoregulation has been studied as discussed in **chapter 3**. Cerebral autoregulatory gain and phase values were similar for AD, MCI and HC which implies that the cerebral autoregulatory mechanism is preserved in AD. However, the cerebrovascular resistance index i.e. the ratio between absolute time-averaged blood pressure and flow velocity, was significantly higher in AD as compared to MCI and HC indicating that vessel stiffness is increased in AD. Indeed, it appeared to be a potential biomarker for AD development of MCI. The cerebrovascular resistance increase in AD was furthermore confirmed by windkessel model findings of a significantly elevated peripheral resistance in AD. Arterial resistance and peripheral compliance were equal for all groups.

From **chapter 4**, the focus was shifted to assessment of local blood flow regulation. Visually-evoked blood flow responses (VEFRs) of formerly (pre-)eclamptic patients and healthy controls have been examined to evaluate neurovascular coupling first in a relative young study population. The aim of the study was to investigate whether possible local (pre)eclampsia-induced endothelial damage was reversible or not. The measured VEFRs have been fitted with the step response of a 2nd order control system model. Although inter-group differences in model parameters were not found, a trend was observed that critical damping ( $\zeta > 1$ ) occurred more frequently in former patients than in controls. Critical damping reflects an atypical VEFR, which is either uncompensated (sluggish,  $\zeta > 1$ ;  $T_v < 20$ ) or compensated by a rise in rate time (intermediate,  $\zeta > 1$ ;  $T_v > 20$ ). Since these abnormal VEFRs were mainly found in former patients (but not exclusively), these response types were hypothesized to result from pathological disturbances.

A revised VEFR analysis procedure to account for reliability and blood pressure dynamics has been proposed in **chapter 5**. This revised procedure consists of the introduction of a reliability measure for model parameters and of a model extension to consider possible blood pressure contribution to the measured VEFR. The effects of these adjustments on study outcomes have been evaluated by applying both the standard VEFR analysis procedure (applied in chapter 4) and the revised procedure to the AD study cohort. Reliability consideration resulted in about 40% VEFR exclusion, mainly due to the models' inability to fit critically damped responses. Reliability consideration reduced parameter variability substantially. Regarding the influence of blood pressure variation, a significantly increased damping was found in AD for the standard but not for the revised model. This reversed the study conclusion from altered to normal neurovascular coupling in AD. Considering their influence on obtained parameters, both aspects i.e. reliability and blood pressure variation should be included in VEFR-

analysis. Regarding clinical study outcomes, neurovascular coupling seems to be unaffected in AD since the finding of an increased damping may be ascribed to ignorance of blood pressure contribution to VEFR.

Study conclusions of earlier chapters (4 and 5) emphasize the need for a model incorporating physiological features. In **chapter 6**, preliminary results have been reported of the application of a newly developed lumped parameter model of the visual cortex vasculature to the 3 different VEFR types. In the new model, regulatory processes i.e. neurogenic, metabolic, myogenic and shear stress mechanisms, act on smooth muscle tone which inherently leads to adjustment of microcirculatory resistance and compliance. This allows the study of effects of pathological changes on the VEFR. It may be concluded that the model provides an improved link between VEFR and physiology. Preliminary results show that the physiology-based model can describe VEFR type representatives reasonably well obtaining physiologically plausible parameter values.

Thus, from a clinical perspective it may be concluded that (Duplex) ultrasonography has great potential as a standard screening tool for MCI patients. It seems worthwhile to examine all future MCI patients on extra- and intracranial blood flow velocity and to determine their cerebrovascular resistance index by simultaneous blood pressure recording. Follow-up of MCI patients will reveal the predictive value of these parameters for future AD development. Furthermore, from a methodological perspective, it can be concluded that the current standard of control system analysis to assess local cerebral blood flow regulation has limitations regarding parameter reliability and VEFR interpretation. Both reliability and interpretation may be improved by optimization and control of data acquisition quality and by use of physiology-based models. Physiological mechanisms influencing VEFR establishment should be incorporated in such a model to possibly explain part of its variance. Efforts should be directed to development and validation of physiology-based models aimed at reliable description of VEFRs by physiologically meaningful parameters.



# Samenvatting

## Op weg naar Klinische Evaluatie van Cerebrale Bloedstroom Regulatie op basis van Ultrageluidsmetingen

### *Model Toepassing in Klinische Studies*

Voor het behoud van zijn vitale functies, is het brein in sterke mate afhankelijk van de aanvoer van voldoende zuurstof en voedingstoffen. De bloedtoevoer naar het brein wordt hoofdzakelijk beheerst door 2 regelsystemen i.e. neurovasculaire koppeling en cerebrale autoregulatie. Cerebrale autoregulatie zorgt voor een constante en voldoende bloedtoevoer door bloeddruk variaties te compenseren via dilatatie of contractie van de kleine weerstands vaatjes. Neurovasculaire koppeling past de bloedtoevoer aan aan de lokale metabole behoefte. Cerebrale perfusie en bloedstroom regulatie kunnen in gevaar komen onder verschillende pathologische omstandigheden. Klinisch onderzoek van cerebrale bloedstroom en zijn regulatie kunnen zorgen voor relevante diagnostische, predictieve en therapeutische informatie. Het in deze thesis gepresenteerde onderzoek is er daarom op gericht om een stap voorwaarts te zetten in de ontwikkeling van betrouwbare en klinisch bruikbare parameters om de cerebrale bloedstroom regulatie te evalueren met behulp van ultrageluid.

Als het gaat om vroege diagnostiek, screening en bewaking van de cerebrale bloedstroom en zijn regulatie, heeft ultrageluid belangrijke voordelen ten opzichte van andere beeldvormende technieken omdat het niet invasief, kosteneffectief en gemakkelijk in gebruik is en omdat het een goede tijdsresolutie heeft. Met behulp van ultrageluid kunnen bloedstroomsnelheden onderzocht worden op verschillende plaatsen in zowel de extra- als intracraniale circulatie en kunnen tevens beide regelsystemen geëvalueerd worden met behulp van overdrachtsfunctie analyse. Voor het onderzoeken van de cerebrale autoregulatie, zijn de transcraniale Doppler bloedstroomsnelheden in de grote middelste hersenvaten tegelijkertijd gemeten en opgenomen met de vinger bloeddruk (via plethysmografie). De versterking (gain) en fase van de druk – bloedstroomsnelheid overdrachtsfunctie zijn bepaald om kwantitatieve maten te verkrijgen voor cerebrale autoregulatie functie. Neurovasculaire koppeling functie is onderzocht door een visuele blokstimulus aan de proefpersoon aan te bieden en tegelijkertijd de bloedstroomsnelheid te meten in het bloedvat dat voor de bloedtoevoer van de visuele cortex zorgt. De visueel opgewekte bloedstroom responsie (VEFR) is vervolgens beschouwd als de stap responsie van een lineair tweede orde regelsysteem model om patiëntspecifieke parameters zoals de versterkingsfactor (gain) en demping als maten voor neurovasculaire koppeling te genereren.

In **hoofdstuk 2** is een klinische studie beschreven waarbij extra- en intracraniale bloedstroomsnelheden (BFVs), gemeten op verschillende plaatsen binnen de circulatie, vergeleken zijn tussen Alzheimer patiënten (AD), patiënten met milde cognitieve

schade (MCI) en gezonde oudere controles (HC). BFVs van AD waren significant lager op proximale plaatsen maar vergelijkbaar ten op zichte van MCI en HC op distale plaatsen in zowel de arteria carotis interna als de arteria cerebri media en posterior. Dit specifieke patroon kan waarschijnlijk worden toegeschreven aan afgenomen distale vaatdiameters als gevolg van AD pathologie. MCI BFV zijn vergelijkbaar met HC BFV in de extracraniële en intracraniële posterieure circulatie, terwijl MCI BFV waarden in de intracraniële anterieure circulatie tussen AD en HC in liggen. Dit suggereert dat intracraniële anterieure vaten het meest geschikt zijn om vroeg pathologische veranderingen als gevolg van AD te detecteren. De studie bevindingen impliceren verder dat uitgebreide ultrageluidsscreening van intra- en extracraniële vaten nuttig is om BFV afname te monitoren in de MCI fase. Toekomstige follow-up van MCI patiënten kan de predictieve waarde van plaats-specifieke BFV voor conversie naar AD laten zien.

Bij hetzelfde studie cohort is tevens de dynamische cerebrale autoregulatie bestudeerd zoals bediscussieerd in **hoofdstuk 3**. Cerebrale autoregulatie gain en fase zijn vergelijkbaar voor AD, MCI en HC wat suggereert dat het cerebrale autoregulatie mechanisme intact is bij AD patiënten. Toch is de cerebrovasculaire weerstand index, m.a.w. de ratio tussen absolute tijdsgemiddelde bloeddruk en bloedstroomsnelheid, significant hoger in AD in vergelijking met MCI en HC wat impliceert dat de vaatweerstand verhoogd is bij AD. Sterker nog, deze index blijkt een potentiële biomarker te zijn voor de ontwikkeling van AD bij MCI patiënten. De cerebrovasculaire weerstand toename in AD wordt bovendien bevestigd door windkessel model bevindingen die aantonen dat de perifere weerstand significant verhoogd is in AD. Arteriële weerstand en perifere compliantie zijn daarentegen gelijk voor alle groepen.

Vanaf **hoofdstuk 4** wordt de focus verschoven naar locale bloedstroom regulatie. Visueel opgewekte bloedstroom responsies (VEFRs) van voormalig (pre-)eclampsie patiënten en gezonde controles zijn onderzocht om neurovasculaire koppeling eerst in een relatief jonge studie populatie te onderzoeken. Het doel van de studie was te onderzoeken of mogelijke (pre-)eclampsie geïnduceerd endotheel schade reversibel is of niet. De gemeten VEFRs zijn daartoe gefit met de stap responsie van een 2e orde regelsysteem model. Ondanks dat er geen groepsverschillen in model parameters gevonden zijn, was er wel een duidelijke trend zichtbaar dat kritische demping ( $\zeta > 1$ ) vaker optreedt bij voormalig patiënten dan bij controles. Kritische demping weerspiegelt een atypische VEFR, die ofwel ongecompenseerd blijft (sluggish,  $\zeta > 1$ ;  $T_v < 20$ ) of gecompenseerd wordt door een stijging in de initiële stijg term (intermediate,  $\zeta > 1$ ;  $T_v > 20$ ). Aangezien deze abnormale VEFRs vaker gezien worden bij voormalige patiënten (maar niet uitsluitend), kan als hypothese gesteld worden dat deze responsies het resultaat zijn van pathologische verstoringen.

Een aangepaste VEFR analyse procedure die rekening houdt met betrouwbaarheid van model parameters en met bloeddruk dynamica wordt geïntroduceerd in **hoofdstuk 5**. Deze aangepaste procedure bestaat uit de introductie van een betrouwbaarheid parameter voor model parameters en uit een model uitbreiding om de mogelijke bijdrage van bloeddruk variaties aan de gemeten VEFR mee te nemen in de analy-

se. De effecten van deze aanpassingen op de studie uitkomsten zijn geëvalueerd door zowel de standaard procedure (toegepast in hoofdstuk 4) als de aangepaste procedure toe te passen op de VEFRs gemeten bij het AD studie cohort. Overweging van de betrouwbaarheid van model parameters resulteerde in exclusie van ongeveer 40% van de VEFRs, vooral door de tekortkoming van het model bij het fitten van kritisch gedempte responsies. Echter, in acht name van de betrouwbaarheid leidde ook tot een aanzienlijke reductie van de parameter variabiliteit. Wat betreft de invloed van bloeddruk variatie, werd een significant verhoogde demping gevonden wanneer de standaard procedure werd toegepast in tegenstelling tot voor de aangepaste procedure. Dit leidde tot omkering van de studie conclusie van gestoorde naar normale neurovasculaire koppeling in AD. Gezien hun invloed op verkregen parameters, zouden beide aspecten m.a.w. betrouwbaarheid en bloeddruk variatie geïncorporeerd moeten worden in VEFR-analyse. De klinische studie uitkomsten in ogenschouw nemend, lijkt neurovasculaire koppeling niet aangetast in AD omdat het vinden van een verhoogde demping toegeschreven zou kunnen worden aan het negeren van mogelijke bloeddruk bijdrage aan de VEFR.

Studie conclusies uit eerdere hoofdstukken (4 en 5) benadrukken de behoefte aan een model met fysiologisch betekenisvolle parameters. In **hoofdstuk 6**, worden de eerste (voorbereidende) resultaten gerapporteerd van de toepassing van een nieuw ontwikkeld lumped parameter model van de visuele cortex vaatboom op de 3 verschillende VEFR types. In het nieuwe model grijpen de regulatie processen m.a.w. neurogene, metabole, myogene en shear stress mechanismen, aan op de tonus van de gladde spiercellen wat inherent leidt tot de aanpassing van de microcirculatie weerstand en compliantie. Dit zorgt ervoor dat effecten van pathologische veranderingen op de VEFR bestudeerd kunnen worden. Er kan geconcludeerd worden dat met dit model de link tussen VEFR en fysiologie wordt verbeterd. De eerste resultaten laten zien dat het op fysiologie gebaseerde model in staat is om representatieve voorbeelden van alle 3 VEFR types redelijk goed te beschrijven waarbij fysiologisch aanvaardbare parameter waarden worden verkregen.

Vanuit een klinisch perspectief kan geconcludeerd worden dat (Duplex) ultrageluidsmetingen duidelijk potentie laten zien als een standaard screening tool bij MCI patiënten. Het lijkt de moeite waard om bij alle toekomstige MCI patiënten de extra- en intracraniale bloedstroomsnelheden te meten en de cerebrovasculaire weerstand te bepalen door simultane bloeddruk opname. Follow-up van MCI patiënten zal de predictieve waarde van deze parameters laten zien voor toekomstige ontwikkeling naar AD. Van een methodologische perspectief kan geconcludeerd worden dat de huidige standaard gebruikte regelsysteem analyse om de locale cerebrale bloedstroom regulatie te evalueren beperkingen heeft qua parameter betrouwbaarheid en VEFR interpretatie. Zowel betrouwbaarheid als interpretatie kunnen mogelijk verbeterd worden door optimalisatie en betere controle van de data acquisitie kwaliteit en door het gebruik van op fysiologie gebaseerde modellen. Fysiologische mechanismen die de totstandkoming van de VEFR beïnvloeden zouden geïmplementeerd in een dergelijk model moeten worden om mogelijk een deel van de VEFR variantie te kunnen verklaren. Er zou gestreefd moeten worden naar de ontwikkeling en validatie van op fysiologie gebaseerde



modellen die ontworpen zijn om VEFs betrouwbaar te kunnen beschrijven aan de hand van parameters met een eenduidige fysiologische betekenis.

# Dankwoord

De totstandkoming van dit boekje is mede mogelijk gemaakt door bijdragen, in welke vorm dan ook, van vele mensen om mij heen. Graag wil ik hen via deze weg bedanken.

Geachte professor van de Vosse, beste Frans, ten eerste wil ik je bedanken dat je mij hebt opgenomen in jouw onderzoeksgroep. Ik voel me bevoorrecht dat ik zoveel van jou heb mogen leren zoals verschillende manieren om naar vraagstukken te kijken en ze te reduceren tot relatief eenvoudige problemen. Daarbij ben je ook nog eens een fijne mentor die ondersteunt waar nodig. Ontzettend bedankt voor al je support!

Geachte professor Mess, beste Werner, uw strenge doch rechtvaardige manier van (concrete) feedback geven zorgde ervoor dat ik na onze besprekingen altijd wegging met het positieve gevoel dat het beste uit me werd gehaald. Bedankt voor uw open-mindedheid en het delen van uw visies als clinicus!

Geachte Dr. Reulen, beste Jos, door onze verschillen in persoonlijkheid, werden we beiden uitgedaagd om een weg in samenwerken te vinden die voor ons allebei werkt. Ik heb heel veel geleerd van uw manier van denken, kritische kijk op onderzoek en innovatieve ideeën hoe dingen in elkaar zitten. Hartelijk bedankt voor de vele keren dat ik gebruik heb mogen maken van al uw goede tips en adviezen!

Dear professor Panerai, it is an honour for me that you accepted the invitation to take part in the committee. Thank you very much for your useful comments on my thesis.

Dear professor Rosengarten, I also felt honoured that you accepted the invitation to take part in the committee. Thanks a lot for your interest and the useful discussions.

Geachte professor Bergmans en professor de Mol, bedankt dat jullie in de oppositie wilden plaatsnemen. Ook gaat mijn dank uit naar de voorzitter, professor Hilbers.

Beste Dr. Peeters, beste Louis, uw gedrevenheid en onstuitbaar enthousiasme wisten mij steeds weer die extra energie te geven om toch door te gaan als het even tegen zat. Hartelijk bedankt voor de prettige samenwerking! Ook wil ik de PERIM groep bedanken met name Inez Schreij die mij alle hulp heeft geboden bij de patiëntinclusie.

Geachte professor Verhey, beste Frans, ik wil u, samen met Pauline Aalten en Inez Ramakers, bedanken voor de fijne samenwerking, waardevolle suggesties en alle ondersteuning bij de 'KNF-studie'. Rosa, Claire en Jeroen, bedankt voor jullie hulp bij de AD-inclusie. Heidi, wij kijken allebei terug op een mooie Boston-tijd, bedankt voor de tips!!

Beste Erik, heel erg bedankt dat de deur altijd open stond en ik met welke vragen dan ook bij jou terecht kon. Ik heb veel van onze discussies en jouw visie op dingen geleerd!

Beste Eri, wij hadden onze weg naar een goede maar ook gezellige samenwerking snel gevonden. Dankjewel dat je zo een fijne collega was en lieve vriendin bent geworden!

Guy Bogaarts en Bart Spronck, het was een eer om jullie mee te mogen begeleiden, hoewel het meer als samenwerken voelde. Bedankt voor jullie inbreng en enthousiasme. Ik heb veel van jullie geleerd en vind het leuk dat jullie collega-aio's zijn geworden!

Alle (oud-)collega's van de KNF: Gertie, Chantal, Jose, Iris, Daisy, Marielle, Nathal, Saskia, Wendy, Manuela, Jacqueline, Anita, Loreen, Kevin, Linda, Ariane, Paul Blijham, Selma, Vivian, Danny, heel erg bedankt voor de leuke, goede werksfeer! Paul Bergs, dankjewel dat je altijd klaarstaat en met mij mee wilt denken. Loes, we hebben altijd genoeg te kletsen als we elkaar weer tegenkomen... bedankt, ook voor de klifio-tips!

Geachte professor Beijerinck, beste Herman, hartelijk bedankt dat je in mij hebt geloofd, dat je zo eerlijk bent (al kon ik het wat minder waarderen op het moment zelf) en dat je me de kans hebt gegeven om mij als persoon verder te ontwikkelen. Ook wil ik de SMPE\e met name Ivonne Lammerts, Ineke en Karlijn bedanken voor hun steun. Saskia en Beatrijs, na de communicatiecursus zijn wij doorgegaan met 'lastige situaties voor jonkies' bespreken tijdens onze etentjes. Bedankt voor de tips en gezelligheid!

Ook wil ik de voormalige BMT-AZM provisorium groep bestaande uit Marielle, Maurice, Erik, Wilco, Lambert, Wouter, Maarten, Ralph, Ellen, Bram, Rob Debije, Manon en Els bedanken dat jullie een tweede 'thuishaven' voor mij vormden. Ook bij de BMT-UM groep o.l.v. Tammo kon ik altijd terecht voor vragen of een leuk gesprek. Met name wil ik Arnold bedanken voor de adviezen en Evelien, Nico en Claire voor hun belangstelling.

Dear Mihai, Alessandro, Nazia, Iulia, Anca and Carole, the 'wannabe-dutchies' as I nicknamed you guys. Most of you I first met during the summer school in Vienna and from then I had a new group of friends. Thank you so much for all great moments we shared, the enjoyable dinner evenings and interesting discussions on important and somehow less important things in life like why Dutch people do not rinse when doing the dishes...

Julienne en Floor, bedankt voor jullie betrokkenheid, voor de goede gesprekken over de meest uiteenlopende onderwerpen tijdens de etentjes en natuurlijk voor alle lol bij het onveilig maken van de dansvloeren al dan niet met wat hulp van de cocktails ;). Floor, ook bedankt voor je telefonische peptalks en onze 'back to nature'-activiteiten.

Lieve Harrie en Ellie, bedankt voor jullie onvoorwaardelijke steun. Het is fijn te weten, dat ik altijd bij jullie terecht kan als ik daar behoefte aan heb. Ook bedankt voor alle hulp bij het klussen in mijn appartement.

Lieve Simone, ondanks dat we elkaar pas aan het begin van onze promoties leerden kennen, heb je me overal mee naar toe gesleept waardoor ik in een mum van tijd heel wat leuke plekjes in Maastricht leerde kennen. Ook de zee-en-strandfestivals in Zee-

land en Almere en onze uitbundige carnivals zijn onvergetelijk ..... Superbedankt voor alle gezelligheid, maar ook dat ik altijd bij je aan mocht kloppen voor statistiek-advies!

Elke en Martijn, wat ontzettend knap hoe jullie ondanks de grote tegenslagen die jullie te verwerken hebben gekregen, nog zo positief in het leven staan. Ik heb hier veel inspiratie uitgehaald hoe om te gaan met de obstakels op mijn pad. De weekendjes weg en dagjes uit hebben voor heel wat leuke afleiding en goede gesprekken gezorgd. Super bedankt voor al je steun, lieve Elke! We gaan er een groot feest van maken in NY!!

Mijn lieve paranimf Carole, wat ben ik blij dat ik een vriendin als jij heb: je bent altijd vrolijk en optimistisch, je ziet overal mogelijkheden en hebt oprechte belangstelling in alles en iedereen. Ontzettend bedankt voor alle bijzondere momenten die ik met en dankzij jou heb meegemaakt zoals de ULM-vlucht en aankomst van 1000-en kuikentjes op de boerderij van je ouders, onze henna tattoo's en limo-ritjes bij Nazia's bruiloft, biertjes drinken met Anca tussen de hippies in Kopenhagen... en hopelijk volgen nog veel meer leuke avonturen, te beginnen met samen onderzoek doen in Vancouver!

Mijn lieve paranimf Rachel, als tweelingzussen hebben we een heel speciale band en begrijpen wij elkaar als geen ander. Het is heerlijk om iemand te hebben bij wie je terecht kan als het even wat minder meezit, maar die ook minstens net zo blij is als jijzelf wanneer er positief nieuws te melden valt! Dankjewel dat ik met wat dan ook bij je terecht kan. En natuurlijk ook voor de vele keren dat ik in 'hotel Rachel' in Eindhoven heb mogen verblijven: dat maakte het bijna wekelijkse gereis tot een waar feestje! Superbedankt dat je zo een geweldige zus voor mij bent!

Als ik ergens heel veel geluk mee heb gehad in mijn leven, dan is dat met een moeder als jij, mama. Je hebt keihard gewerkt om mij een toekomst te geven waarin ik alle kansen heb gekregen om mij te ontwikkelen. Ik hoop daarom ook dat je dit boekje ook een beetje als jouw boekje zult beschouwen, want dat is het met recht. Woorden schieten tekort om je te bedanken voor al je liefde, steun en geloof in mij.



# Curriculum Vitae



Esther Martens was born on the 11<sup>th</sup> of February, 1979 in Sittard, the Netherlands. After obtaining her high school diplomas (HAVO 1996, VWO 1998) at the Bisschoppelijk College in Sittard, she started to study (bio-)medical engineering at the Eindhoven University of Technology in Eindhoven, the Netherlands. Her interest in a course on the physics of the senses led to an internship on the influence of foot-sole pressure on perceived body position during short-radius centrifugation at the Man Vehicle Lab

of the Massachusetts Institute of Technology (MIT) in Cambridge, MA, USA. She continued to work in the field of function research by performing her graduation project on cerebral autoregulation and neurovascular coupling after (pre)eclampsia at the department of Clinical Neurophysiology of the Maastricht University Medical Centre. She received her master's degree in medical engineering in 2005. After a short period of being employed as a research assistant at the Clinical Neurophysiology department, she got the opportunity to continue her research on cerebral blood flow regulation as part of a PhD trajectory established by collaboration between the Clinical Neurophysiology department of the Maastricht University Medical Centre and the Cardiovascular Biomechanics group of the Biomedical Engineering department of the Eindhoven University of Technology. The project of which the results are presented in this dissertation was focused on reliable clinical assessment of cerebral blood flow regulation by ultrasonography. Esther combined the PhD trajectory with a post-academic educational program on Qualified Medical Engineering at the School of Medical Physics and Engineering (SMPE/e) of the Eindhoven University of Technology. As part of the program, she spent 3 months at the Syncope and Fall in Elderly (SAFE) laboratory of the Beth Israel Deaconess Medical Centre, a training hospital of Harvard Medical School, in Boston, MA, USA. She obtained her Qualified Medical Engineer (QME) degree in 2010. Since 2011, she is employed as a medical physicist trainee by the Maastricht University Medical Centre.

